3.0 VOLCANIC HAZARD ANALYSIS

This section presents the probabilistic volcanic hazard analysis (PVHA) model developed for this study. Section 3.1 describes the mathematical formulation for the PVHA. Details of the mathematical model are developed in Appendix F. Section 3.2 translates the individual experts' assessments into a common hazard model format and summarizes their assessments of various components of the model. The results of the hazard analysis are presented in Section 4.

3.1 VOLCANIC HAZARD MODEL FORMULATION

3.1.1 Basic Formulation

The quantitative product of the PVHA study is the probability that the proposed repository site will be intersected by a volcanic event during the next 10,000 years. Because the probability is small it can be estimated to a very close (and conservative) approximation by the expected number of intersections regardless of the appropriate temporal model for volcanic event occurrence.[1] The specific measure of volcanic hazard used in this analysis is the mean number of intersections per year or mean annual frequency of intersection, termed ν_I. Given the fact that the time period of interest for the PVHA assessment is very small compared to the time scale for changes in volcanic rates (millions of years), the mean annual frequency of intersection is not expected to vary significantly during 10,000 years. Thus the mean number of intersections is very close to $\nu_I \cdot 10^{-4}$, which is, in turn, slightly greater than the probability of intersection. For simplicity, we shall refer below to this "mean annual frequency" as the "frequency."

The frequency of intersection can be represented as the product of two quantities, the frequency of occurrence and the likelihood that the event will intersect the repository. Figure 3-1 shows schematically the basic formulation for PVHA calculation. If one assumes that volcanic events occur randomly in time with a constant rate, then a natural estimate of the frequency of occurrence is the number of observed events divided by the time period of observation. If one assumes that volcanic events occur randomly within a region R with uniform spatial density, then a natural

[1] This is shown by comparing the mean number of intersections [equal to $0 \cdot P(0)+1 \cdot P(1)+2 \cdot P(2)+....$] to the probability of one or more intersections [equal to $P(1)+P(2)+....$]. When P(2) is much smaller than P(1), which is the case for rare events, the mean number if events is close to P(1 event).

estimate of the spatial density of events is one over the area of region R. Using these estimates, the estimated annual frequency of intersection, ν_I, is given by the expression

$$\nu_I = \frac{N(R,T)}{T} \cdot \frac{a_r^e}{A_R} \qquad \textbf{(3-1)}$$

where $N(R,T)$ is the number of events that have occurred in region R in time period T, A_R is the area of region R, and a_r^e is the area of the repository, adjusted for the dimensions of the effect of the event. For example, if the repository were circular, with radius r_r, and events that occur within a distance d_e of the repository result in intersection, then $a_r^e = \pi(r_r+d_e)^2$ (see Figure 3-1).

The members of the expert panel used a variety of methods to model the volcanic hazard at the proposed Yucca Mountain repository site. All of these models can be represented by a generalized form of Equation **(3-1)**:

$$\nu_I(t) = \iint_R \lambda(x,y,t) \cdot P_I(x,y)\, dx\, dy \qquad \textbf{(3-2)}$$

In Equation **(3-2)** $\lambda(x,y,t)$ is the rate density (frequency of events per unit time, per unit area) at point (x,y) and time t in the region of interest, R, and $P_I(x,y)$ is the conditional probability that a volcanic event occurring at point (x,y) will intersect the repository. The generalized model allows for a spatially and temporally varying rate of volcanic events.

The generalized model of Equation **(3-2)** can be related to the basic model of Figure 3-1 and Equation **(3-1)** by considering the rate density of volcanic events to be uniform over region R and time T. Thus the estimate of $\lambda(x,y,t)$ is $N(R,T)/(T \cdot A_R)$, a constant value independent of location in region R and independent of time within time period T. The conditional probability of intersection becomes a step function, $P_I(x,y) = 1$ for (x,y) inside of the effective region of the repository, r^e, and 0 everywhere else. As a result:

$$\nu_I(t) = \iint_R \lambda(x,y,t) P_I(x,y)\, dx\, dy = \frac{N(R,T)}{TA_R} \iint_{r^e} dx\, dy = \frac{N(R,T)}{TA_R} a_r^e \qquad \textbf{(3-3)}$$

The generalized model of Equation **(3-2)** used in this analysis separates the PVHA into two parts: (1) an assessment of the spatial and temporal frequency of volcanic events, and (2) an assessment

of the spatial extent of an event, given that it occurs. This separation provides a means of easily incorporating the variety of approaches to volcanic hazard published in the literature (and used by the experts) into the common model. The published approaches (e.g., Crowe et al., 1982, 1992; Ho et al., 1991; Sheridan, 1992; Connor and Hill, 1995) consider volcanic events to be represented by points and use various point process methods to model the distribution of future events in time and space. For the most part, these models consider the temporal and spatial aspects of the problem in such a way that the rate density parameter, $\lambda(x,y,t)$, can be written as the product of a rate parameter, $\lambda(t)$, and a spatial density, $f(x,y)$. The generalized model of Equation **(3-2)** becomes:

$$v_j(t) = \int\int_R \lambda(t) \cdot f(x,y) \cdot P_j(x,y)\, dx\, dy \qquad \textbf{(3-4)}$$

Referring again to the simple example of Figure 3-1, the estimate of $\lambda(t)$ is $N(R,T)/T$ and the estimate of $f(x,y)$ is $1/A_R$.

Below, we describe the various models used by the experts to represent the temporal and spatial distribution of future volcanic events in the following sections of the report. First, however, we discuss the approach used to address the uncertainty in specifying volcanic hazard models and model parameters.

3.1.2 Treatment of Uncertainty

The PVHA model of Equation **(3-2)** or **(3-4)** represents the randomness inherent in the natural phenomena of the occurrence of volcanic events. In all assessments of the effects of rare phenomena one is faced with considerable uncertainty in selecting the appropriate models and model parameters arising from limited data and/or alternative interpretations of the available data. It has become a standard-of-practice to explicitly incorporate these additional uncertainties into probabilistic hazard assessments. The most prominent example is probabilistic seismic hazard analysis (PSHA) methodologies used for hazard assessments at critical facilities (National Research Council, 1988).

For this study, we employ the logic tree methodology to incorporate the uncertainty in modeling the spatial and temporal distribution of future volcanic events in the region surrounding the proposed Yucca Mountain site. The logic tree formulation has been well developed for probabilistic seismic hazard analysis (e.g., Kulkarni et al., 1984; Coppersmith and Youngs, 1986; EPRI, 1987; National Research Council, 1988, SSHAC, 1995). The methodology involves setting

out the sequence of assessments that must be made in order to perform the analysis and then addressing the uncertainties in each of these assessments in a sequential manner. The logic tree allows for alternative models, hypotheses, and parameter values to be weighted and incorporated into the analysis in a logical and transparent way. Thus, it provides a convenient approach for breaking a large, complex assessment into a sequence of smaller, simpler components that can be more easily addressed.[2]

The simple volcanic hazard model shown on Figure 3-1 will be used to illustrate the logic tree methodology. The three parameters of the hazard model are the time period, T, over which the rate of occurrence of volcanic events is assumed to be constant and representative of the current rate, the region, R, over which the spatial distribution of volcanic events can be considered uniform during time period T, and the actual number of events, $N(R,T)$, that have occurred in region R in time period T. Figure 3-2 shows the alternative assessments that could be made. These involve considering alternative time periods, alternative regions, and the uncertainty in determining the actual number of events that have occurred in the past.

The general structure of a logic tree is shown on Figure 3-3. The logic tree is composed of a series of nodes and branches. Each node represents an assessment of a state of nature (e.g., alternative models or hypotheses) or an input parameter value that must be made to perform the analysis. Each branch leading from the node represents one possible discrete alternative for the state of nature or parameter value being addressed. If the variable in question is continuous, it can be discretized at a suitable increment. The branches at each node are intended to represent mutually exclusive and collectively exhaustive states of the input parameter. In practice, a sufficient number of branches are placed at a given node to adequately represent the uncertainty in the parameter estimation.

Probabilities are assigned to each branch that represent the relative likelihood or degree of belief that the branch represents the correct value or state of the input parameter. These probabilities are assessed conditional on the assumption that all the branches leading to that node represent the true state of the preceding parameters. Because they are conditional probabilities for an assumed mutually exclusive and collectively exhaustive set of values, the sum of the conditional probabilities at each node is unity. The probabilities depend strongly upon expert judgment

[2] Note that, although it is similar in appearance, the logic tree is neither an "event" tree nor a "decision" tree; the logic tree deals solely with model and parameter uncertainty associated with limited information.

(subjective probabilities) because the available data are too limited to allow for objective statistical analysis, and because scientific judgment is needed to weigh alternative scientific interpretations of the available data. The logic tree approach simplifies these subjective assessments because the uncertainty in a single parameter is considered individually with all other parameters leading up to that parameter assessment assumed to be known with certainty. Thus, the nodes of the logic tree are sequenced to provide for the conditional aspects or dependencies among the parameters and to provide a logical progression of assumptions from the general to the specific in defining the input parameters for an evaluation. So, for example, the distribution for N, the number of past events, depends on what time period T (e.g., 2 Ma vs. 5 Ma) and region R (R_1 vs. R_2) are under consideration at the node (Figure 3-3).

In most cases, the probabilities assigned to the branches at a node are in units of tenths, unless there is a basis for finer resolution. Usually the weights represent one of two types of probability assessments. In the first, a range or distribution of parameter values is represented by the logic tree branches for that parameter and their associated weights. For example, the volume of basalt erupted during a single past volcanic event is uncertain because of uncertainties in geochronologic analyses of materials and in interpreting eroded land forms. The resulting volume may be represented by a preferred value and a range of higher and lower values, similar to a normal or log normal statistical distribution. This type of distribution can be represented by three (or more) branches of a logic tree. Keefer and Bodily (1983) have shown that most distributions can be reliably represented by three values: the median estimate (with a weight of 0.63) and a higher and lower value (each with weights of 0.185) that represent the 5th and 95th percentiles (e.g., plus or minus 1.65 standard deviations for a normal distribution). Although a large number of branches for an individual assessment can be included on a logic tree, usually the results are not sensitive to having more than about three branches at any one node in a logic tree having many nodes. If the assessments are provided in the form of a specific probability density function or in the form of a cumulative probability distribution, the assessment can be discretized into a suitable increment for input into the logic tree format.

In some instances, the uncertainty in a parameter assessment can be estimated using formal statistical estimation techniques and the resulting continuous distribution discretized for use in the logic tree formulation. For example, the rate of occurrence of volcanic events in Equation **(3-1)** is estimated by the quantity N/T. If one assumes that the occurrence of volcanic events conforms to a Poisson process, then there are explicit probabilistic models that describe the probability distribution for the rate parameter of a Poisson process estimated from a data set of finite size.

Appendix F describes the procedure used in this study to develop a discrete distribution describing the uncertainty in the rate of occurrence estimated from an observed number of events.

A second type of probability assessment to which logic trees are suited is in indicating a relative preference for, or degree of belief in, two (or more) alternative hypotheses. For example, the appropriate geologic time period for assessing the current rate of volcanic events is uncertain. Two possible alternatives might be the Quaternary period (past 2 million years) or the Pliocene and Quaternary (past 5 million years). Based on the pertinent data, a relative preference for these alternatives can be expressed by the logic tree weights. A strong preference for one over the other is usually represented by weights such as 0.9 and 0.1 for the two alternatives. If there is no preference for either hypothesis, they are usually assigned equal weights (0.5 and 0.5 for two hypotheses). Increasing the weight assigned to one hypothesis from 0.5 to 0.9+ reflects an increasing preference for that alternative. Although the logic tree weights are ultimately subjective judgments based on available information, it is important to document the data and interpretations that led to the assessment of the alternatives being considered and the assignment of weights in order that the process can be reviewed by others.

The example logic tree shown on Figure 3-3a contains three nodes, one for each of the three parameters of the simplified model of Equation **(3-2)**. In this example, the parameter that is clearly dependent on the other assessments is the event counts, $N(R,T)$, which is a function of the time period and region. Therefore, this node is logically placed last (farthest to the right) in the logic tree. However, the sequence of the nodes is not fixed and is decided primarily as a matter of convenience in making the assessments. Once a logic tree has been developed, one can invert the order of the nodes, as will be illustrated later in Section 3.2.

The simplified model shown on Figures 3-2 and 3-3a considered two alternative time periods (3.2 and 10.0 My) and two alternative regions (R_1 with area 10,000 km^2 and R_2 with area 5,000 km^2). The assessment has been made that the shorter time period is strongly preferred (probability 0.8) to the longer time period (0.2) and that region R_1 is slightly preferred (probability 0.6) to region R_2 (0.4). For each combination of T and R, two alternative values of $N(R,T)$ have been assessed. These alternatives are based on the assumption that the larger volcanic centers represent one or more events. Two hypotheses are considered, all of the larger centers represent single events or all of the centers represent multiple (2 or 3) events. These two hypotheses are considered equally likely to represent the true history of volcanism in the region and are given equal weight.

The logic tree shown on part (a) of Figure 3-3 defines a discrete distribution for the frequency of intersection, ν_I, computed using Equation **(3-2)**. The eight possible parameter combinations, the probability of each parameter combination, and the resulting frequency of intersection are listed on part (b) of Figure 3-3 for an effective repository area, a_r^e of 10 km^2. The resulting distribution is shown on part (c) of Figure 3-3. The probability that the frequency of intersection will take one of the eight possible values is equal to the joint probability of the set of parameters T, R, and $N(T,R)$ being the true parameter values and is equal to the product of the conditional probabilities following a particular path through the logic tree. For example, the probability that the frequency of intersection equals $4 \cdot 10^{-9}$ equals the product of the probability that T should be 3.2 Ma, the probability that R_j is the appropriate region, and that $N(T,R)$ equals 13 events.

The discrete distribution for the frequency of intersection shown on part (c) of Figure 3-3 can be used to compute the expected or mean value of ν_I given the uncertainty in the input parameters T, R, and $N(T,R)$. The expected value, $E[\nu_I]$, is obtained by summing the individual estimates of ν_I multiplied by the probability that they are the "correct" estimate:

$$\begin{aligned} E[\nu_I] &= 0.24 \cdot 4.0 \cdot 10^{-9} + 0.24 \cdot 3.8 \cdot 10^{-9} + 0.16 \cdot 6.9 \cdot 10^{-9} + 0.16 \cdot 6.3 \cdot 10^{-9} + \\ &\quad 0.06 \cdot 2.0 \cdot 10^{-9} + 0.06 \cdot 1.5 \cdot 10^{-9} + 0.04 \cdot 3.2 \cdot 10^{-9} + 0.04 \cdot 2.4 \cdot 10^{-9} \\ &= 4.4 \cdot 10^{-9} \text{ events/year} \end{aligned}$$

Formally, this is given by the equation

$$E[\nu_I] = \sum_i \sum_j \sum_k \frac{N_k(T_i,R_j)}{T_i \cdot A_{R_j}} \cdot P(T=T_i) \cdot P(R=R_j) \cdot P(N=N_k \mid T_i,R_j) \qquad \textbf{(3-5)}$$

The variance in the estimate of ν_I is computed in a similar fashion and is defined formally by:

$$Var[\nu_I] = \sum_i \sum_j \sum_k \left(\frac{N_k(T_i,R_j)}{T_i \cdot A_{R_j}} - E[\nu_I] \right)^2 \cdot P(T=T_i) \cdot P(R=R_j) \cdot P(N=N_k \mid T_i,R_j) \qquad \textbf{(3-6)}$$

The resulting coefficient of variation (square root of the variance/mean) is 0.37.

Part (d) of Figure 3-3 shows the cumulative distribution for the frequency of intersection, ν_I, developed from the discrete distribution shown on part (c). This distribution can be used to obtain

confidence intervals for the frequency of intersection that reflect the uncertainties in defining the hazard analysis models and parameters. The actual logic trees developed to represent the volcanic hazard models of each of the experts have thousands of branches, resulting much smoother density estimates that those show on Figure 3-3 for this simple example.

In the following sections the various hazard models used by the experts are described in terms of the basic formulation and the treatment of uncertainty. Details of the mathematical formulations are provided in Appendix F.

3.1.3 Locally Homogeneous Spatial and Temporal Model

The basic assumption of the homogeneous model is that one can identify a region where the rate of occurrence of volcanic events can be considered uniform in both time and space over the time period of interest to the hazard assessment. The simplified hazard model of Figure 3-1 is an example of a homogeneous spatial and temporal model. It is of course recognized that the rate of volcanic events is not spatially and temporally homogeneous over the entire western United States. One must identify zones where the assumption of homogeneity can be applied. Therefore, we use the term "locally homogeneous" to describe the model in which the region of interest is divided into one or more zones, each with its own homogeneous rate of volcanic events.

The assumption of a uniform spatial and temporal rate density of volcanic events within a locally homogeneous zone is consistent with a homogeneous Poisson process. Homogeneous Poisson models are commonly used to represent the hazard from rare events. In particular, the Poisson model forms the basis of the probabilistic seismic hazard methodology developed by Cornell (1968, 1971). It has also been shown that the Poisson model provides a reasonable representation for the combined effects of the contributions from multiple independent processes, even when the individual processes are non-Poisson in nature (Brillinger, 1982).

The locally homogeneous spatial and temporal model is implemented by dividing the region of interest into a number of non-overlapping zones, Z_i, $i = 1$ to n. Figure 3-4 shows an example of subdividing the region shown on Figure 3-1 into two zones, a large region with diffuse activity, Zone A, and a smaller region with a concentration of activity, Zone B. In this type of zonation the larger zone is often called a background zone that is used to represent a "background" rate of activity in the region outside of the more active volcanic fields.

Within each zone the rate density of volcanic events can be modeled by separating the temporal and spatial aspects using Equation **(3-4)**. Given the assumption of a uniform spatial density, the density parameter is equal to the inverse of the zone area, A_i [$f(x,y) = 1/A_i$]. If the rate of occurrence, λ, is to be estimated from the observed data for the zone, then the maximum likelihood estimate is given by the number of observed events within a specified time interval, $N(Z_i,T)$, divided by the time interval, T [$\lambda = N(Z_i,T)/T$]. The frequency of intersection due to the occurrence of volcanic events in zone i is thus given by

$$\nu_{I_i} = \frac{N(Z_i,T)}{T} \iint_{Z_i} \frac{1}{A_i} \cdot P_I(x,y)\, dx\, dy = \frac{N(Z_i,T)}{T} \cdot (\bar{P}_I)_i \qquad \textbf{(3-7)}$$

where $(\bar{P}_I)_i$ is the spatial average of the conditional probability of intersection within zone i. The total hazard is obtained by summing the hazard contributed by each zone

$$\nu_I = \sum_{i=1}^{n} \frac{N(Z_i,T)}{T} \cdot (\bar{P}_I)_i \qquad \textbf{(3-8)}$$

The boundary between two zones represents a point where there is an abrupt step function in the volcanic event rate density. Several of the experts chose to consider a gradual transition between zones in areas where there was a large change in rate density and the modeling of this change is important to the site hazard. The eastern edge of Crater Flat is an example in which the hazard is very sensitive to the manner of the rate density changes. The gradual transition was implemented by assuming that the rate density within zone i decays linearly to zero with distance from the zone boundary over a specified distance, h. The effect is an increase in the area of the zone approximately equal to $h/2$ times the length of the zone perimeter along the portion of the zone where a gradual transition is assumed to occur, and an increase in the area over which the spatial average of P_I is computed (see Appendix F).

The uncertainties in the homogeneous spatial and temporal model include defining the appropriate zones, defining the appropriate time period, and estimating the number of events that have occurred within that time period. These uncertainties are modeled in the PVHA by considering alternative zonations, alternative time periods, alternative estimates of the number of events that have occurred at each volcanic center, and alternative boundary conditions (abrupt versus gradual transition). In addition, there is uncertainty in estimating the true rate of volcanic events given that there is only a

limited data set. The uncertainty in the rate parameter, λ, can be estimated using objective statistical techniques. Weichert (1980) presents a method of estimating confidence intervals for a Poisson rate. His approach (described in Appendix F) uses a χ^2 distribution to represent the confidence interval in λ. In the PVHA, the uncertainty in λ was represented by the three point approximation of Keefer and Bodily (1983) discussed above. The maximum likelihood value, $N(Z,T)/T$, was given a weight of 0.63. The 5th and 95th percentiles of the confidence interval for λ were estimated using Weichert's χ^2 approach and each was given a weight of 0.185.

3.1.4 Nonhomogeneous Spatial Models

Nonhomogeneous spatial models provide a means of specifying a smooth variation of the spatial density of volcanic events, $f(x,y)$, within the region of interest. Two types of nonhomogeneous spatial models were used by the experts, parametric models and nonparametric models.

Parametric Spatial Density Function. Sheridan (1992) has developed a model for volcanic fields in which the spatial density of events is represented by a bivariate Gaussian distribution. The resulting volcanic field has an elliptical shape defined by five parameters, the coordinates of the center of the field, the length of the major and minor axes, and the orientation of the major axis. Figure 3-5 shows an example of a bivariate Gaussian field representation of the volcanic events in Crater Flat. The spatial density of future events associated with the field is given by the expression

$$f(x,y) = \frac{e^{-[(x-\mu)^T \Sigma^{-1}(x-\mu)]/2}}{2\pi|\Sigma|^{1/2}} \qquad (3\text{-}9)$$

where x is the location of point (x,y), μ is the location of the center of the field (mean of x and y for all past and future events) and Σ is the covariance matrix describing the distribution about the field center for the x and y locations of all past and future events associated with the field. The covariance matrix defines the size and shape of the field. For example, the ellipse that encloses 50 percent of the density of the field has dimensions that are approximately 1.2 times the standard deviation of the x and y coordinates of the population of events within the field.

The specification of the Gaussian field parameters can be through reference to better developed fields considered analogous (e.g. Sheridan, 1992; Crowe et al., 1995) or they can be estimated directly from the observed events associated with the field. The experts chose to estimate the parameters of Gaussian volcanic fields from the local data using two approaches.

In the first approach, a set of volcanic events that constitute a field was identified. The five parameters of a bivariate Gaussian distribution were then estimated directly from the x and y locations of the observed events using standard maximum likelihood estimators of the mean of x and y and the covariance matrix of x and y. These parameters provide a best estimate of the field and Equation **(3-9)** can then be used to compute the spatial density function for future events associated with the field.

Uncertainty in the field parameters results from uncertainty in defining the appropriate set of volcanic events that constitute the field. In addition, there is uncertainty in estimating the field parameters because of the limited size of the data set. This uncertainty was incorporated into the PVHA by defining a joint distribution for the five field parameters. Asymptotic standard errors were estimated for each of the field parameters from the maximum likelihood fit to the observed data. The five parameters were then varied by ±one standard error to create 3^5 (243) possible sets of field parameters. The likelihood that each parameter set describes the population producing the observed field data was then computed and the resulting set of likelihoods were normalized to define relative weights to assign to each parameter set. For example, Figure 3-6 shows the set of possible field shapes obtained from fitting the data shown on Figure 3-5 in Crater Flat. Shown are only the 27 field shapes arising from uncertainty in the field size and shape parameters defined by the three parameters of the covariance matrix of x and y.

The second approach for specifying the field parameters is based on the use of the local geology to define the likely geometry of a field. For example, a zone may be defined that is considered to represent a volcanic field. However, instead of assuming that the zone represents a locally homogeneous field, it is assumed that the zone boundary approximately defines a specified density contour of the field (such as the 90th percentile). A set of field parameters is then found that minimizes the difference between the defined approximate field boundary and the bivariate Gaussian ellipse that encompasses the specified density percentile. Figure 3-7 shows an example of fitting a 95th percentile density ellipse to a specified field boundary. Uncertainty in the field parameters defined in this approach was specified by considering alternative zone boundaries and/or alternative values for the density percentile contained within the specified boundary.

The bivariate Gaussian volcanic field model defines the spatial density of future events associated with a field. The rate of occurrence of the events can be computed using the number of observed events in the field and the homogeneous temporal model defined above. The frequency of intersection is then computed using Equation **(3-4)**. It application, the volcanic field was often

considered to be superimposed on a larger spatially homogeneous background zone representing the hazard from random volcanic events not associated with an identifiable field.

Nonparametric Spatial Density Function. Nonparametric spatial densities of events can be estimated using various types of smoothing operators combined with the observed data. Connor and Hill (1995) present three types of nonhomogeneous spatial models for estimating volcanic hazards, spatial-temporal nearest neighbor density estimation, kernel density estimation, and nearest neighbor kernel density estimation. Of the three, the kernel density estimation technique probably is the most widely used in the general field of density estimation, and was the method selected by the experts for nonparametric estimation of the spatial density of future volcanic events.

Nonparametric density estimation assumes that future events are likely to occur "near" the existing events. In the kernel density estimation technique, near is defined by a parametric density function, with characteristic dimension h, centered on each event. The process is illustrated in one dimension on Figure 3-8. Three events are located along the x axis, as indicated on plot (a) of the figure. At the location of each event a parametric kernel function is placed. The kernel has the properties of a symmetric probability density function such that the area under each kernel equals unity. The combined density function at a point is computed by summing the values of the individual kernel density functions at that point. The function is then normalized by its integral, which is equal to the number of points for infinite boundary conditions. The resulting density function is shown on plot (b) of Figure 3-8.

A wide variety of kernel functions have been developed for density estimation. Two common forms are the Epanechnikov and Gaussian kernels. The Epanechnikov kernel was used by Connor and Hill (1995) and has the following form for two-dimensional density estimation (Silverman, 1986)

$$K^{E}(\boldsymbol{d}_i) = \frac{2}{\pi h^2}\left[1 - \frac{\boldsymbol{d}_i^{T}\boldsymbol{d}_i}{h^2}\right] \quad \text{for } \frac{\boldsymbol{d}_i^{T}\boldsymbol{d}_i}{h^2} < 1$$
$$= 0 \quad \text{otherwise} \qquad \textbf{(3-10)}$$

where $\boldsymbol{d}_i^T\boldsymbol{d}_i$ is the distance between point (x,y) and event i ($\boldsymbol{d}_i$ is the vector of relative coordinates), and h is the smoothing constant. The Epanechnikov kernel is shown on plot (a) of Figure 3-9 for h equal to 1. The Epanechnikov kernel has an abrupt termination at a distance h from each data

point (volcanic event) and thus results in zero density at distances greater than h from all data points.

The Gaussian kernel has the form of a two-dimensional Gaussian density function:

$$K^{G}(d_i) = \frac{e^{-d_i^T d_i / 2h^2}}{2\pi h^2} \quad \textbf{(3-11)}$$

The parameter h in the Gaussian kernel represents one standard deviation of a normal distribution. Plot (b) of Figure 3-9 shows a Gaussian kernel with h also equal to 1. The Gaussian kernel does not have the abrupt edge of the Epanechnikov kernel and is much more diffuse for the same value of h.

Silverman (1986) indicates that similar results can be achieved with a variety of kernel types, with the choice primarily motivated by ease of computation. In particular, Silverman indicates that equivalent results can be achieved using the Gaussian and Epanechnikov kernels if the value of h used with the Gaussian kernel is a factor of ~2.5 times smaller than the value of h used with the Epanechnikov kernel. Plot (c) on Figure 3-9 shows a Gaussian kernel with h equal to 0.4. The resulting kernel density function has approximately 99 percent of density with the limits of ±1, compared to 100 percent for the Epanechnikov kernel with h equal to 1.

The kernel functions defined by Equations **(3-10)** and **(3-11)** are axisymmetric. However, anisotropic kernel functions can be used to introduce a preferred orientation for smoothing, perhaps representing the interpretation of an underlying structural control. In this approach a covariance matrix is defined to describe the shape of the kernel density function in a similar manner to the parametric Gaussian field model defined in Equation **(3-9)**. The details of the use of an anisotropic kernel are presented in Appendix F. Using the kernel smoothing approach, the spatial density of volcanic events in the region is given by:

$$f(x,y) = \frac{1}{N(R,T)} \sum_{i=1}^{N(R,T)} K(d_i,h) \quad \textbf{(3-12)}$$

The normalizing constant of $1/N(R,T)$ is introduced to make $f(x,y)$ a density function that integrates to unity.

If the kernel density function is to be limited to the boundaries of a specific zone, Z, then the normalizing constant is replaced by the integral of the smoothing function over the source zone and Equation **(3-12)** becomes:

$$f(x,y) = \frac{\sum_{i=1}^{N(R,T)} K(d_i,h)}{\iint_Z \sum_{i=1}^{N(R,T)} K(d_i,h)\,dx\,dy} \qquad \textbf{(3-13)}$$

This is the edge effect discussed by Connor and Hill (1995).

The primary issue in applying kernel density estimation is the selection of the appropriate value of the smoothing constant, h. Silverman (1986) discusses multiple approaches for selecting h, including subjective judgment, simple formulas based on the scatter in the data, and various statistical methods. Connor and Hill (1995) use cluster analysis techniques to identify maximum cluster lengths in the Yucca Mountain data. They then use these lengths as smoothing distances for the Epanechnikov kernel, which has an abrupt edge or limiting distance.

The volcanic experts used two approaches for selecting h. They either used physical arguments, such as those employed by Connor and Hill (1995), or used a technique similar to that illustrated on Figure 3-7 for the parametric Gaussian field. In the second approach, a zone boundary is defined that is assumed to approximate a specified density contour of all past and future events associated with a local volcanic field. The mapped volcanic events associated with the field are then used to construct kernel density functions using a range of values for h. The appropriate value of h is selected to be the one that results in the minimum difference between the zone boundary and the specified density contour computed from the data. This method is completely analogous to that used for the Gaussian field except that the overall field shape is defined by the distribution of the data. Figure 3-10 illustrates the application of this method to the zone boundary shown on Figure 3-7 with a set of possible events that have occurred within the zone. Examples are shown for both the Epanechnikov and Gaussian kernels. The values of h resulting in the best fits are 5.3, and 2.0, respectively. The ratio of the two is 2.6, consistent with the relative values for h discussed by Silverman (1986).

The nonparametric spatial density function defined by Equations **(3-12)** or **(3-13)** is then used to compute the hazard using Equation **(3-4)**. Uncertainty in the density function is modeled by the uncertainty in the event data and by specifying weighted alternative values of h.

3.1.5 Nonhomogeneous Temporal Models

Nonhomogeneous temporal models provide a means of allowing for a time varying rate of volcanic events, $\lambda(t)$, within a zone or region of interest. To a first approximation, this is achieved by considering alternative time periods for the homogeneous Poisson model, assuming that the instantaneous rate changes very slowly (over millions of years). Nonhomogeneous temporal models provide an approach for estimating the instantaneous rate of volcanic events when it is assumed to vary over time scales on the order of the period of interest for hazard estimation. The nonhomogeneous temporal models considered by the experts were of the general form that defines a monotonic change in the rate with time. Two models were considered, the nonhomogeneous Poisson process with a Weibull rate function (Ho, 1991, 1992), and a volume predictable model.

Nonhomogeneous (Weibull) Poisson Process Ho (1991, 1992) proposed that the rate of volcanic activity in the Yucca Mountain region was not stationary in time and that the time varying rate could be modeled as a nonhomogeneous Poisson process with the time varying rate, $\lambda(t)$ represented by the Weibull function

$$\lambda(t) = \frac{\beta}{\theta}\left(\frac{t}{\theta}\right)^{\beta-1} \qquad \textbf{(3-14)}$$

where t is time measured from t_0 when the process starts, and β and θ are parameters. The homogeneous Poisson process is a special case of Equation **(3-14)** with β equal to 1. The instantaneous rate increases with time when β is greater than 1 and decreases with time for β less than 1. Ho (1991, 1992) presents maximum likelihood relationships for estimating the parameters β and θ (see Appendix F).

Uncertainty in the volcanic event rate is incorporated in the PVHA through uncertainty in the event counts and considering alternative start times, t_0. In addition, the confidence intervals in the Weibull rate parameter were estimated using the formulation developed by Crow (1982) (see Appendix F). In the same manner as discussed above for the homogeneous rate parameter, a three point discrete distribution was used to model the uncertainty in the instantaneous rate parameter. The maximum likelihood value was given a weight of 0.63 and the end points of the 90-percentile confidence interval (the 5th and 95th percentiles) were each given weights of 0.185.

Instantaneous Volume Predictable Rate Crowe et al. (1995) present estimates of the rate of volcanic events based on the model

$$\lambda(t) = \frac{\dot{V}_M(t)}{V_E(t)} \quad \textbf{(3-15)}$$

where $\dot{V}_M(t)$ is the instantaneous rate of magma production and $V_E(t)$ is the time varying volume per volcanic event. One of the volcanic experts adapted this general approach for estimating the instantaneous rate by specifying parametric formulations for $\dot{V}_M(t)$ and $V_E(t)$ and estimating the model parameters by regression analysis. The particular functional forms used are discussed below in the section describing the individual expert's model. Uncertainty in $\lambda(t)$ was modeled by developing three point representations of the uncertainty in both $\dot{V}_M(t)$ and $V_E(t)$ from the regression analyses and then using the resulting nine possible values assuming the two parameters are independent.

The above set of spatial and temporal models were used by the experts in various combinations by substituting the desired relationships for $\lambda(t)$ and $f(x,y)$ into Equation **(3-4)**. The specific models developed by each of the experts are presented in Section 3.2.

3.1.6 Conditional Probability of Intersection

The remaining piece of the hazard model is the computation of the probability that a volcanic event occurring at point (x,y) will produce an intersection of the repository. The conditional probability of intersection, $P_I(x,y)$, depends on the geometry assumed for an event. Most previous PVHA analyses have used a point representation for events [Figure 3-11, part (a)] and have accounted for the dimensions of the event through an increase in the effective area of the repository used in the hazard calculation (e.g., Crowe et al., 1982, 1992; Ho et al., 1991; Connor and Hill, 1995). Using this representation, $P_I(x,y)$ will be 1 within the effective footprint of the repository, and 0 everywhere else.

Sheridan (1992) developed an alternative approach to PVHA in which events are explicitly modeled as linear dike-like features centered on the point representation of the event [Figure 3-11, part (b)]. This approach provides a more physically realistic model of basaltic volcanic events and allows the distribution of possible event lengths and event orientations to be incorporated into the computation of the conditional likelihood that an event will intersect the repository. Thus, $P_I(x,y)$ will vary with both distance and azimuth from the repository.

For this study we have extended the linear dike model to consider the dike to be randomly placed on the point event [Figure 3-11, part (c)]. The parameters of an event thus are the event length, the event azimuth, and the relative location of the dike on the event. These parameters all are modeled as probability density functions defined by the experts. The event length probability distributions were supplied either in the form of a standard probability function (such as a lognormal distribution) or as a subjectively defined cumulative density function. The event azimuths were defined by the experts typically as normally distributed with a specified mean azimuth and a standard deviation. These distributions were then modeled as doubly truncated normal density functions with truncation points at ±90° from the mean azimuth. In some cases, bimodal density distributions were defined for event azimuth. The placement of the dike on the event was modeled by a symmetric density function.

The general procedure for computing $P_I(x,y)$ is illustrated on Figure 3-12. A dike extending length l from point (x,y) will intersect the repository over the azimuth range ϕ_1 to ϕ_2. The probability

that a dike extending length l toward the repository will intersect is equal to the probability that its azimuth will fall in range of ϕ_1 to ϕ_2. This is given by

$$P_I(x,y|l) = \int_{\phi_1|x,y,l}^{\phi_2|x,y,l} f(\phi)d\phi \qquad \textbf{(3-16)}$$

where $f(\phi)$ is the dike azimuth distribution function defined by the experts. As indicated in Equation **(3-16)**, this probability is conditional on the point (x,y) and on l through the range of possible azimuths for intersection. The process is repeated for all possible values of l, each being multiplied by the probability that the dike will extend a distance l beyond the event, yielding the relationship

$$P_I(x,y) = \int_0^{L_{max}} f(l) \cdot \int_{\phi_1|x,y,l}^{\phi_2|x,y,l} f(\phi)d\phi\, dl \qquad \textbf{(3-17)}$$

The density function $f(l)$ defines the probability that a dike will extend a distance l toward the repository. This probability is a function of how the event is represented. If the dikes are assumed to be centered on the events, then l represents a half-length of an event and $f(l)$ is obtained directly from the density function for total event length. For the randomly placed dikes, the density function $f(l)$ is obtained by convolving the event length and event placement distributions. Figure

3-13 shows examples of expert-specified density functions for dike length and dike location on an event. In this example, the expert developed a cumulative distribution for total dike length. This distribution was fit with a smooth interpolation curve to develop the density function.

Figure 3-14 shows examples of the computation of the conditional probability of intersection, $P_I(x,y)$, using the event length distributions shown on Figure 3-13. Results are shown for both unimodal and bimodal event azimuth distributions. The effect of considering randomly placed dikes is to extend the area of influence where the conditional probability of intersection is very low (<0.001). The area enclosed within the 0.001 probability contour is similar for both event representations.

The probability functions used in Equation **(3-17)** to compute the conditional probability of intersection model the placement of a random dike or dike set, given that an event occurs at point *(x,y)*. These probability functions are considered to represent the randomness inherent in the physical process of emplacement of basaltic dikes. In addition, there is scientific uncertainty in specifying the parameters of the process. This uncertainty is expressed by defining alternative probability functions for the length and orientation of the dikes associated with basaltic volcanic events and assigning relative weights to the alternatives.

3.2 EXPERT VOLCANIC HAZARD MODELS FOR YUCCA MOUNTAIN

The previous section describes the set of spatial and temporal models used to define the occurrence frequency of volcanic events in the Yucca Mountain region and the model used to compute the probability that a event occurring at point *(x,y)* will intersect the repository footprint. This section presents the ways in which the experts used these models to assess the volcanic hazard at the proposed Yucca Mountain repository site. First, the general logic tree framework for treatment of uncertainty in the PVHA is developed. Then the individual expert's PVHA models presented in Appendix E are translated into this common framework. Finally, the experts' assessments of key components of the PVHA model are compared.

3.2.1 Logic Tree Structure For PVHA Model

The PVHA models developed by each of the experts were transformed into a common logic tree structure for clarity of presentation and convenience in performing sensitivity analyses. Figures 3-15 and 3-16 show the general logic tree structure used to represent the scientific uncertainties in the PVHA computation. The logic tree is structured to move from the assessment of the general framework on the left (Figure 3-15) to specific assessments of individual volcanic zones and

volcanic centers on the right (Figure 3-16). The specific definition of a specific zone or estimation of the number of events that may have occurred at a volcanic center commonly are dependent upon more general assessments of the appropriate time period or region of interest. Thus, the dependent assessments are placed to the right, and the independent assessments are placed to the left. However, the specific order of the nodes in the tree is purely a matter of convenience in conforming to an expert's thought process. The sequence of the nodes can be easily inverted, as will be demonstrated below in translating some of the experts' hazard models into the general framework of Figure 3-15.

The first two nodes of the logic tree address specification of alternative distributions for the length and orientation of dikes associated with the events. These parameters are used to compute the conditional probability of intersection, $P_I(x,y)$. The assessments of these two distributions are placed first in the logic tree because it is assumed that whichever models are the "correct" models for the dike length and dike orientation distributions, they apply to all events that may occur in the region.

The next two nodes address the assessment of the appropriate temporal models. The first node considers the uncertainty in whether homogeneous or nonhomogeneous temporal models are appropriate. Then, given the appropriate model, the following node addresses the uncertainty in selecting the appropriate time period over which the model parameters are to be evaluated.

The next four nodes address the assessment of the appropriate spatial models. The first node addresses identification of the appropriate region of interest. This region functions as a background volcanic source zone. The second node of this set addresses the uncertainty in specifying the appropriate form of the spatial density of future events. The alternatives considered by the experts include spatially homogeneous over the entire region of interest, locally homogenous within specific zones, or parametric and nonparametric nonhomogeneous spatial models. Given the selection of the region of interest and the appropriate spatial model, the next two nodes addresses specification of the appropriate zonation of the region. Alternative zonations usually are considered only when using the locally homogeneous, or "zonation," approach to spatial modeling.

At this point, the logic tree is expanded into subtrees, one for each of the identified volcanic sources. The vertical bar without a dot denotes additive hazard from multiple sources, (e.g., a local source zone and a background source). To the right of this point of the logic tree the parameter distributions for each source is considered to be probabilistically independent from

those of the other sources, and the distribution in the total computed hazard is obtained by convolving the independent hazard distributions obtained for each source.

The logic tree structure for each volcanic source subtree is shown on Figure 3-16. The first node of the subtree addresses consideration of alternative age estimates of volcanic events in the source zone. Alternative age estimates may impact the rate estimates obtained using the Weibull process nonhomogeneous Poisson model.

The next two nodes address the parameters of the spatial models. The first deals with the treatment of the boundary of the source zone in the locally homogeneous spatial model. Alternatives considered by the experts were either an abrupt or a gradual change in the rate density of events across the boundary between zones of high and low activity. The second node addresses uncertainty in the specification of the basic parameters of the nonhomogeneous spatial models. If a parametric Gaussian field is to be fit to a specified zone boundary, then the uncertainty in specifying the density level represented by the boundary is addressed at this node. Similarly, the uncertainty in specifying the smoothing parameter of the nonparametric spatial models is addressed at this node.

The next two nodes address the basis for establishing the rate of activity in the source, given the appropriate temporal model. In most cases, this is just the event counts at the volcanic centers contained within the source for the specified time period. However, some source zones do not contain mapped events within the appropriate time period, and the experts used other means of specifying the rate of events, either comparisons to other zones or the use of other time periods. The second node is used for those cases where the rate of activity in a specific source zone is estimated from other source zones or time periods. The node addresses the uncertainty in specifying the appropriate multiplying factor to scale the rate from one zone to another.

The next seven nodes address the uncertainty in estimating the number of events that have occurred at each of the seven volcanic centers of primary interest to assessing the hazard at the repository: Lathrop Wells (LW), northwestern Crater Flat (NWCF), southeastern Crater Flat (SECF), the Amargosa Valley aeromagnetic anomalies (AV), Sleeping Butte (SM), Thirsty Mesa (TM), and Buckboard Mesa (BM). These assessments are represented individually in the logic tree so that the contribution of the uncertainty in the event counts at specific centers to the uncertainty in the total hazard can be readily identified. This approach also allows for explicit treatment of the impact of alternative event counts on application of the nonhomogeneous spatial models.

The next node of the logic tree addresses the statistical uncertainty in the parameters of the Gaussian field model [Equation **(3-9)**]. As discussed above in Section 3.1, a joint distribution for the five parameters of the Gaussian field model is computed from relative likelihood estimates using the observed events in the field. This node is placed at this point because the field parameters are conditional on the specific set of events that make up the field.

The next two nodes address uncertainty in the event counts at other volcanic centers and uncertainty in specifying the amount of additional events that may be undetected in the source region—so-called "hidden" events. The effect of hidden events is typically modeled as a range of possible multiples of the rate of activity computed from the observed events.

The final node addresses the statistical uncertainty in estimating the volcanic rate parameter for the given temporal model and data set. This includes the uncertainty in the homogenous or nonhomogeneous Poisson rates and the uncertainty in the volume predictable rate.

3.2.2 Individual Expert PVHA Models

This section presents a translation of the experts' assessments into the common logic tree framework of Figures 3-15 and 3-16. The models are listed in alphabetical order by first initial: Alexander McBirney, Bruce Crowe, George Thompson, George Walker, Mel Kuntz, Michael Sheridan, Richard Carlson, Richard Fisher, Wendell Duffield, and William Hackett. Appendix E contains summaries of the elicitation of each of the experts documenting the basis for the development of each PVHA model.

Alexander McBirney Figure 3-17 presents the logic tree that describes the basic framework for the PVHA model developed by Alexander McBirney (AM). Uncertainty in the size and orientation of dikes associated with the events is modeled by alternative maximum dike lengths of 15 and 20 km. Figure 3-18 shows the resulting distributions for $f(l)$ used to compute the conditional probability of intersection, $P_I(x,y)$.

A single temporal model, the homogeneous Poisson model, is used with two alternative time periods, post-1 Ma and post-5 Ma. A single region of interest is defined and two alternative spatial models are considered: the zonation (locally homogeneous) approach and the kernel smoothing approach. Following the zonation approach, a single zonation model is proposed. Figure 3-19 shows the zonation model proposed by AM. It consists of five zone types distinguished by differences in geology. The transition in the rate density across zone boundaries was assumed to be abrupt for all zones.

Table 3-1 summarizes the data used to define volcanic event rates for the individual source zones for both the zonation and kernel smoothing approaches. Zone types 4 and 5 do not contain any mapped volcanic events for the post-5 Ma time periods and the rate of volcanic events is based on other zones, as indicated. For the post-1 Ma time period, the rate of events in Zone types 3, 4, and 5 is assumed to be the same as that for the post-5 Ma time period. Table 3-2 summarizes the uncertainties in the event counts at each of the volcanic centers. The rate factors to account for hidden events were assessed to be 1.0 for the post-1 Ma time period and 1.1 for the post-5 Ma time period.

Following the kernel smoothing approach, three alternative values of the smoothing parameter h were selected. These values initially were chosen to span the range of 15 to 30 km used by Connor and Hill (1995) with the Epanechnikov kernel. However, AM chose to use a Gaussian kernel and the corresponding values of h were reduced by a factor of 2.5. Kernel density estimates were computed using three equally weighted values for h of 6, 9, and 12 km. The density estimates were computed for all possible combinations of the event counts in the northern AVIP zone for both time periods. Figure 3-20 shows an example of the kernel density estimate obtained using the most likely (highest probability) event counts for the post-5 Ma time period and a smoothing parameter of 9 km.

Bruce Crowe Figure 3-21 presents the logic tree that describes the basic framework for the PVHA model developed by Bruce Crowe (BC). Uncertainty in the size and orientation of dikes associated with the events is modeled by two alternative distributions for total event length. Figure 3-22 shows the resulting distributions for $f(l)$ used to compute the conditional probability of intersection, $P_I(x,y)$. A bimodal density function was specified for dike azimuth.

Two alternative temporal models are considered, the homogeneous Poisson model and the Weibull process nonhomogeneous Poisson model. Because the development of the PVHA model presented in BC's elicitation summary (Figure BC-1 of Appendix E) follows a different order than that of the general model shown on Figure 3-15, the remaining levels of the logic tree must be reordered from the assessments presented in the elicitation summary. This reordering was accomplished using Bayes' Theorem. Bayes' Theorem states that if one defines two types of events, A and B, each with several possible values (A_i and B_j), and provides probability assessments for the different values of

A, $P(A_i)$ and for different values of B conditional on the value of A, $P(B_j|A_i)$, then one can compute the conditional probability $P(A_i|B_j)$ by the expression

$$P(A_i|B_j) = \frac{P(B_j|A_i)\cdot P(A_i)}{\sum_k P(B_k|A_i)\cdot P(A_i)} \quad \textbf{(3-18)}$$

For example, in Figure BC-1 of Appendix E, the first assessment is the appropriate type of zonation model, one based on volcanic event distributions (ED) or one based on structural models (S). The probability assessments for the zonation type are $P(\text{ED})=0.4$, and $P(\text{S})=0.6$. The appropriate time period for computing event rates is assessed conditionally on the type of zonation model. Three time periods are considered: the Quaternary (Q) time period (post-1.15 Ma), the Plio-Quaternary (PQ) time period (post-5.05 Ma), and the Mio-Plio-Quaternary (MPQ) time period (post-9.15 Ma). If we place the assessment of time period before the assessment of zonation type in the logic tree, then we need to compute the probability of the zonation type conditionally on the time period. The following example illustrates computation of the probability of zonation type, either event-distribution (ED) based or structurally (S) based, conditional on time period Q being the appropriate time period.

Given zonation type ED, the probability assigned to time period Q is

$$P(\text{Q}|\text{ED}) = 0.8\cdot 0.5 = 0.4$$

and given zonation type A, the probability assigned to time period Q is the sum of the assessments for the various Quaternary zones.

$$P(\text{Q}|\text{S}) = 0.6\cdot 0.33+0.6\cdot 0.33+0.25\cdot 0.5+0.15\cdot 0.5 = 0.6$$

The probabilities assigned to the zonation models ED and S, given time period Q are obtained using Equation **(3-18)**.

$$P(\text{ED}|\text{Q}) = 0.4\cdot 0.4/(0.4\cdot 0.4+0.6\cdot 0.6) = 0.308$$
$$P(\text{S}|\text{Q}) = 0.6\cdot 0.6/(0.4\cdot 0.4+0.6\cdot 0.6) = 0.692$$

Proceeding in this manner, the logic tree shown on Figure BC-1 of Appendix A was transformed into that shown on Figure 3-21.

Three alternative regions of interest are considered for the PQ and MPQ time periods (Figure 3-23). The smallest of the tree, the post-caldera basalt zone (PCB) is not considered appropriate for computing background event rates for the Q time period because it does not contain any events.

Only the locally homogeneous, or zonation, spatial model is used in the assessment. Two alternative methods of defining zones are used, one based on event distributions and one based on structural considerations. The relative weights assigned to these two models display a shift in preference from the structural approach toward the event distribution approach as longer time periods are considered. Given the time period and the type of zonation model, various alternative source zones are defined. Figures 3-24 and 3-25 show the alternative zones for the Q and PQ time periods, respectively. Only the PCB zone (Figure 3-23) is used for the MPQ time period. The transition in the rate density across zone boundaries was assumed to be abrupt for all zones.

Table 3-3 summarizes the data to define the volcanic event rates for the individual source zones. Note that the full length of the Quaternary (2 My) is used to define the rate of events in the background zones for the Q time period models. Table 3-4 summarizes the uncertainties in the event counts at each of the volcanic centers. Bruce Crowe explicitly provided estimates of the number of hidden events at each volcanic center rather than general rate factors to multiply the rates computed from observed events. Three equally weighted alternative sets of event ages are defined in the elicitation summary for use in the nonhomogeneous Weibull process model. The resulting average values of parameter β computed over all alternative estimates of event counts and ages were 0.69 ±0.16 for the Q time period, 0.90 ±0.11 for the PQ time period, and 0.67 ±0.25 for the MPQ time period.

George Thompson Figure 3-26 presents the logic tree that describes the basic framework for the PVHA model developed by George Thompson (GT). Uncertainty in the size and orientation of dikes associated with the events is modeled by alternative maximum dike lengths of 10 and 12 km. Figure 3-27 shows the resulting distributions for $f(l)$ used to compute the conditional probability of intersection, $P_f(x,y)$.

A single temporal model, the homogeneous Poisson model, is used with two alternative time periods, post-1 Ma and post-4 Ma. Two alternative regions of interest are defined (see Figure 3-28). Only the zonation (locally homogeneous) approach is considered in the PVHA model. Two overlapping zones, a volcanic domain (VD) and a Quaternary faulting domain (QF) are specified. The controlling source zone in the region of overlap depends on the time period considered appropriate, as illustrated on Figure 3-29. Assuming that the post-1 Ma time period is appropriate,

the Quaternary faulting zone is the dominant source. If the 4 Ma time period is considered to be the appropriate time period, the volcanic domain is the dominant source. Two alternatives are considered for the transition in the rate density across the boundary of the volcanic and Quaternary faulting zones, one in which there is an abrupt transition (weight 0.67) and one in which there is a gradual transition over a distance of 5 km (weight 0.33).

Table 3-5 summarizes the data used to define volcanic event rates for the individual source zones. The Quaternary faulting zone does not contain any mapped volcanic events, and the rate of volcanic events is assessed to be one-tenth of the rate in the volcanic domain. Table 3-6 summarizes the uncertainties in the event counts at each of the volcanic centers. The rate factors to account for hidden events were assessed to be 1.0 (weight 0.5) or 2.0 (weight 0.5).

George Walker Figure 3-30 presents the logic tree that describes the basic framework for the PVHA model developed by George Walker (GW). Uncertainty in the size and orientation of dikes associated with the events is modeled by alternative maximum dike lengths of 15 and 20 km. Figure 3-31 shows the resulting distributions for $f(l)$ used to compute the conditional probability of intersection, $P_f(x,y)$. A bimodal distribution for dike azimuths is specified.

A single temporal model—the homogeneous Poisson model— is used with a single time period of post-5 Ma. A single region of interest is defined containing one source zone (Figure 3-32). Three alternative approaches to spatial modeling are considered, the zonation (locally homogeneous) approach, Epanechnikov kernel smoothing, and fitting a Gaussian field to the observed volcanic events. Both the kernel smoothing and the Gaussian field approaches are applied to the events in the Crater Flat Volcanic Zone (CFVZ) shown on Figure 3-32. The smoothing parameter h for the kernel density estimate is estimated by minimizing the difference between the 90 percent density contour and the CFVZ boundary. The transition in the rate density across the CFVZ boundary is assumed to be abrupt.

Table 3-7 summarizes the data used to define volcanic event rates for the CFVZ and background source zones. Table 3-8 summarizes the uncertainties in the event counts at each of the volcanic centers. Kernel density estimates and Gaussian volcanic fields were computed for all possible combinations of the event counts in the CFVZ. The mean value of the smoothing parameter computed over all possible combinations of event counts is 6.0 ±0.4 km. Figure 3-33 shows an example of the kernel density estimate obtained using the most likely event counts. Figure 3-34 shows an example of a Gaussian field fit to the most likely event counts in the CFVZ.

The rate factors to account for hidden events were assessed to be 1.0 (0.3), 2.0 (0.2), 3 (0.167), 4 (0.166), or 5 (0.167).

Mel Kuntz Figure 3-35 presents the logic tree that describes the basic framework for the PVHA model developed by Mel Kuntz (MK). Uncertainty in the size and orientation of dikes associated with the events is modeled by alternative maximum dike lengths of 10, 12, 15, and 18 km. Figure 3-36 shows the resulting distributions for $f(l)$ used to compute the conditional probability of intersection, $P_I(x,y)$. A bimodal distribution for dike azimuths is specified.

Two alternative temporal models are considered, the homogeneous Poisson model (weight 0.8) and the Weibull process nonhomogeneous Poisson model (weight 0.2). Alternative time periods of post-2 Ma, post-5 Ma and post-11 Ma are considered in the analysis. A single region of interest is considered (Region A on Figure 3-37). Four alternative approaches to spatial modeling are considered, a uniform model within the region of interest, the zonation (locally homogeneous) approach, Gaussian kernel smoothing, and fitting a Gaussian field to the observed volcanic events. Five source zones are defined for the zonation model (Zones B through F on Figure 3-37). The transition in the rate density across the boundary between Zone C (Crater Flat) and Zone E to the east is modeled as being either abrupt (weight 0.5) or gradual over a distance of 5 km (weight 0.5). Both the kernel smoothing and the Gaussian field approaches are applied to the events in Zone C of the zonation mode shown on Figure 3-37. The smoothing parameter for the kernel density, h, is estimated by minimizing the difference between 90 percent (weight 0.6) or 95 percent (weight 0.4) density contours and the Zone C boundary.

Table 3-9 summarizes the data used to define volcanic event rates for the various source zones. Several of the source zones do not contain events in certain time periods, and the event rates are specified as multiples of the rates for other zones. Table 3-10 summarizes the uncertainties in the event counts at each of the volcanic centers. The resulting average values of parameter β computed over all alternative estimates of event counts and ages were 2.36 ±0.51 for the post-2 Ma time period, 1.05 ±0.13 for the post-5 Ma time period, and 3.02 ±0.92 for the post-11 Ma time period. Kernel density estimates and Gaussian volcanic fields were computed for all possible combinations of the event counts in Zone C. The mean values of the smoothing parameter computed over all possible combinations of event counts and time periods are 3.1 ±0.3 km for the 90 percent density constraint and 2.9 ±0.5 km for the 95 percent density constraint. Figure 3-38 shows an example of the kernel density estimate obtained using the most likely event counts for the post-2 Ma time period and the 90 percent density constraint. Figure 3-39 shows an example of a Gaussian field fit to the same data.

The rate factors to account for hidden events were assessed to be 1.0 (0.25), 1.1 (0.5), 1.5 (0.2), or 2 (0.05).

Michael Sheridan Figure 3-40 presents the logic tree that describes the basic framework for the PVHA model developed by Michael Sheridan (MS). Uncertainty in the size and orientation of dikes associated with the events is modeled by nine alternative lognormal distributions for dike length. Figure 3-41 shows the resulting distributions for $f(l)$ used to compute the conditional probability of intersection, $P_I(x,y)$.

The homogeneous Poisson model is considered the appropriate temporal model and the post-5 Ma time period is considered the appropriate time period. Two regions of interest are considered, the region within 200 km of the proposed Yucca Mountain site and the region within 40 km of the site (Figure 3-42). Two alternative approaches to spatial modeling are considered, a uniform model within the 40-km region of interest and fitting a Gaussian field to the observed volcanic events in three specified fields, Crater Flat, Sleeping Butte/Thirsty Mesa, and Buckboard Mesa. In addition, there is a 0.25 probability that the event at Lathrop Wells is still continuing. This is modeled by placing a point source at Lathrop Wells with the specified event frequency of 1 event in 100,000 years, MS's specified duration of an event.

Table 3-11 summarizes the data used to define volcanic event rates. When using the Gaussian field approach, the rate of events outside of the three fields is specified as the frequency of new field occurrence. Table 3-12 summarizes the uncertainties in the event counts at each of the volcanic centers and the rate of new field occurrence in the regions of interest. Gaussian volcanic fields were computed for all possible combinations of the event counts in each of the field areas. Figure 3-43 shows an example of Gaussian fields fit to the most likely event counts at each of the three fields. Because of the limited spatial extent of events at the Sleeping Butte/Thirsty Mesa field, the aspect ratio was fixed at 3.0. The events at Buckboard Mesa are very closely spaced and a circular field with standard error of 1 km was used to define the field.

The rate factors to account for hidden events were assessed to be 1.33 (0.185), 1.67 (0.63), or 2 (0.185).

Richard Carlson Figure 3-44 presents the logic tree that describes the basic framework for the PVHA model developed by Richard Carlson (RC). Uncertainty in the size and orientation of dikes associated with the events is modeled by three alternative maximum dike lengths. Figure 3-45

shows the resulting distributions for $f(l)$ used to compute the conditional probability of intersection, $P_I(x,y)$.

Two alternative temporal models are included in the hazard model, a homogeneous Poisson model applicable for the post-1 Ma time period, and a volume predictable model applicable for the post-5 Ma time period. Two regions of interest are considered (Figure 3-46), the Amargosa Valley Isotopic Province (AVIP) for the post-1 Ma time period and the northern portion of AVIP for the post-5 Ma time period. Two alternative approaches to spatial modeling are considered, a uniform model within the region of interest and kernel smoothing using a fixed Epanechnikov kernel with an aspect ratio of 2:1 and an orientation of N20°W. Uncertainty in the smoothing parameter, h, was modeled by considering alternative values for the major axis value of h.

Table 3-13 summarizes the data used to define volcanic event rates. Table 3-14 summarizes the uncertainties in the event counts in the regions of interest. Kernel density functions were computed for all possible combinations of the event counts. Figure 3-47 shows an example for h equal to 10 km and the most likely event counts for the post-5 Ma time period.

Richard Carlson's PVHA model incorporates the volume predictable rate model defined by Equation **(3-15)**. The rate of magma generation in the northern AVIP zone was specified by fitting the following functional form to the cumulative volume data.

$$V_M(t) = C_1 + C_2 \cdot (C_3 - t)^{1/2} \qquad \textbf{(3-19)}$$

In Equation **(3-19)**, time is measured from the present and parameter C_3 acts as a starting time. This formulation was fit to the data by nonlinear least squares using the data given in RC's elicitation. The result is the relationship $V_M(t) = 2.288 + 1.400 \cdot (5.026 - t)^{1/2}$. Figure 3-48 shows the resulting fit. Differentiation of this relationship yields the rate of magma generation today, $V_M(t=0)$, of 0.312 km^3/Ma. Using the asymptotic errors obtained from the fit of the data, 5th and 95th percentiles of $V_M(t=0)$ were computed to be 0.105 km^3/Ma and 0.515 km^3/Ma, respectively. These three values were used with weights of 0.63 for the best estimate and 0.185 for the 5th and 95th percentiles to compute the volume predictable rates.

The volume per event, $V_E(t)$, was obtained by fitting a relationship of the form

$$V_E(t) = C_4 \cdot (C_3 - t)^{C_5} \qquad \textbf{(3-20)}$$

where C_3 was fixed at the value of 5.026 obtained from the fit to the cumulative volume data. The cumulative volume data for the region consists of volumes estimated for each center, e.g. 0.92 km^3 for the basalts of Buckboard Mesa. Thus, the volume per event data depends on how many events have occurred at each center. For the hazard analysis, the volume per event was computed for every possible combination of event counts in the northern AVIP region by a least squares fit of the log of Equation **(3-20)** to the volume per event data resulting from dividing the volume at each center by the number of events estimated to have occurred at the center. Figure 3-48 shows an example of the fit to the most likely counts in the region. In this example $V_E(t=0)$ is 0.096 km^3 with a 90-percent confidence interval of 0.030 to 0.306 km^3. Uncertainty in the volume predictable rate for each possible event count was modeled be considering the three possible values for $V_M(t=0)$ listed above and a similar three point distribution for $V_E(t=0)$ estimated from the regression fit to the specific event counts. The weighted average over all possible event counts of the volume per event was 0.080 km^3.

The rate factors to account for hidden events were assessed to be 1.1 for both the post-1 Ma and post-5 Ma time periods.

Richard Fisher Figure 3-49 presents the logic tree that describes the basic framework for the PVHA model developed by Richard Fisher (RF). Uncertainty in the size and orientation of dikes associated with the events is modeled by alternative maximum dike lengths of 20 and 25 km. Figure 3-50 shows the resulting distributions for $f(l)$ used to compute the conditional probability of intersection, $P_I(x,y)$. A bimodal distribution for dike azimuths is specified.

The homogeneous Poisson model is used to compute the event rates for alternative time periods of post-1 Ma and post-2 Ma. Two alternative regions of interest were considered (Figure 3-51). Three alternative approaches to spatial modeling are considered, the zonation (locally homogeneous) approach using the zones shown on Figure 3-52, Epanechnikov kernel smoothing, and fitting Gaussian field shapes to the Crater Flat and Sleeping Butte zones shown on Figure 3-52. The transition in the rate density across the boundary between zones was assumed to be abrupt. The smoothing parameter for the kernel density h and the Gaussian field shape parameters were estimated by minimizing the difference between 90 percent (0.8), 95 percent (0.1), or 98 percent (0.1) density contours and the Crater Flat boundary.

Table 3-15 summarizes the data used to define volcanic event rates for the various source zones. Table 3-16 summarizes the uncertainties in the event counts at each of the volcanic centers. Kernel density estimates and Gaussian volcanic fields were computed for all possible

combinations of the event counts in the Crater Flat zone. The mean values of the smoothing parameter computed over all possible combinations of event counts and time periods are 9.9 ±0.6 km for the 90 percent density constraint, 9.2 ±0.7 km for the 95 percent density constraint, and 8.7 ±0.6 km for the 98 percent density constraint. Figure 3-53 shows an example of the kernel density estimate obtained using the most likely event counts for the post-2 Ma time period and the 90 percent density constraint. Figure 3-54 shows an example of a Gaussian field fit to the Crater Flat zone boundary.

The rate factors to account for hidden events were assessed to be 1.15 (0.25), 1.32 (0.25), 1.5 (0.25), or 2 (0.25).

Wendell Duffield Figure 3-55 presents the logic tree that describes the basic framework for the PVHA model developed by Wendell Duffield (WD). Uncertainty in the size and orientation of dikes associated with the events is modeled by alternative maximum dike lengths of 20, 30, and 40 km. Figure 3-56 shows the resulting distributions for $f(l)$ used to compute the conditional probability of intersection, $P_I(x,y)$.

A single temporal model, the homogeneous Poisson model, is used with a single time period of post-1 Ma. The region of interest is defined as the region within 40 km of the repository (Figure 3-57). Only the zonation (locally homogeneous) approach is considered in the PVHA model. Figure 3-57 shows the defined source zones. Two alternatives are considered, one with separate zones B and C_n, and one in which these two zones are combined. The transition in the rate density across the boundary of the zones is considered to be abrupt.

Table 3-17 summarizes the data used to define volcanic event rates for the individual source zones. The rate for those zones that do not contain any mapped volcanic events is based on estimates of the number of undetected events or a multiple of the rate in other zones. Table 3-18 summarizes the uncertainties in the event counts at each of the volcanic centers. The number of hidden events in the region for the time frame of interest (1 Ma) were assessed to be either 0 (weight 0.99) or 1 (weight 0.01).

William Hackett Figure 3-58 presents the logic tree that describes the basic framework for the PVHA model developed by William Hackett (WH). Uncertainty in the size and orientation of dikes associated with the events is modeled by alternative maximum dike lengths of 20, 30, and 40 km. Figure 3-59 shows the resulting distributions for $f(l)$ used to compute the conditional probability of intersection, $P_I(x,y)$. A bimodal distribution for dike azimuths is specified.

The homogeneous Poisson model is used to compute the event rates for alternative time periods of post-1 Ma, post-5 Ma and post-11 Ma. A single region of interest is defined (Figure 3-60). Two alternative approaches to spatial modeling are considered, the zonation (locally homogeneous) approach and Gaussian kernel smoothing. The zonation models are dependent on the time period considered appropriate (Figure 3-60). The transition in the rate density across the boundary between zones was assumed to be abrupt. The smoothing parameter for the kernel density, h, was specified as alternative values of 3.2 km (0.5), 6.4 km (0.4), and 9.6 km (0.1).

Table 3-19 summarizes the data used to define volcanic event rates for the various source zones. Table 3-20 summarizes the uncertainties in the event counts at each of the volcanic centers. The potential for hidden events are accounted for in defining the distribution of event counts at each center. Kernel density estimates were computed for all possible combinations of the event counts in the appropriate time period. Figure 3-61 shows an example of the kernel density estimate obtained using the most likely event counts for the post-1 Ma time period.

3.2.3 Summary of Assessments

Figures 3-62 and 3-63 present summaries of the experts' assessments of various components of the PVHA model. The summaries are in the form of histograms with the histogram bins defining alternative models or parameter values. The probability assigned to each bin is the equally weighted average of the probabilities specified by the experts. For example, the top plot on Figure 3-62 shows the aggregate relative preference for the four types of spatial models. In aggregate, the experts preferred the use of locally homogeneous zonation models to represent the spatial distribution of future volcanic events. The least favored model is the uniform model that assumes the spatial density is homogeneous throughout the region. The homogeneous temporal model is strongly favored with the preferred time periods of post-1 Ma or post-5 Ma. The experts also indicate that the number of hidden events in the region is likely to be less than the number of observed events. There is a wide distribution for the maximum length of a dike or dike set associated with an individual event. This wide distribution reflects the large uncertainties for maximum dike length specified individually by the experts. Figure 3-63 shows the aggregate distributions for the event counts at the seven primary volcanic centers. The aggregate distributions are generally similar to those developed individually by the experts.

TABLE 3-1
DATA USED TO DEFINE VOLCANIC EVENT RATES FOR SOURCE ZONES
ALEXANDER R. MCBIRNEY SOURCE MODEL

TIME PERIOD	COUNT METHOD FOR ZONES	NOTES
Post 1 Ma (0.1)	Zone 1: (NCF+SB) Zone 2: (LW) Zone 3: Use Post-5 Ma rate Zone 4: Use Post-5 Ma rate Zone 5: Use Post-5 Ma rate	NCF: Northern (1.0 Ma) Crater Flat SB: Sleeping Butte LW: Lathrop Wells 3.7: 3.7 Ma Crater Flat TM: Thirsty Mesa AV: Amargosa Valley BM: Buckboard Mesa
Post 5 Ma (0.9)	Zone 1: (NCF+SB+3.7+TM) Zone 2: (LW+AV) Zone 3: (BM) Zone 4: (BM) Zone 5: 0.5 x rate of Zone 3	

TABLE 3-2
ESTIMATED UNCERTAINTIES IN EVENT COUNTS
ALEXANDER R. McBIRNEY SOURCE MODEL

LOCATION	COUNTS (CONES)	WEIGHT	NOTES
Lathrop Wells	1 I - IV 2 I, II 3 I, II, III 4 I, II, III, IV	(0.3) (0.2) (0.4) (0.1)	BC: Black Cone HC: Hidden Cone 2HC: 2 events at Hidden Cone LBP: Little Black Peak LC: Little Cones 2LC: 2 events at Little Cones M: Makani Cone I - IV: Chronostratigraphic units of Crowe et al. (1995) RC: Red Cone
Sleeping Butte	1 (HC+LBP) 2 (HC, LBP) 3 (2HC, LBP)	(0.05) (0.8) (0.15)	
1.0 Ma Crater Flat	1 (all) 2 (LC+RC+BC, M) 3 (LC, RC+BC, M) 4 (LC, RC, BC, M) 5 (2LC, RC, BC, M)	(0.9) (0.05) (0.025) (0.015) (0.01)	
Buckboard Mesa	0 1 2	(0.8) (0.1) (0.1)	
3.7 Ma Crater Flat	1 2 3 4 5 6	(0.75) (0.05) (0.05) (0.05) (0.05) (0.05)	
Amargosa Valley	2 3 4 5 6 7 8	(0.02) (0.03) (0.05) (0.2) (0.5) (0.15) (0.05)	
Thirsty Mesa	1 2	(0.9) (0.1)	

TABLE 3-3
DATA USED TO DEFINE VOLCANIC EVENT RATES FOR SOURCE ZONES
BRUCE M. CROWE SOURCE MODEL

TIME PERIOD	COUNT METHOD FOR ZONES	NOTES
Quaternary (post-1.15 Ma)	CF: (LW+NCF+SB) PA: (LW+NCF) WL: (LW+NCF+SB) NE: (LW+NCF) SGB: (DV2+U+CV) AVIP: (DV2)	AV: Amargosa Valley AVIP: Amargosa Valley Isotopic Province of Yogodzinski (1995) BM: Buckboard Mesa CF: Crater Flat CV: Clayton Valley DV2: Death Valley (2 Ma) DV5: Death Valley (3-5 Ma) GV: Grapevine Canyon LW: Lathrop Wells NC: Nye Canyon NCF: Northern (1.0 Ma) Crater Flat NE: North East PCB: Post Caldera Basalts PA: Pull apart and Pull apart with fault PM: Pahute Mesa PR: Paiute Ridge RW: Rocket Wash SB: Sleeping Butte SC: Scarp Canyon SGB: Southern Great Basin TM: Thirsty Mesa TP: Towne Pass U: Ubehebe WL: Walker Lane YF: Yucca Flat YPCB: Younger Post-Caldera Basalts 3.7: 3.7 Ma Crater Flat
Plio-Quaternary (post-5.05 Ma)	CF: (LW+NCF+3.7+AV+SB+TM) YPCB: (LW+NCF+3.7+AV+SB+TM +BM) PA: (LW+NCF+3.7+AV) WL: (LW+NCF+3.7+AV+SB+TM) NE: (LW+NCF+3.7+AV+BM) SGB: (DV2+DV5+U+CV+TP+GV) AVIP: (DV2+DV5)	
Mio-Plio-Quaternary (post-9.05 Ma)	PCB: (LW+NCF+3.7+AV+SB+TM +BM+PM+PR+SC+RW+YF +NC)	

TABLE 3-4
ESTIMATED UNCERTAINTIES IN EVENT COUNTS
BRUCE M. CROWE SOURCE MODEL

LOCATION	COUNTS (CONES)	WEIGHT	NOTES
Lathrop Wells	1	(0.9)	A-G: Aeromagnetic anomalies of V. Langenheim, USGS BC: Black Cone HC: Hidden Cone 2HC: 2 events at Hidden Cone LBP: Little Black Peak LC: Little Cones 2LC: 2 events at Little Cone M: Makani Cone RC: Red Cone SC: Split Cone SB: Shoreline Butte 2SB: 2 events at Shoreline Butte 3SB: 3 events at Shoreline Butte u: undetected
	2	(0.06)	
	3	(0.03)	
	4	(0.01)	
Sleeping Butte	1 (LBP+HC)	(0.35)	
	2 (LBP, HC)	(0.45)	
	3 (LBP, 2HC)	(0.2)	
1.0 Ma Crater Flat	1 (all)	(0.1)	
	2 (RC+LC,BC+M)	(0.1)	
	3 (LC, RC+BC, M)	(0.45)	
	4 (LC,RC,BC,M)	(0.2)	
	5 (2LC, RC, BC, M)	(0.1)	
	6 (A, RC, BC, M, 2LC)	(0.025)	
	7 (u)	(0.025)	
Buckboard Mesa	1	(0.7)	
	2	(0.25)	
	3 (u)	(0.05)	
3.7 Ma Crater Flat	1	(0.1)	
	2	(0.25)	
	3	(0.25)	
	4	(0.1)	
	5	(0.1)	
	6	(0.1)	
	7 (u)	(0.05)	
	8 (2u)	(0.05)	
Amargosa Valley	3	(0.05)	
	4	(0.12)	
	5	(0.2)	
	6	(0.2)	
	7 (u)	(0.2)	
	8 (u)	(0.1)	
	9 (2u)	(0.07)	
	10 (3u)	(0.03)	
	11 (4u)	(0.02)	
	12 (5u)	(0.01)	
Thirsty Mesa	1	(0.85)	
	2	(0.09)	
	3	(0.06)	

TABLE 3-4 (Continued)
ESTIMATED UNCERTAINTIES IN EVENT COUNTS
BRUCE M. CROWE SOURCE MODEL

LOCATION	COUNTS (CONES)	WEIGHT	NOTES
Death Valley (2 Ma)	2 (SC, SB) 3 (2SB, SC) 4 (3SB, SC) 5 (3SB, SC+u) 6 (3SB, SC +2u)	(0.3) (0.3) (0.25) (0.1) (0.05)	
Death Valley (3-5 Ma)	22 Density Estimates 44 " " 89 " "	(0.185) (0.63) (0.185)	
Clayton Valley	1 2 (u) 3 (2u)	(0.85) (0.1) (0.05)	
Ubehebe	1 2 3 4 5 (u) 6 (2u)	(0.6) (0.15) (0.1)	
Towne Pass	11 Density Estimates 22 " " 44 " "	(0.185) (0.63) (0.185)	
Grapevine Canyon	6 Density Estimates 12 " " 24 " "	(0.185) (0.63) (0.185)	
Nye Canyon	1 2 3 4 5 6 (u) 7 (2u) 8 (3u) 9 (4u)	(0.02) (0.2) (0.2) (0.16) (0.16) (0.12) (0.08) (0.04) (0.02)	

TABLE 3-4 (Continued)
ESTIMATED UNCERTAINTIES IN EVENT COUNTS
BRUCE M. CROWE SOURCE MODEL

LOCATION	COUNTS (CONES)	WEIGHT	NOTES
Paiute Ridge	1	(0.35)	
	2	(0.35)	
	3	(0.15)	
	4	(0.1)	
	5 (u)	(0.05)	
Yucca Flat	1	(0.4)	
	2	(0.4)	
	3 (u)	(0.2)	
Pahute Mesa	3	(0.5)	
	4	(0.2)	
	5	(0.15)	
	6 (u)	(0.1)	
	7 (u)	(0.05)	

TABLE 3-5
DATA USED TO DEFINE VOLCANIC EVENT RATES FOR SOURCE ZONES
GEORGE A. THOMPSON SOURCE MODEL

TIME PERIOD	COUNT METHOD FOR ZONES	NOTES
Post 1 Ma (0.3)	VD: (LW+NCF) QFD: 1/10 VD B200 km: (200 k) BAVIP: (SB+DV1)	AV: Amargosa Valley BAVIP: Background, Amargosa Valley Isotopic Province B200 km: Background, 200 km Radius BM: Buckboard Mesa DV1: Death Valley (1 Ma) DV4: Death Valley (4 Ma) LW: Lathrop Wells NAVIP: Northern Amargosa Valley Isotopic Province of Yogodzinski (1995) NCF: Northern (1.0 Ma) Crater Flat QFD: Quaternary Faulting Domain SB: Sleeping Butte VD: Volcanic Domain 3.7: 3.7 Ma Crater Flat 200 km: 200 km Radius Field Counts
Post 4 Ma (0.7)	VD: (LW+NCF+3.7+AV) QFD: 1/10 VD B200 km: (200 k) NAVIP: (SB+BM+DV4)	

TABLE 3-6
ESTIMATED UNCERTAINTIES IN EVENT COUNTS
GEORGE A. THOMPSON SOURCE MODEL

LOCATION	COUNTS (CONES)	WEIGHT	NOTES
Lathrop Wells	1 2 3 4	(0.75) (0.09) (0.08) (0.08)	BC: Black Cone LC: Little Cones 2LC: 2 events at Little Cones M: Makani Cone RC: Red Cone SB: Shoreline Butte 2SB: 2 events at Shoreline Butte 3SB: 3 events at Shoreline Butte SC: Split Cone
Sleeping Butte	1 2	(0.35) (0.65)	
1.0 Ma Crater Flat	1 (all) 2 (LC+RC+BC, M) 3 (LC, RC+BC, M) 4 (LC, RC, BC, M) 5 (2LC, RC, BC, M)	(0.2) (0.15) (0.1) (0.5) (0.05)	
Buckboard Mesa	1 2	(0.7) (0.3)	
3.7 Ma Crater Flat	1 2 3 4 5 6	(0.4) (0.5) (0.04) (0.03) (0.02) (0.01)	
Amargosa Valley	5 7	(0.9) (0.1)	
Background 200 km radius	16 in 5 Ma	(1.0)	
Background AVIP (1 Ma)	1 in 1 Ma (SC)	(1.0)	
Background AVIP (4 Ma)	2 (SC+SB) 3 (SC+2SB) 4 (SC+3SB)	(0.35) (0.35) (0.3)	

TABLE 3-7
DATA USED TO DEFINE VOLCANIC EVENT RATES FOR SOURCE ZONES
GEORGE P.L. WALKER SOURCE MODEL

TIME PERIOD	COUNT METHOD FOR ZONES	NOTES
Post 4.6 Ma (1.0)	- CFVZ zone: NCF, 3.7, LW, TM, SB, AV - Background Node: BM	NCF: Northern (1.0 Ma) Crater Flat 3.7: 3.7 Ma Crater Flat LW: Lathrop Wells TM: Thirsty Mesa SB: Sleeping Butte AV: Amargosa Valley BM: Buckboard Mesa

TABLE 3-8
ESTIMATED UNCERTAINTIES IN EVENT COUNTS
GEORGE P.L. WALKER SOURCE MODEL

LOCATION	COUNTS (CONES)	WEIGHT	NOTES
Lathrop Wells	1 2 3 4	(0.9) (0.07) (0.02) (0.01)	BC: Black Cone LC: Little Cones M: Makani Cone RC: Red Cone
Sleeping Butte	1 2	(0.4) (0.6)	
1.0 Ma Crater Flat	1 (all) 3 (LC, RC+BC, M) 4 (LC, RC, BC, M)	(0.1) (0.35) (0.55)	
Buckboard Mesa	1 2	(0.75) (0.25)	
3.7 Ma Crater Flat	2 3 4 5	(0.5) (0.25) (0.2) (0.05)	
Amargosa Valley	2 3 5 6	(0.3) (0.4) (0.15) (0.15)	
Thirsty Mesa	1 2 3	(0.85) (0.09) (0.06)	

TABLE 3-9
DATA USED TO DEFINE VOLCANIC EVENT RATES FOR SOURCE ZONES
MEL A. KUNTZ SOURCE MODEL

TIME PERIOD	COUNT METHOD FOR ZONES	NOTES
Post 2 Ma (0.5)	A: (NCF+LW+SB)	AV: Amargosa Valley BM: Buckboard Mesa LW: Lathrop Wells NCF: Northern (1.0 Ma) Crater Flat RW: Rocket Wash SB: Sleeping Butte SC: Solitario Canyon TM: Thirsty Mesa 3.7: 3.7 Ma Crater Flat
	B: (SB)	
	C: (NCF+LW)	
	D: 1.0 of E (0.1) 0.5 of E (0.5) 0.1 of E (0.4)	
	E: 1.0 of F (0.01) 0.5 of F (0.25) 0.1 of F (0.55) 0.01 of F (0.19)	
	F: 1/3 of B (0.7) 1/6 of C (0.3)	
Post 5 Ma (0.45)	A: (NCF+3.7+LW+TM+SB+AV+BM)	
	B: (TM+SB)	
	C: (NCF+3.7+LW+AV)	
	D: 1.0 of E (0.1) 0.1 of E (0.5) 0.1 of E (0.2)	
	E: 0.5 of F (0.25) 0.1 of F (0.55) 0.01 of F (0.19)	
	F: (BM)	
Post 11 Ma (0.05)	A: (NCF+3.7+LW+TM+SB+AV+BM+RW +SC)	
	B: (TM+SB+RW)	
	C: (NCF+3.7+LW+AV)	
	D: 1.0 of E (0.1) 0.1 of E (0.5) 0.1 of E (0.2)	
	E: (SC)	
	F: (BM)	

TABLE 3-10
ESTIMATED UNCERTAINTIES IN EVENT COUNTS
MEL A. KUNTZ SOURCE MODEL

LOCATION	COUNTS (CONES)	WEIGHT	NOTES
Lathrop Wells	1 I - IV 2 I+II 3 I, II, III 4 I, II, III, IV	(0.95) (0.03) (0.019) (0.001)	BC: Black Cone B-G: Aeromagnetic anomalies of V. Langenheim, USGS HC: Hidden Cone 2HC: 2 events at Hidden Cone LBP: Little Black Peak LC: Little Cones M: Makani Cone I - IV: Chronostratigraphic units of Crowe et al. (1995) RC: Red Cone
Sleeping Butte	1 (LBP+HC) 2 (LBP, HC) 3 (LBP, 2HC)	(0. 6) (0.3) (0.1)	
1.0 Ma Crater Flat	1 (all) 2 (LC+RC+BC, M) 3 (RC+BC, LC, M) 4 (RC, BC, LC, M)	(0.6) (0.3) (0.05) (0.05)	
Buckboard Mesa	1 2	(0.95) (0.05)	
3.7 Ma Crater Flat	1 2 3 4 5 6	(0.75) (0.05) (0.15) (0.02) (0.02) (0.01)	
Amargosa Valley	1 (B) 2 (B, D) 3 (B, C, D) 4 (B, C, D, E) or (B, C, D, F+G) 5 (B, C, D, F, G) or (B, C, D, E, F) or (B, C, D, E, G) 6 (B, C, D, E, F, G)	(0.02) (0.1) (0.6) (0.075) (0.075) (0.033) (0.034) (0.033) (0.03)	
Thirsty Mesa	1 2 3	(0.95) (0.04) (0.01)	
Rocket Wash	1	(1.0)	
Solitario Canyon	1	(1.0)	

TABLE 3-11
DATA USED TO DEFINE VOLCANIC EVENT RATES FOR SOURCE ZONES
MICHAEL F. SHERIDAN SOURCE MODEL

TIME PERIOD	COUNT METHOD FOR FIELDS	NOTES
5 MA (1.0)	CFF: (LW+3.7+NCF, AV) SBTMF: (SB+TM) BMF: (BM) 200 km: 10 Ma (0.75) 5 Ma (0.25) 40 km: 10 km (0.75) 5 Ma (0.25)	CFF: Crater Flat Field SBTMF: Sleeping Butte/Thirsty Mesa Field BMF: Buckboard Mesa Field NCF: Northern (1.0 Ma) Crater Flat 3.7: 3.7 Ma Crater Flat LW: Lathrop Wells TM: Thirsty Mesa SB: Sleeping Butte AV: Amargosa Valley BM: Buckboard Mesa 200 km: 200 km Radius 40 km: 40 km Radius

TABLE 3-12
ESTIMATED UNCERTAINTIES IN EVENT COUNTS
MICHAEL F. SHERIDAN SOURCE MODEL

FIELD COUNTS

REGION	TIME PERIOD	COUNTS	WEIGHT
Within 200 km	Post 10 Ma	30	(1.0)
	Post 5 Ma	16	(1.0)
Within 40 km	Post 10 Ma	5	(1.0)
	Post 5 Ma	2	(1.0)

EVENT COUNTS

LOCATION	COUNTS (CONES)	WEIGHT	NOTES
Lathrop Wells	1	(0.9)	
	2	(0.1)	
Sleeping Butte	1	(0.67)	
	2	(0.33)	
1.0 Ma Crater Flat	1	(0.7)	
	2	(0.2)	
	3	(0.1)	
Buckboard Mesa	1	(0.75)	
	2	(0.05)	
	3	(0.05)	
	4	(0.05)	
	5	(0.05)	
	6	(0.05)	
3.7 Ma Crater Flat	1	(0.1)	
	2	(0.6)	
	3	(0.2)	
	4	(0.1)	
Amargosa Valley	5	(0.25)	
	6	(0.5)	
	7	(0.25)	
Thirsty Mesa	1	(0.9)	
	2	(0.033)	
	3	(0.034)	
	4	(0.033)	

TABLE 3-13
DATA USED TO DEFINE VOLCANIC EVENT RATES FOR SOURCE ZONES
RICHARD W. CARLSON SOURCE MODEL

TIME PERIOD	COUNT METHOD FOR ZONES	NOTES
1.0 Ma (0.3)	AVIP: (LW+SB+NCF+DV)	AVIP: Amargosa Valley Isotopic Province of Yogodzinski (1995) AV: Amargosa Valley BM: Buckboard Mesa DV: Death Valley LW: Lathrop Wells NCF: Northern (1.0 Ma) Crater Flat NAVIP: Northern Amargosa Valley Isotopic Province TM: Thirsty Mesa SB: Sleeping Butte 3.7: 3.7 Ma Crater Flat
5.0 Ma (0.7)	NAVIP: (LW+SB+NCF+3.7+AV+TM+BM)	

TABLE 3-14
ESTIMATED UNCERTAINTIES IN EVENT COUNTS
RICHARD W. CARLSON SOURCE MODEL

LOCATION	COUNTS (CONES)	WEIGHT	NOTES
Lathrop Wells	1 2	(0.95) (0.05)	BC: Black Cone B-G: Aeromagnetic anomalies of V. Langenheim, USGS HC: Hidden Cone 2HC: 2 events at Hidden Cone LBP: Little Black Peak LC: Little Cones 2LC: 2 events at Little Cones M: Makani Cone RC: Red Cone SC: Split Cone
Sleeping Butte	1 (LBP+HC) 2 (LBP, HC) 3 (LBP, 2HC)	(0.7) (0.2) (0.1)	
1.0 Ma Crater Flat	1 (all) 3 (LC, RC+BC, M) 5 (2LC, RC, BC, M)	(0.6) (0.3) (0.1)	
Buckboard Mesa	1 2	(0.9) (0.1)	
3.7 Ma Crater Flat	1 2 3 4 5 6	(0.8) (0.1) (0.05) (0.02) (0.02) (0.01)	
Amargosa Valley	3 (B,C,D) 4 (B,C,D,E) 5 (B,C,D,E,F) 6 (B,C,D,E,F,G)	(0.3) (0.5) (0.1) (0.1)	
Thirsty Mesa	1 2	(0.9) (0.1)	
Death Valley (1 Ma)	1 (SC)	(1.0)	

TABLE 3-15
DATA USED TO DEFINE VOLCANIC EVENT RATES FOR SOURCE ZONES
RICHARD V. FISHER SOURCE MODEL

TIME PERIOD	COUNT METHOD FOR ZONES	NOTES
Post 1 Ma (0.8)	CFF: (NCF+ LW) SBF: (SB) BK100: (DV1, UH) BKEZ: (DV1, UH, LC, C)	CFF: Crater Flat Field BK100: 100 km radius Background Zone BKEZ: Eastern Background Zone NCF: Northern Crater Flat LW: Lathrop Wells SB: Sleeping Butte SBF: Sleeping Butte Field DV1: Death Valley (1 Ma) DV2: Death Valley (2 Ma) UH: Ubehebe LC: Lunar Crater C: Cima
Post 2 Ma (0.2)	CFF: (NCF+ LW) SBF: (SB) BK100: (DV2, UH) BKEZ: (DV2, UH, LC, C)	

TABLE 3-16
ESTIMAZTED UNCERTAINTIES IN EVENT COUNTS
RICHARD V. FISHER SOURCE MODEL -

LOCATION	COUNTS (CONES)	WEIGHT	NOTES
Lathrop Wells	1 I-IV 2 I, II+III 3 I, II, III 4 I, II, III, IV	(0.6) (0.3) (0.05) (0.05)	BC: Black Cone HC: Hidden Cone 2HC: 2 events at Hidden Cone LBP: Little Black Peak LC: Little Cone M: Makani Cone RC: Red Cone SB: Shoreline Butte SC: Split Cone I-IV: Chronostratigraphic units of Crowe et al. (1995)
Sleeping Butte	1 (LBP+HC) 2 (LBP, HC) 3 (LBP, 2HC)	(0.7) (0.25) (0.05)	
1.0 Ma Crater Flat	1 (all) 2 (LC+RC, BC+M) 3 (LC, RC+BC, M) 4 (LC, RC, BC, M)	(0.8) (0.05) (0.05) (0.1)	
N. Death Valley (1 MA)	1 (SC)	(1.0)	
N. Death Valley (2 Ma)	2 (SC, SB)	(1.0)	
Lunar Crater	1 2 3 28	(0.05) (0.30) (0.60) (0.05)	
Cima	1 7 22 29	(0.1) (0.05) (0.35) (0.14)	

TABLE 3-17
DATA USED TO DEFINE VOLCANIC EVENT RATES FOR SOURCE ZONES
WENDELL A. DUFFIELD SOURCE MODEL

TIME PERIOD	COUNT METHOD FOR SUBZONES	NOTES	NOTES
Post 1 Ma (1.0)	Subzone A: (NCF+LW) Subzone B: (AV) Subzone Cn: 1 event/1 Ma (0.01) 0 events/1 Ma (0.99) Subzone Cwl: 10 x Cn rate Subzone D: (SB)		AV: Amargosa Valley LW: Lathrop Wells NCF: Northern (1.0 Ma) Crater Flat SB: Sleeping Butte

TABLE 3-18
ESTIMATED UNCERTAINTIES IN EVENT COUNTS
WENDELL A. DUFFIELD SOURCE MODEL

LOCATION	COUNTS (CONES)	WEIGHT	NOTES
Lathrop Wells	1 I-IV 2 I, II-IV	(0.90) (0.10)	BC: Black Cone C-G: Aeromagnetic anomalies of V. Langenheim, USGS HC: Hidden Cone LBP: Little Black Peak LC: Little Cones 2LC: 2 separate Little Cones M: Makani Cone RC: Red Cone I-IV: Chronostratigraphic units of Crowe et al. (1995)
Sleeping Butte	1 (LBP+HC) 2 (LBP, HC)	(0.05) (0.95)	
1.0 Ma Crater Flat	1 (all) 2 (LC, RC+BC, M) 3 (LC, RC+BC, M) 4 (LC, RC, BC, M) 5 (2LC, RC, BC, M)	(0.07) (0.14) (0.26) (0.34) (0.19)	
Armagosa Valley	0 1 (D) 2 (C,D) 3 (C,D,E) 4 (C,D,E,F) 5 (C,D,E,F,G)	(0.95) (0.03) (0.01) (0.005) (0.003) (0.002)	

TABLE 3-19
DATA USED TO DEFINE VOLCANIC EVENT RATES FOR SOURCE ZONES
WILLIAM R. HACKETT SOURCE MODEL

TIME PERIOD	COUNT METHOD FOR ZONES	NOTES
Post 1 Ma (0.6)	- 1 Ma Zone: (NCF+ LW+SB) - Background (10 Ma Zone): Post-10 Ma rate (0.33) (3.7+TM+BM+RW+PR+PM+NC+YF+SC) 10 - 1 Ma rate (0.33) (3.7+TM+BM+RW+PR+PM+NC+YF+SC) 10 - 5 Ma rate (0.33) (RW+PR+PM+NC+YF+SC)	AV: Amargosa Valley BM: Buckboard Mesa LW: Lathrop Wells NC: Nye Canyon NCF: Northern Crater Flat PM: Pahute Mesa PR: Paiute Ridge RW: Rocket Wash SB: Sleeping Butte SC: Solitario Canyon TM: Thirsty Mesa YF: Yucca Flat 3.7: 3.7 Ma Crater Flat
Post 5 Ma (0.3)	- 5 Ma Zone: (NCF+LW+SB+TM+BM+AV) - Background (10 Ma Zone): Post 10 Ma rate (0.33) (PR+PM+NC+YF+ 3.7) 10 - 1 Ma rate (0.33) (PR+PM+NC+YF+3.7) 10 - 5 Ma rate (0.33) (PR+PM+NC+YF)	
Post 10 Ma (0.1)	- 10 Ma Zone: (NCF+LW+SB+TM+BM+AV+RW+ PM+PR+NC+YF+SC+3.7)	

TABLE 3-20
ESTIMATED UNCERTAINTIES IN EVENT COUNTS
WILLIAM R. HACKETT SOURCE MODEL

LOCATION	COUNTS (CONES)	WEIGHT	NOTES
Lathrop Wells	1 (0.4) 2 (0.1) 3 (0.4) 4 (0.05) 5 (u) (0.05)		A-G: Aeromagnetic anomalies of V. Langenheim, USGS BC: Black Cone HC: Hidden Cone 2HC: 2 events at Hidden Cone LBP: Little Black Peak LC: Little Cone 2LC: 2 events at Little Cones M: Makani Cone RC: Red Cone u: undetected events
Sleeping Butte	1 (LBP+HC) (0.4) 2 (LBP, HC) (0.5) 3 (LBP, 2HC) (0.1)		
1.0 Ma Crater Flat	1 (all) (0.1) 2 (LC, RC+BC+M) (0.3) 3 (LC, RC+BC, M) (0.4) 4 (LC, RC, BC, M) (0.1) 5 (2LC, RC, BC, M) (0.05) 6 (u, 2LC, RC, BC, M) (0.05)		
Buckboard Mesa	1 (0.8) 2 (0.2)		
3.7 Ma Crater Flat	1 (0.05) 2 (0.1) 3 (0.3) 4 (0.2) 5 (0.2) 6 (0.1) 7 (u) (0.025) 8 (2u) (0.025)		
Amargosa Valley	1 (B) (0.0184) 2 (B+C) or (B+D) 0.0817 (0.0816) 3 (B+C+D) or (B+C+G) or (B+D+E) (0.2949) (0.0660) (0.0660) 4 (B+C+D+E) or (B+C+D+G) (0.1473) (0.1473) 5 (B+C+D+E+G) (0.0853) 6 (B+C+D+E+F+G) (0.0110) 7 (A-G) (0.0005)		
Thirsty Mesa	1 (0.7) 2 (u) (0.2) 3 (2u) (0.1)		
Rocket Wash	1 (0.8) 2 (u) (0.2)		

TABLE 3-20 (Cont'd)
ESTIMATED UNCERTAINTIES IN EVENT COUNTS
WILLIAM R. HACKETT SOURCE MODELS

LOCATION	COUNTS (CONES)	WEIGHT	NOTES
Pahute Mesa	1	(0.1)	
	2	(0.6)	
	3	(0.2)	
	4 (u)	(0.1)	
Paiute Ridge	1	(0.05)	
	2	(0.4)	
	3	(0.3)	
	4	(0.1)	
	5	(0.1)	
	6 (u)	(0.05)	
Nye Canyon	1	(0.05)	
	2	(0.1)	
	3	(0.2)	
	4	(0.5)	
	5	(0.1)	
	6 (u)	(0.05)	
Yucca Flat	1	(0.9)	
	2 (u)	(0.1)	
Solitario Canyon	1	(1.0)	

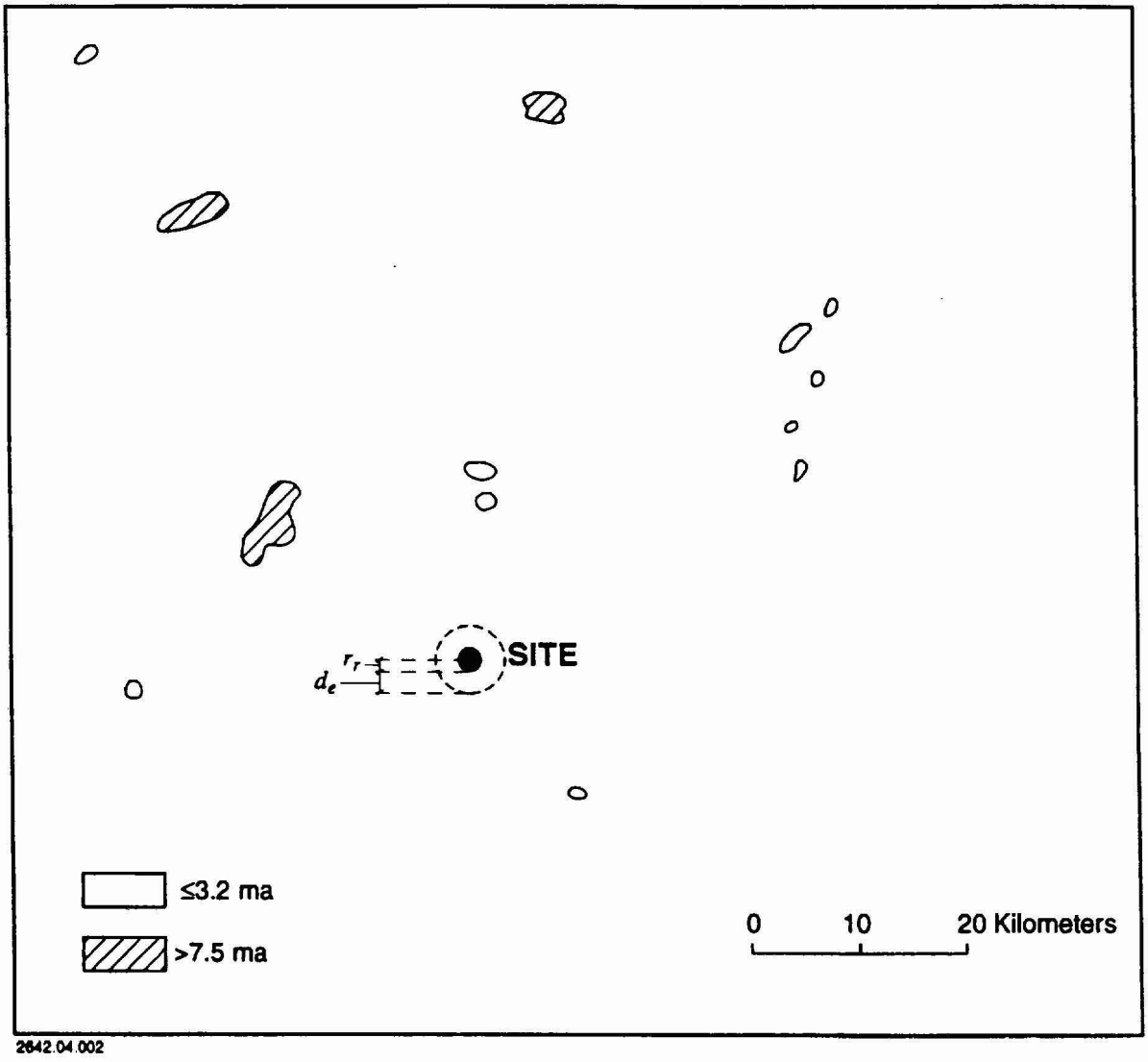

Figure 3-1 Example of simplified volcanic hazard model for a region R. Volcanic events are denoted by the irregular patches.

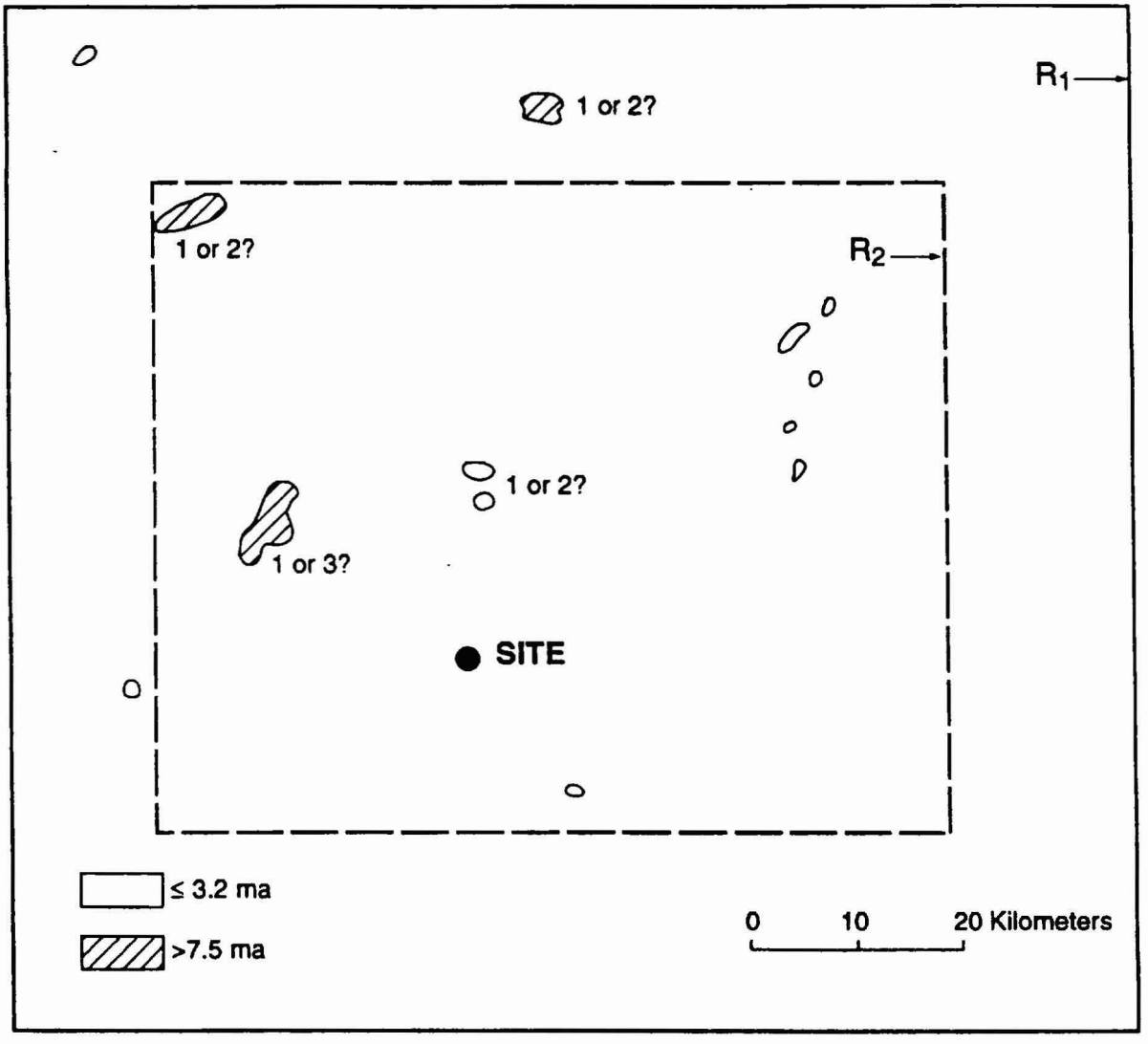

Figure 3-2 Alternative interpretations of the parameters of the simplified volcanic hazard model of Figure 3-1. Shown are alternative definitions of the region of interest and alternative estimates of the numbers of events at various volcanic centers.

(a)

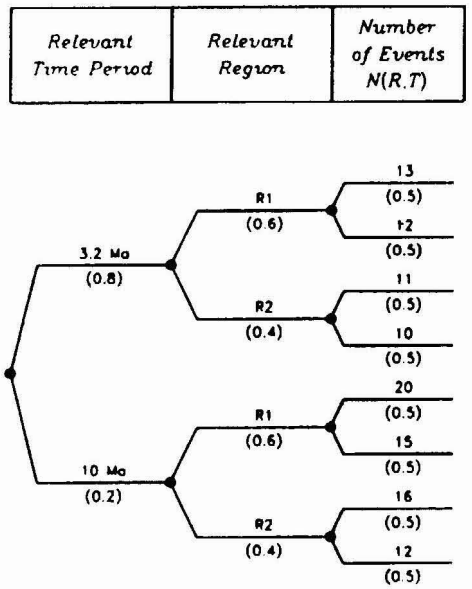

(b)

T (my)	Area of R (sq. km)	N	v	P(v)
3.2	10^4	13	$4.0 \cdot 10^{-9}$	0.24
3.2	10^4	12	$3.8 \cdot 10^{-9}$	0.24
3.2	$0.5 \cdot 10^4$	11	$6.9 \cdot 10^{-9}$	0.16
3.2	$0.5 \cdot 10^4$	10	$6.3 \cdot 10^{-9}$	0.16
10	10^4	20	$2.0 \cdot 10^{-9}$	0.06
10	10^4	15	$1.5 \cdot 10^{-9}$	0.06
10	$0.5 \cdot 10^4$	16	$3.2 \cdot 10^{-9}$	0.04
10	$0.5 \cdot 10^4$	12	$2.4 \cdot 10^{-9}$	0.04

(c)

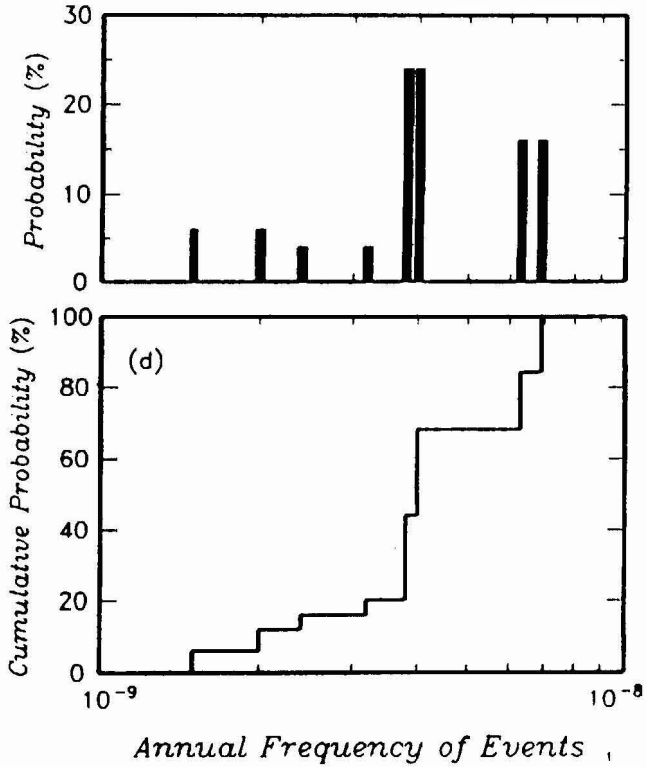

Figure 3-3 Example of logic tree formulation for treatment of uncertainty in PVHA. (a) Logic tree representing uncertainty in region of interest, time period, and event counts. (b) Table of alternate computed hazard estimates. (c) Resulting discrete distribution for frequency of intersection. (d) Cummulative distribution of frequency of intersection.

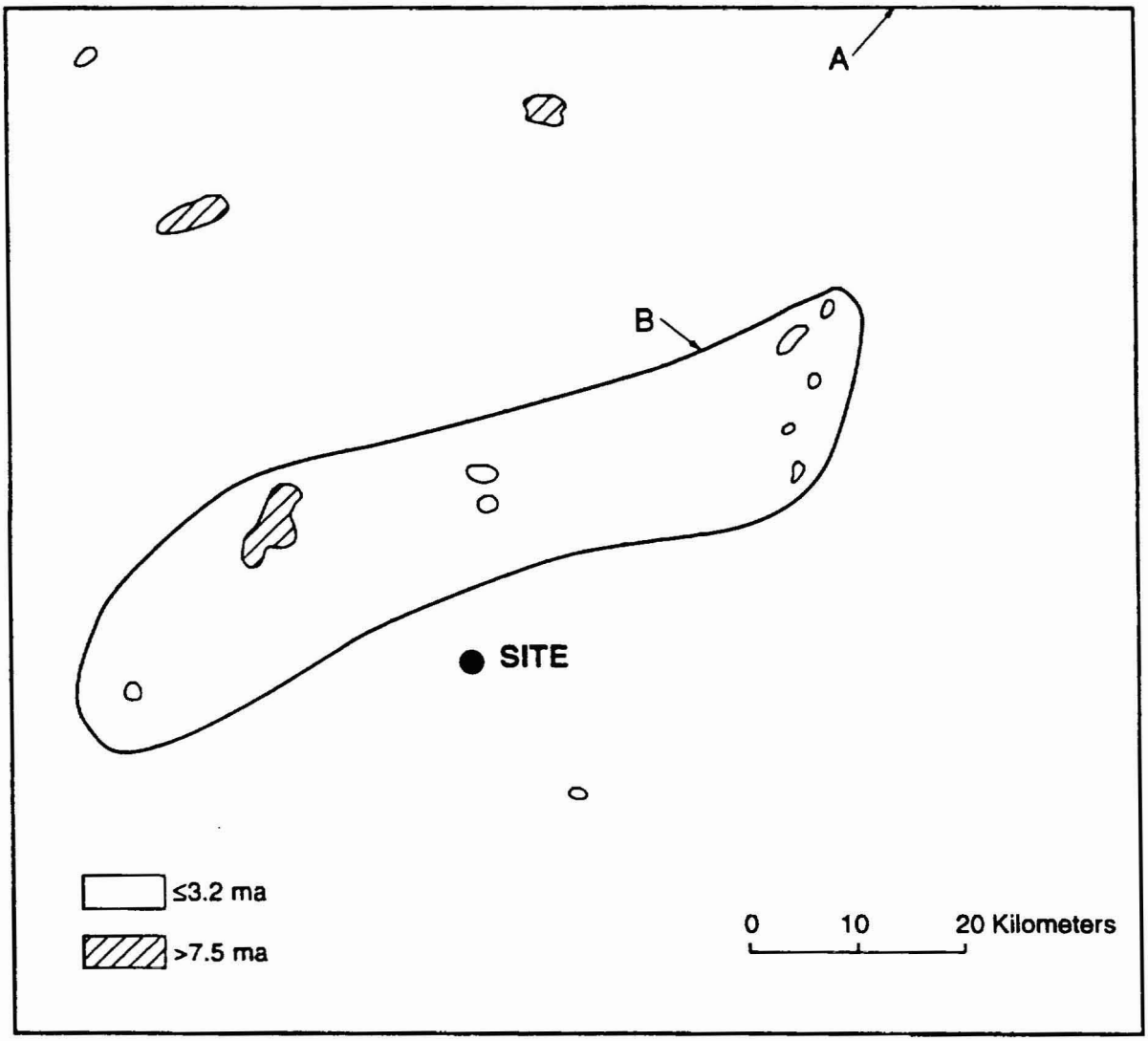

Figure 3-4 Example of subdividing the region of Figure 3-1 into locally homogeneous zones.

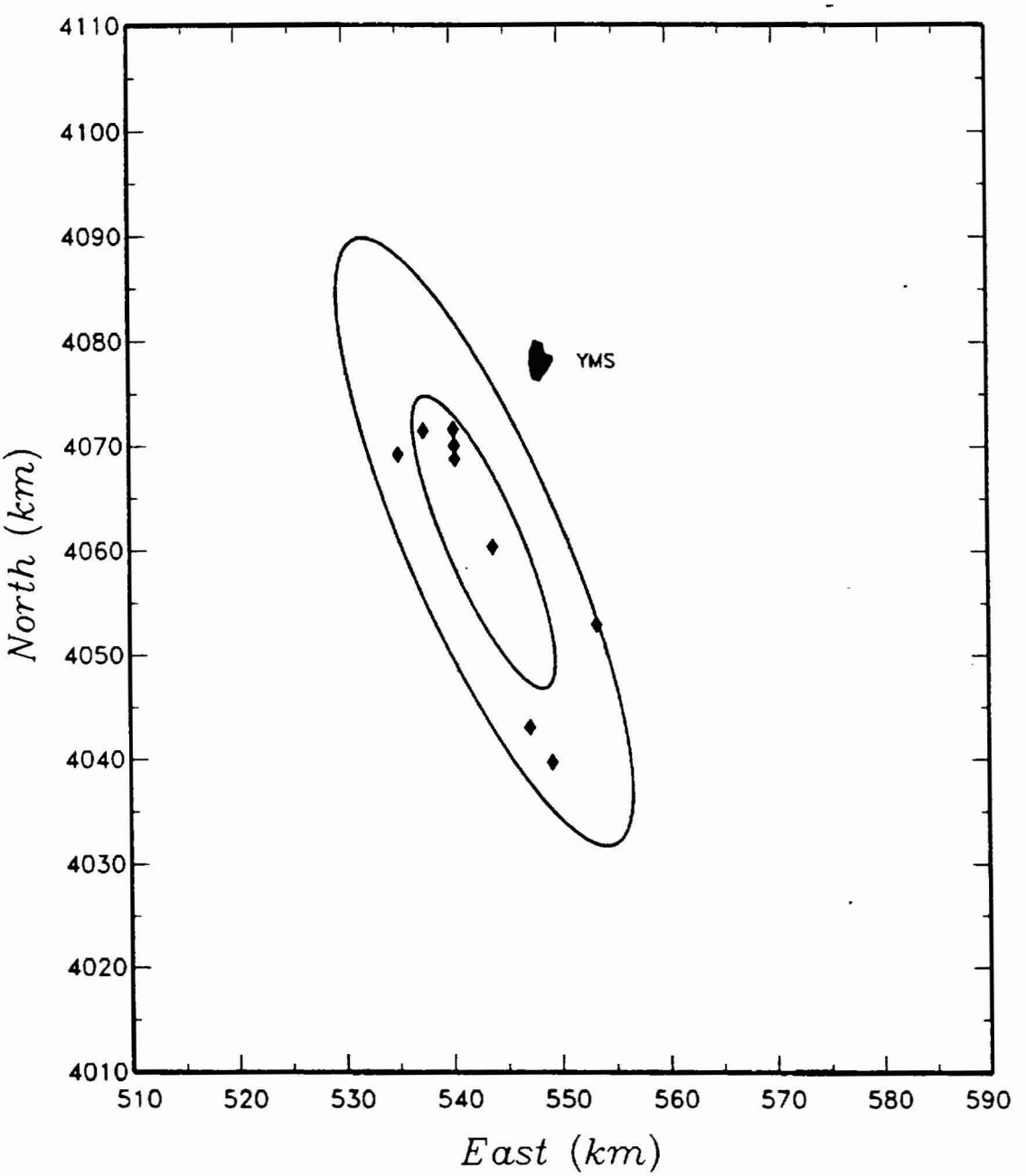

Figure 3-5 Representation of the volcanic events in Crater Flat by a bivariate Gaussian field. Lines enclose regions expected to contain 50 and 95-percent of future events associated with the field. YMS refers to the proposed Yucca Mountain repository site.

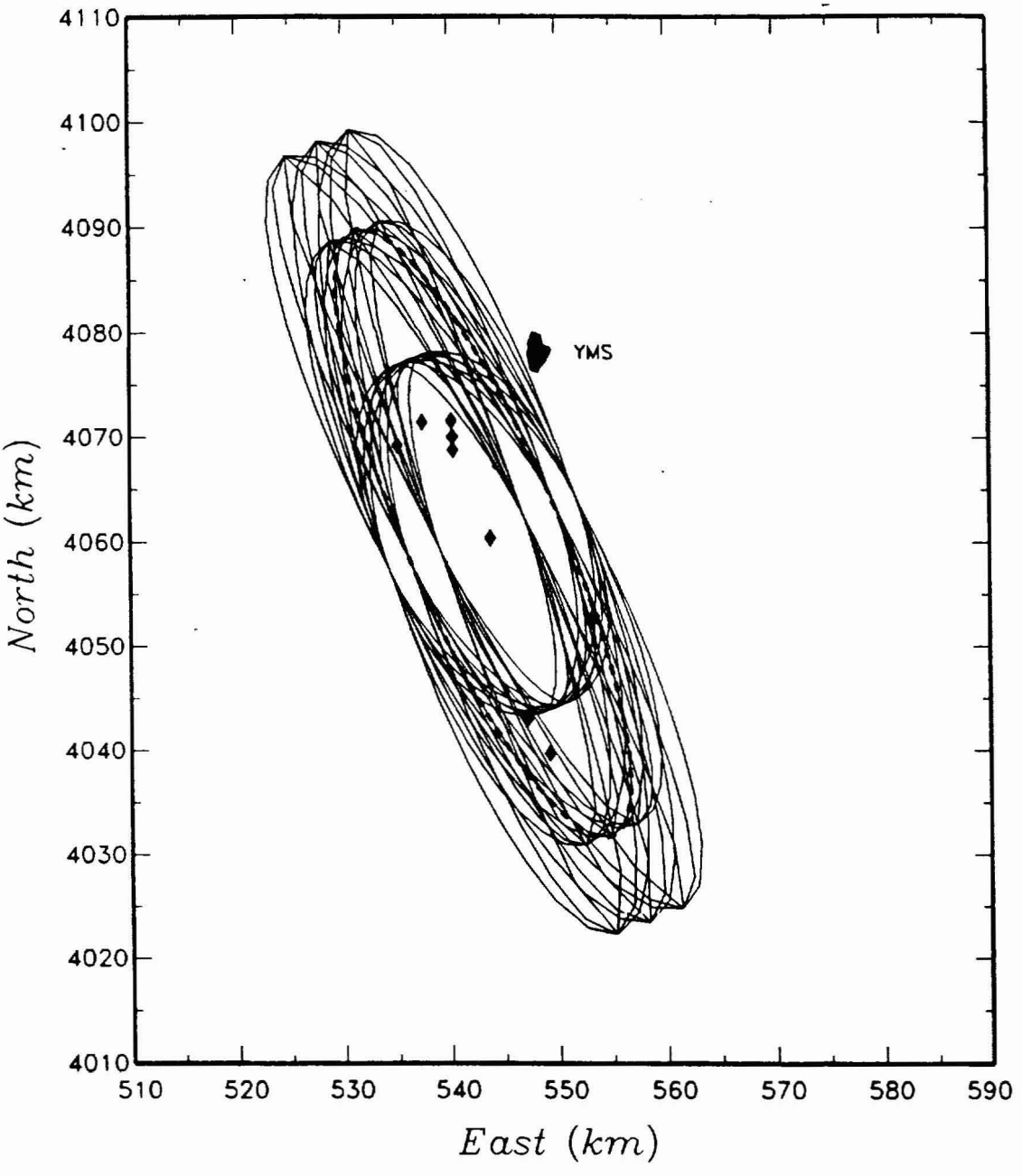

Figure 3-6 Example of set of 27 possible Gaussian volcanic fields considering uncertainty in field size and orientation (covariance of x and y). Each curve is a possible 95-percent density ellipse for the field. The heavy dashed curve denotes the maximum likelihood 95-percent density ellipse. YMS refers to the proposed Yucca Mountain repository site.

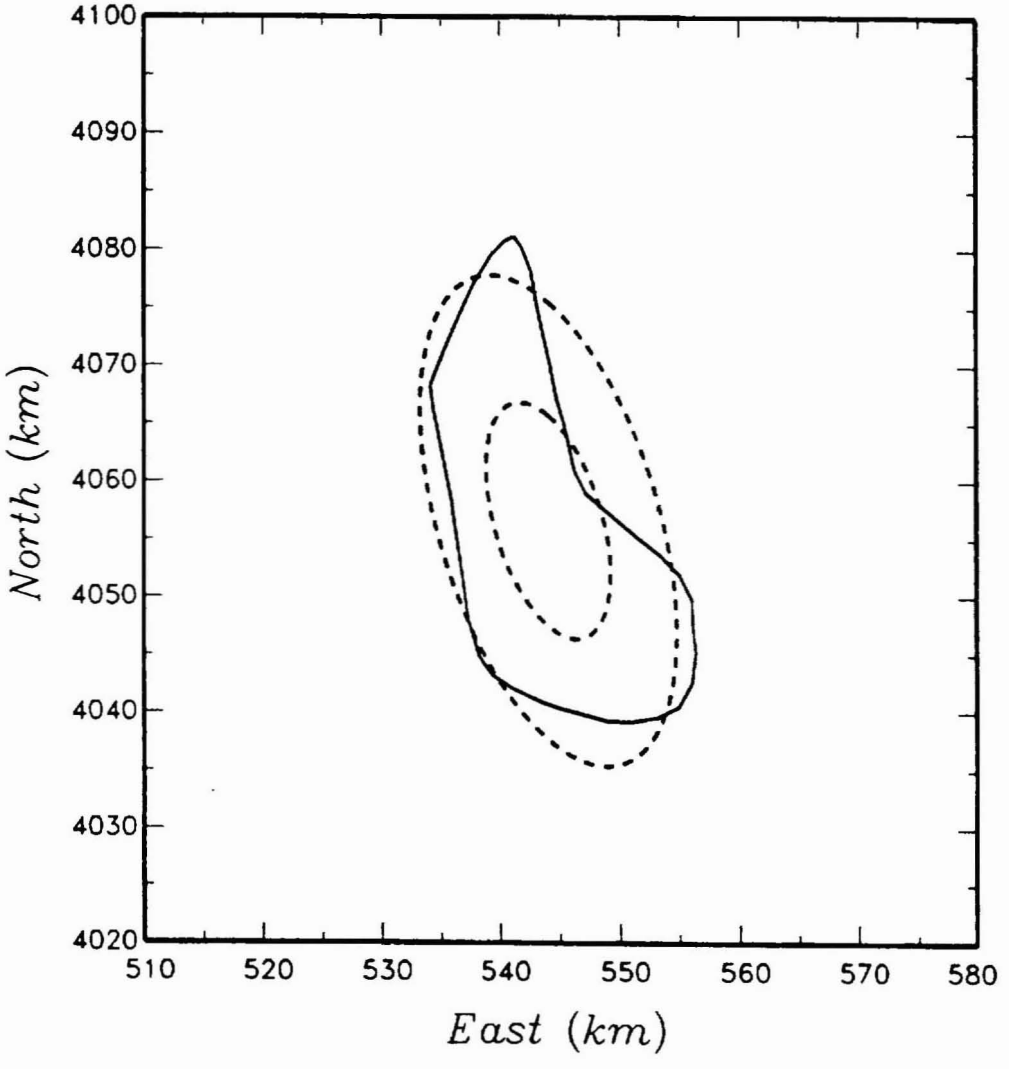

Figure 3-7 Example of fitting a 95-percent density bivariate Gaussian field shape to boundary of a volcanic zone defined by geology. The 50-percent density ellipse is also shown.

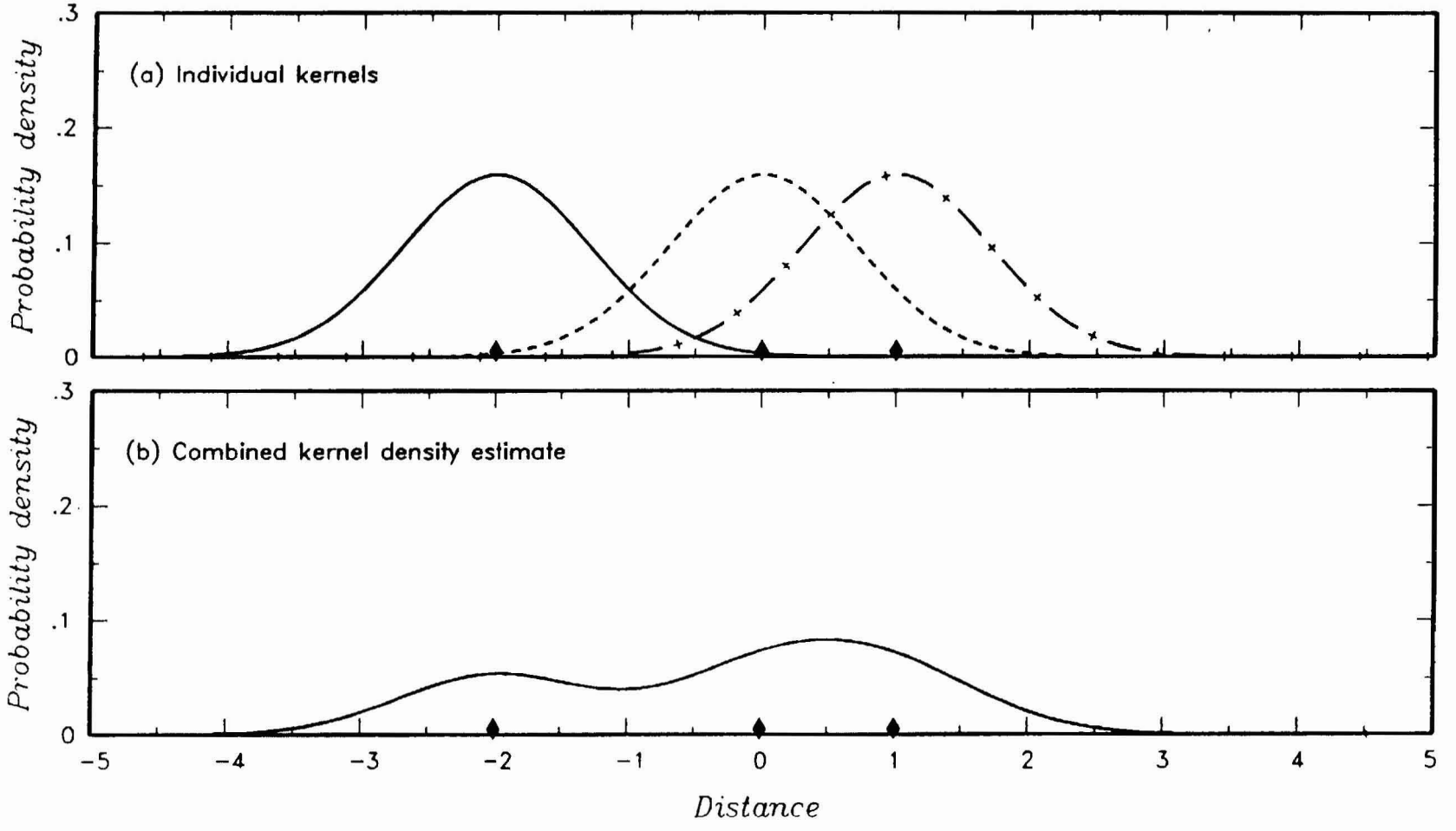

Figure 3-8 Example of kernel density estimation in one dimension. (a) Individual kernel functions centered on the data points. (b) Summation of individual kernels normalized to unity to produce a composite estimate of the spatial density function.

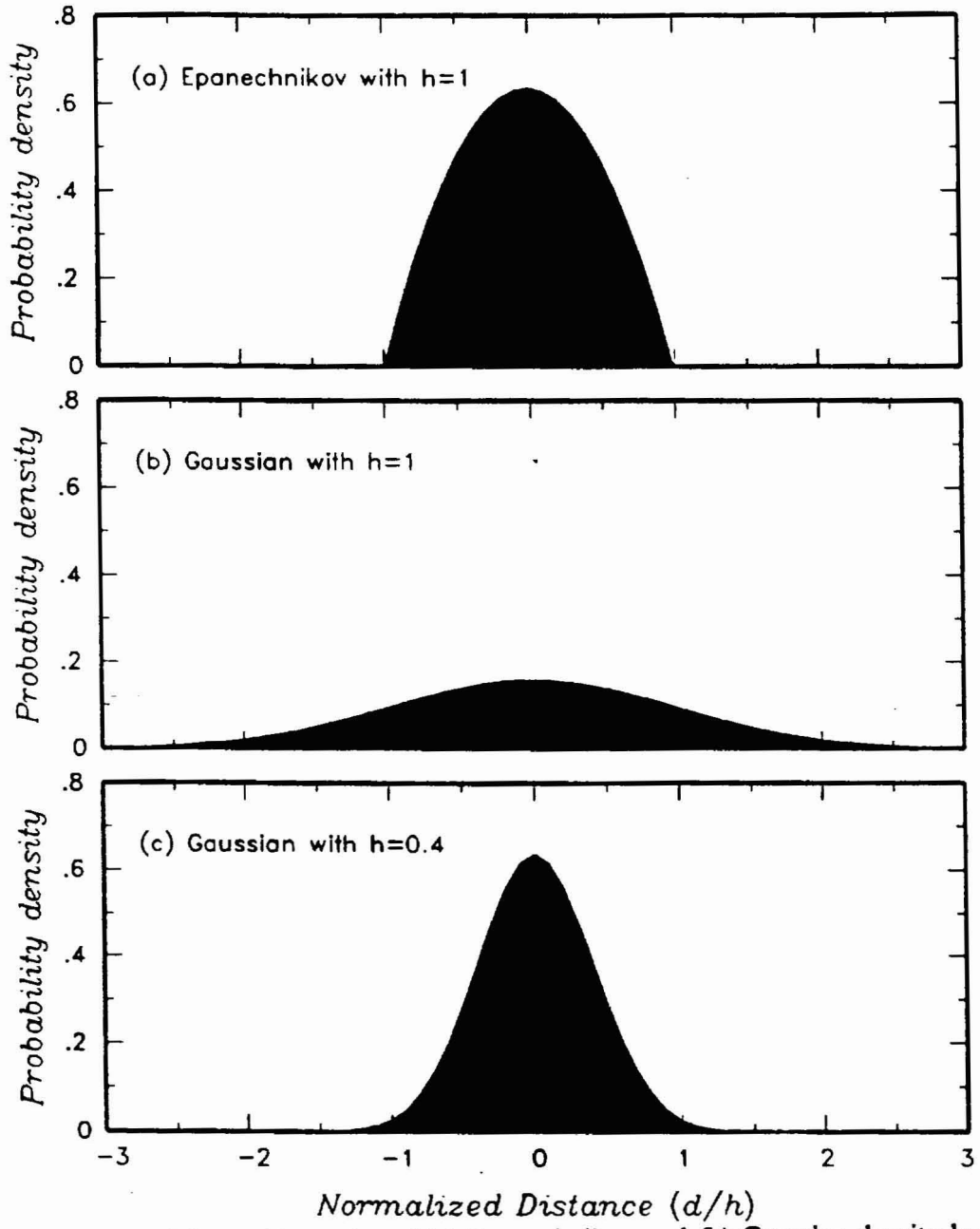

Figure 3-9 Examples of (a) Epanechnikov and (b) Gaussian density kernels with the same value of h. In (c) the Gaussian kernel is adjusted to have an h 2.5 times smaller than the h of the Epanechnikov kernel in (a).

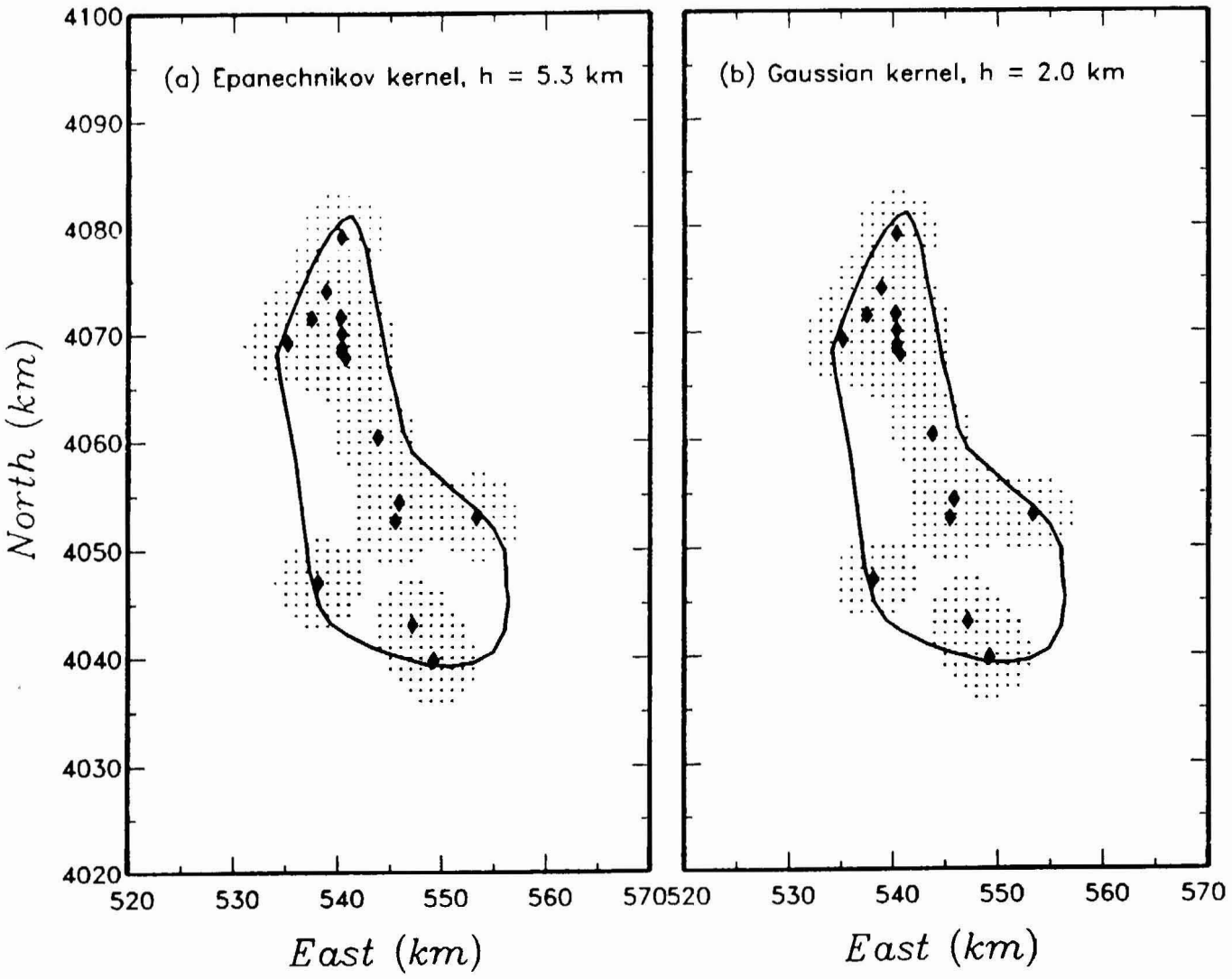

Figure 3-10 Example of fitting kernel density to boundary of a volcanic zone defined by geology. Stippled area defines the 95 percent density contour obtained using (a) a Epanechnikov kernel and (b) a Gaussian kernel.

(a) Point Event

(b) Event-Centered Dike

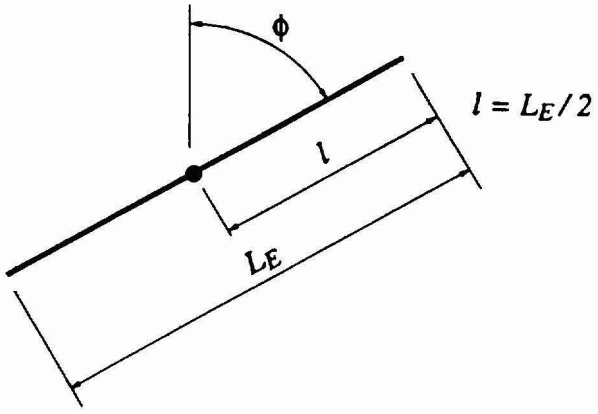

(c) Randomly Located Dike

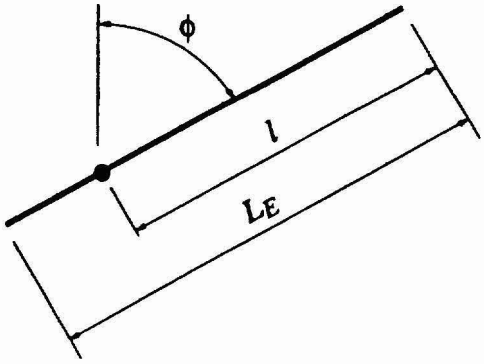

Figure 3-11 Example representations of the locations of volcanic events used in the PVHA. Each event is considered to be either (a) a point, (b) a linear dike centered on the event, or (c) a linear dike randomly located on the event.

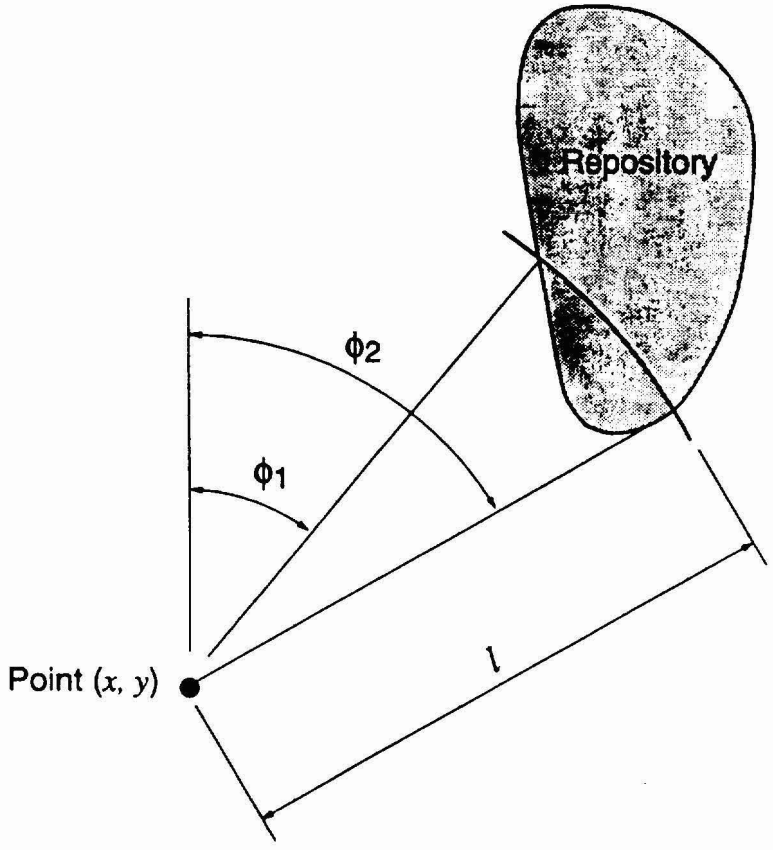

Figure 3-12 Procedure for computing conditional probability of intersection, $P_I(x,y)$.

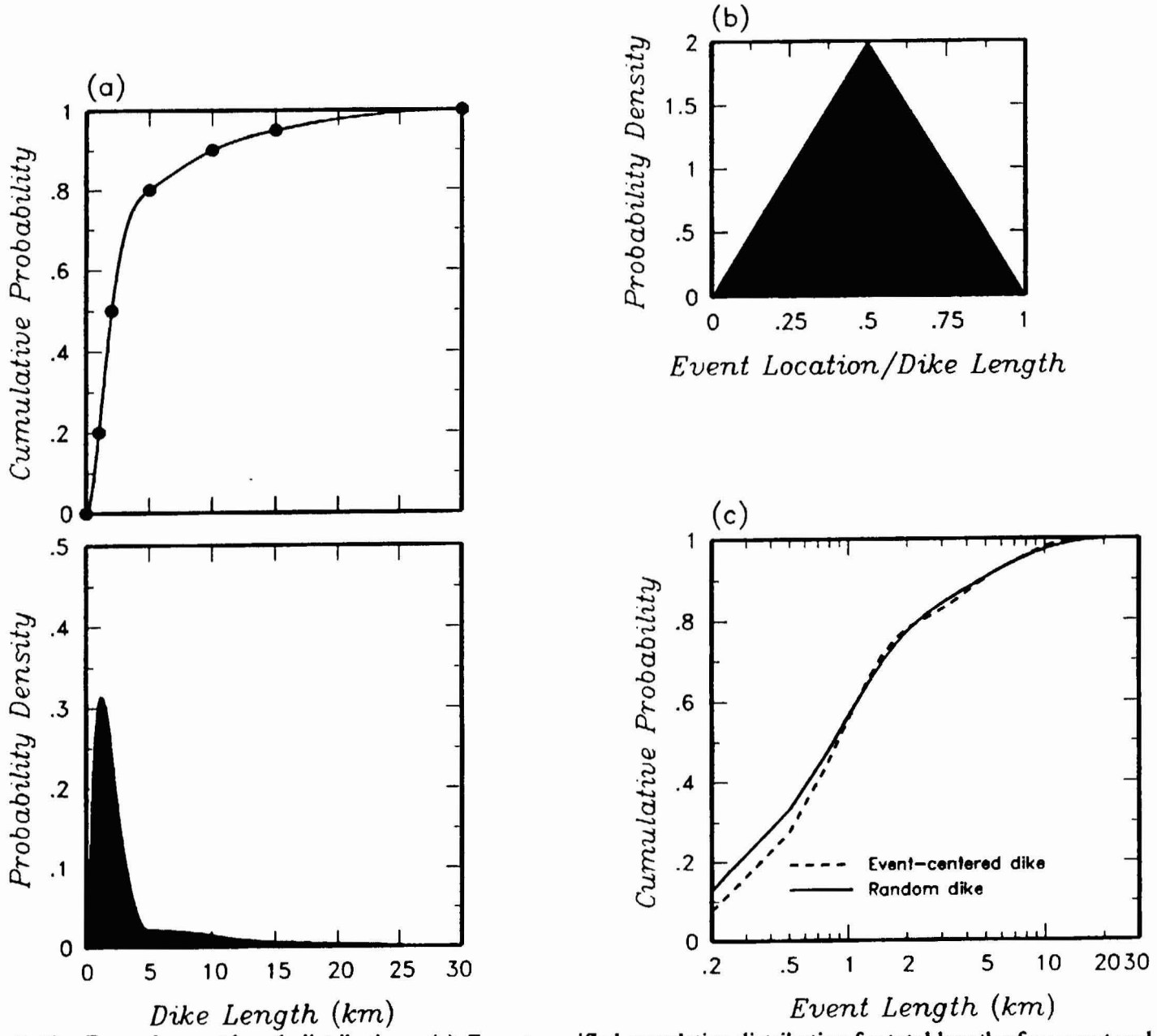

Figure 3-13 Example event length distributions. (a) Expert specified cumulative distribution for total length of an event and the resulting density function. (b) Expert specified distribution for location of an event along the dike. (c) Resulting density functions for distance from the event to the end of the dike for event-centered dikes and randomly placed dikes.

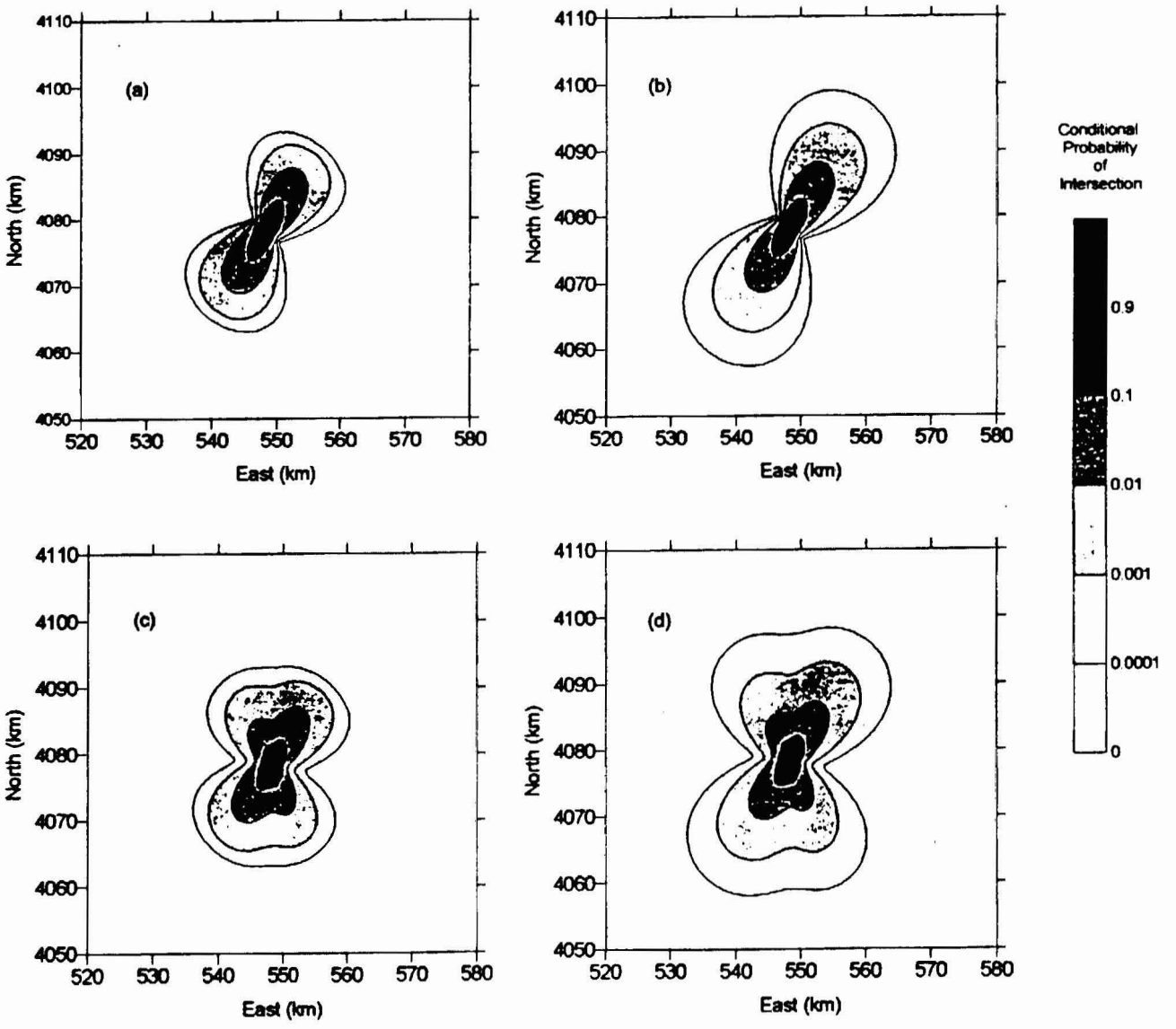

Figure 3-14 Examples of conditional probability of intersection computations. The event length distributions are shown on Figure 3-13(c). (a) Event-centered dikes with bimodal azimuth distribution N30°E ± 15°, (b) Random dikes with azimuth distribution N30°E ± 15°, (c) Event-centered dikes with bimodal azimuth distribution 70-percent frequency N30°E ± 15°, 30-percent frequency N20°W ± 15°, and (d) Random dikes with bimodal azimuth distribution 70-percent frequency N20°W ±15°. 30-percent frequency N20°W± 15°.

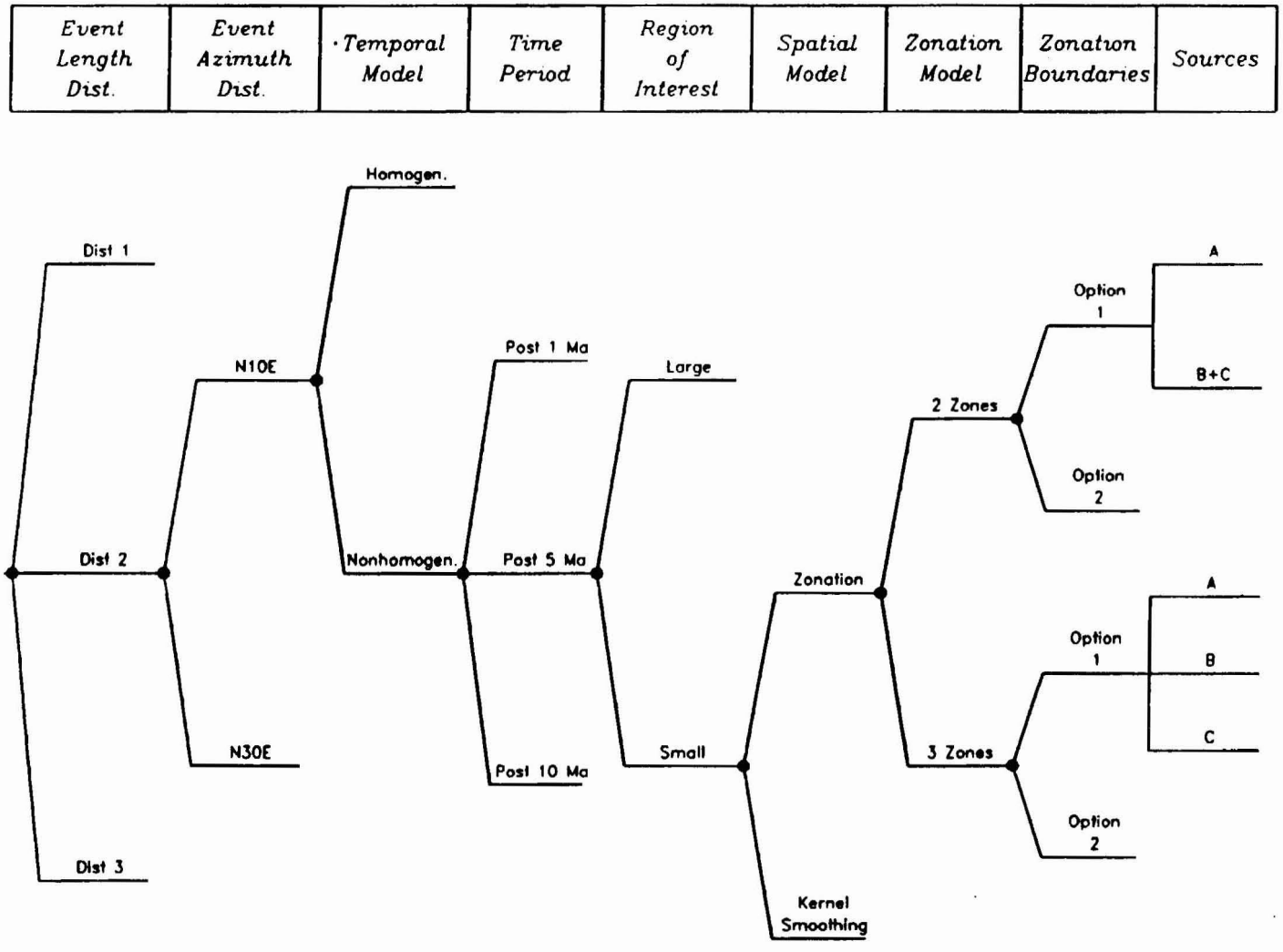

Figure 3-15 General logic tree structure used to construct PVHA computation model.

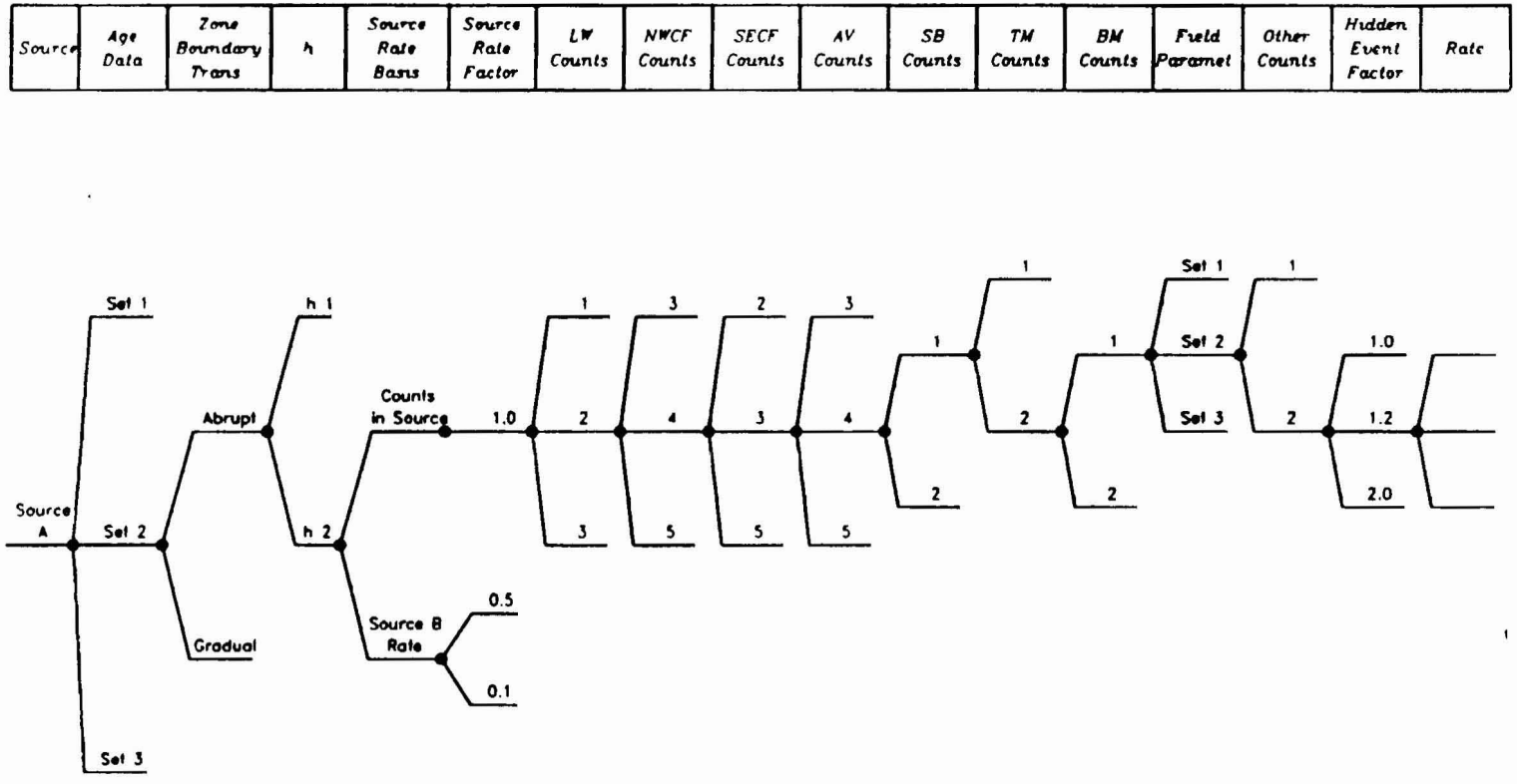

Figure 3-16 Logic tree structure for subtrees addressing the uncertainty in modeling the hazard from specific sources. These subtrees are attached to the overall logic tree shown on Figure 3-15.

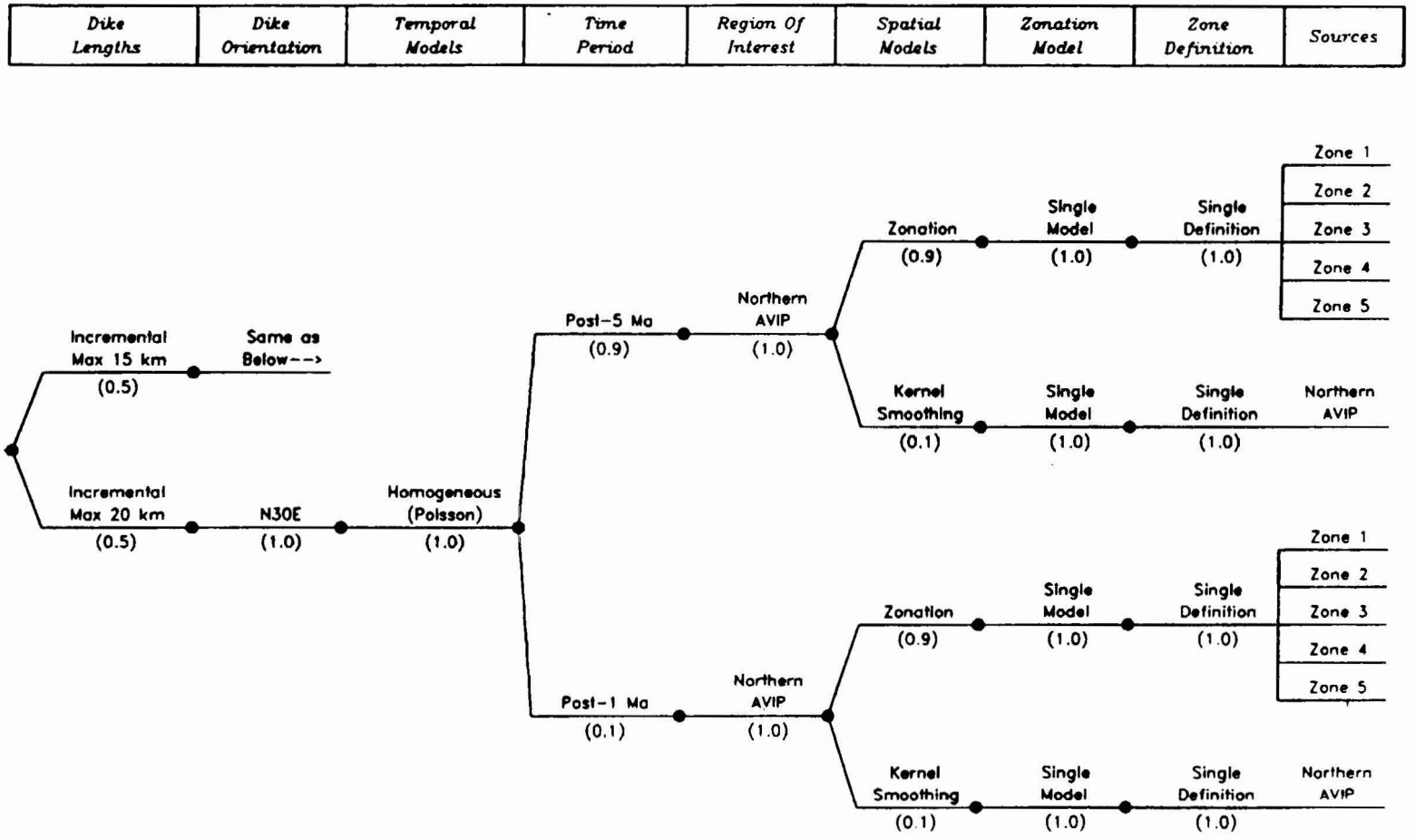

Figure 3-17 Logic tree for the PVHA model developed by Alexander McBirney.

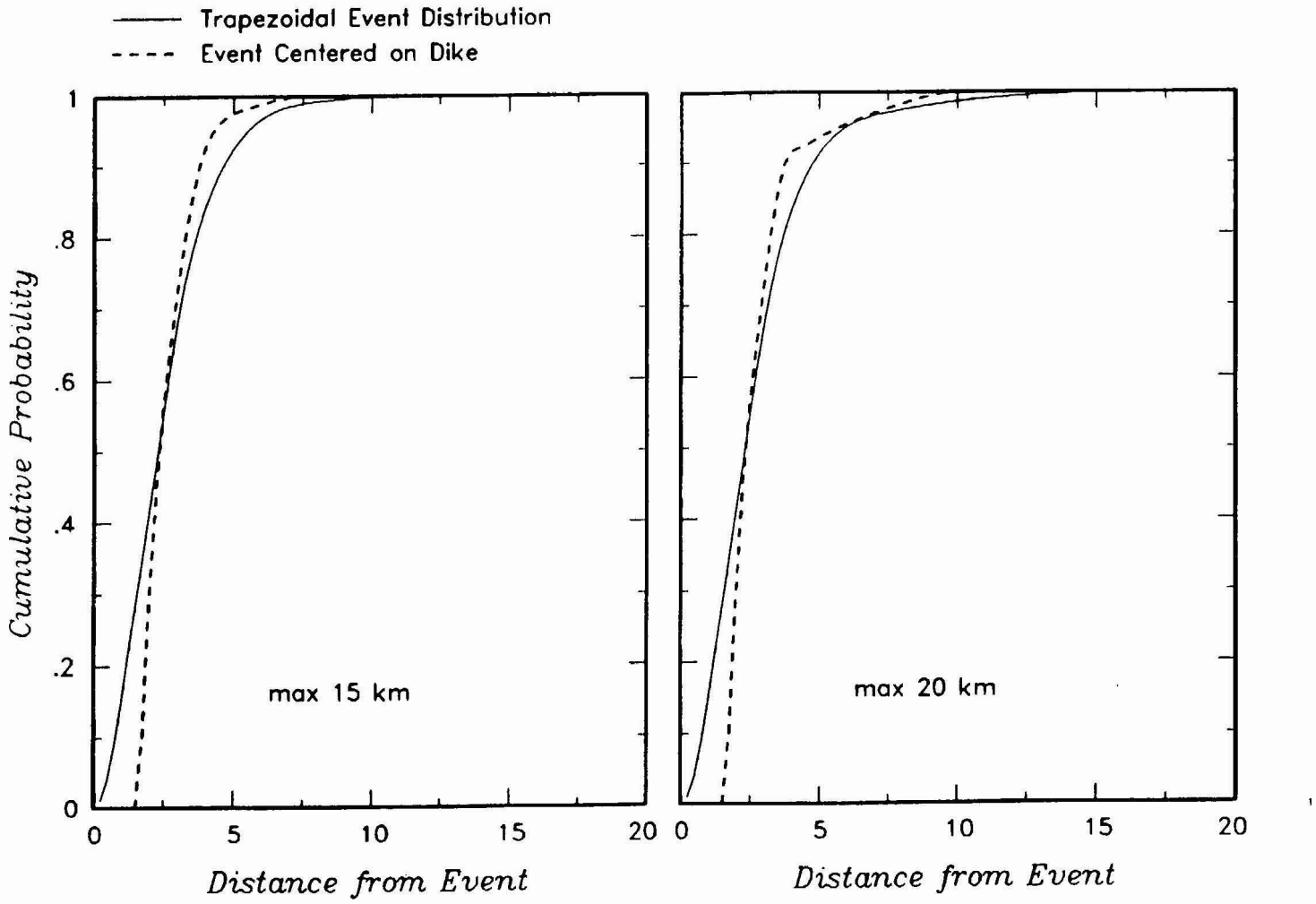

Figure 3-18 Alternative distributions for the length of an event *f(l)* developed from the assessments by Alexander McBirney.

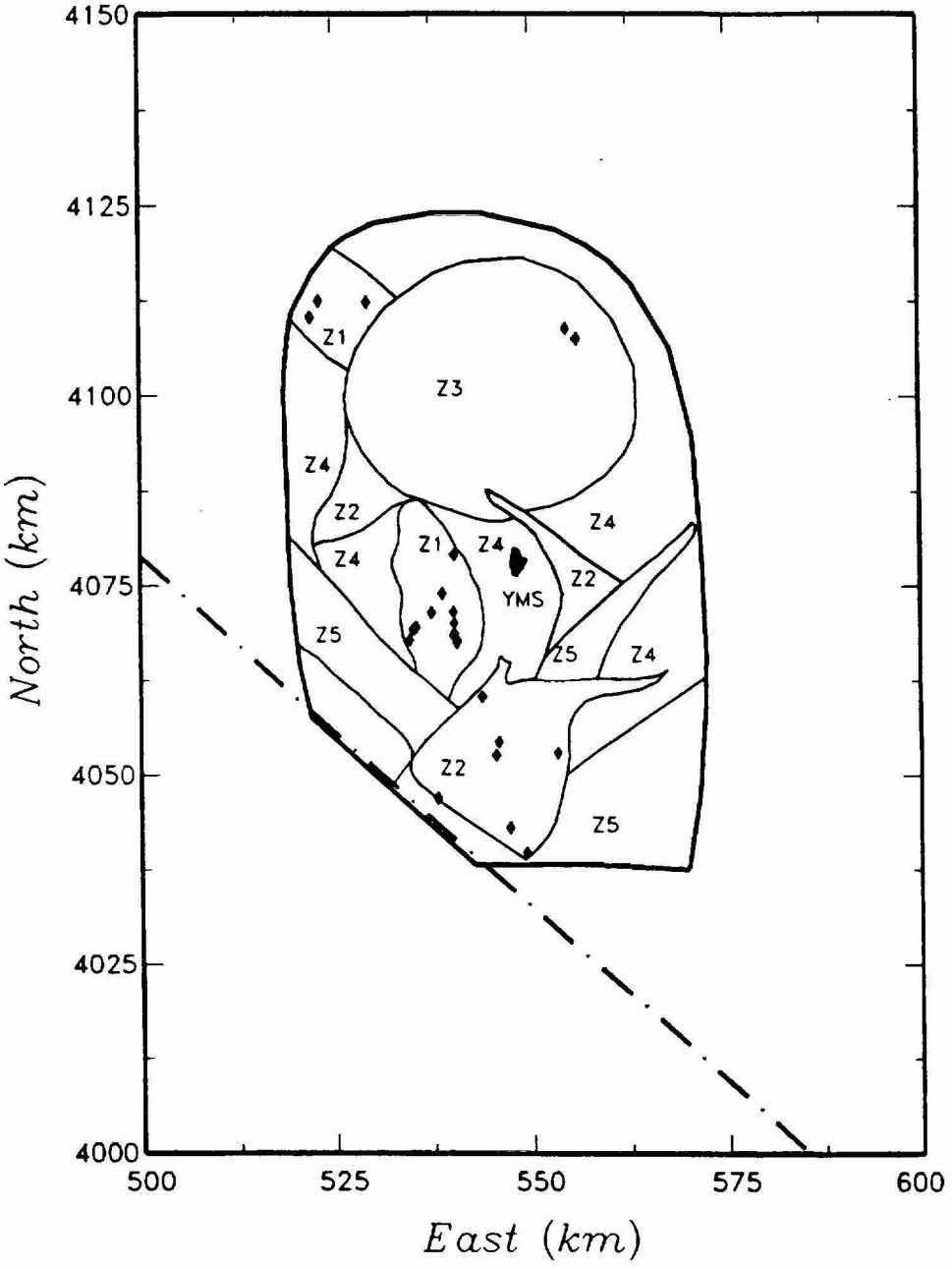

Figure 3-19 Volcanic source zone model developed by Alexander McBirney. Diamonds represent volcanic events for the post-5 Ma time period. YMS refers to the proposed Yucca Mountain repository site and the dash-dot line is the Nevada-California border.

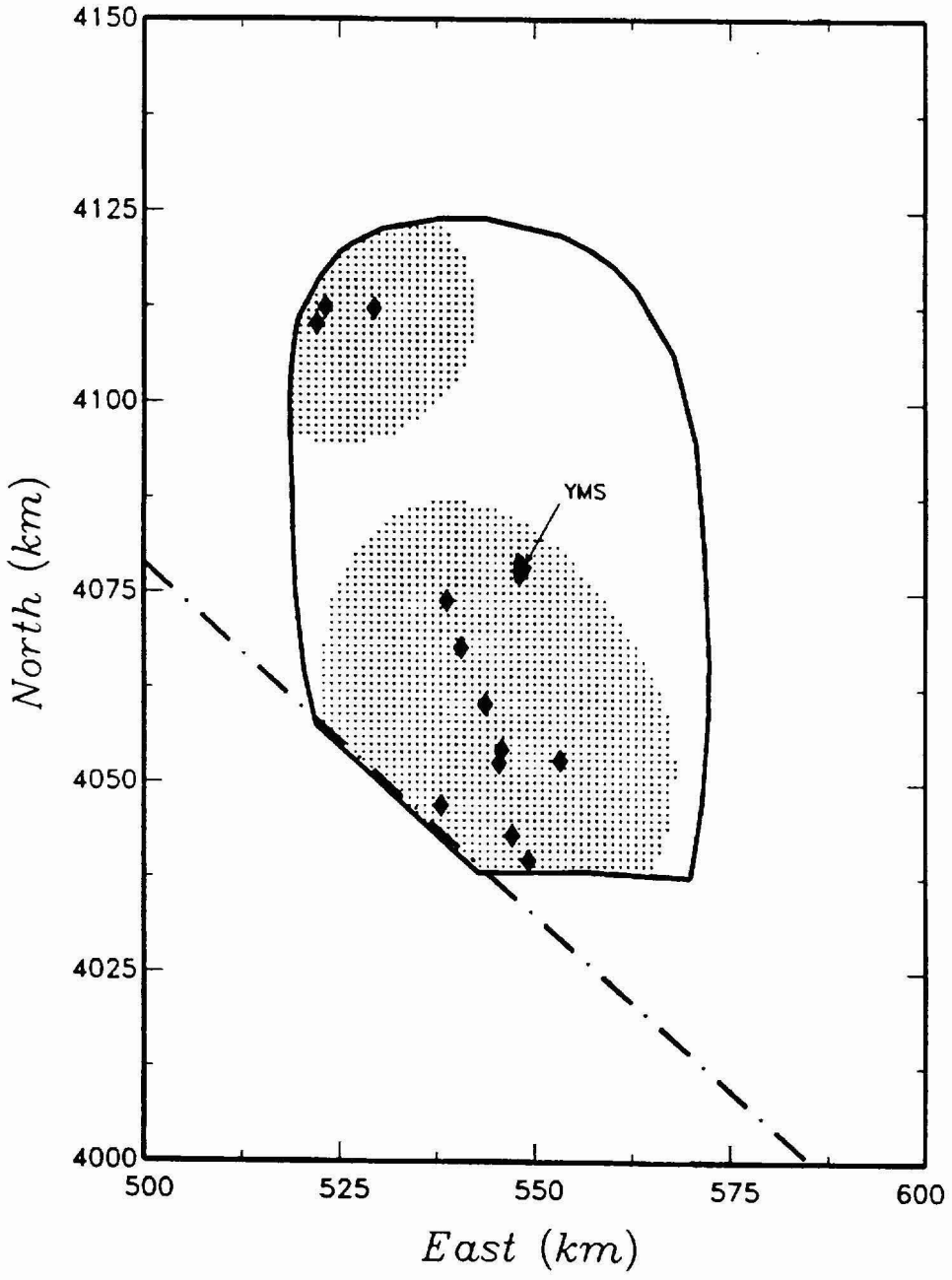

Figure 3-20 Example of a kernel density estimate based on Alexander McBirney's preferred event counts for the post-5 Ma time period and a Gaussian kernel with h = 9 km. The stippled area contains 95-percent of the spatial density. YMS refers to the proposed Yucca Mountain repository site and the dash-dot line is the Nevada-California border.

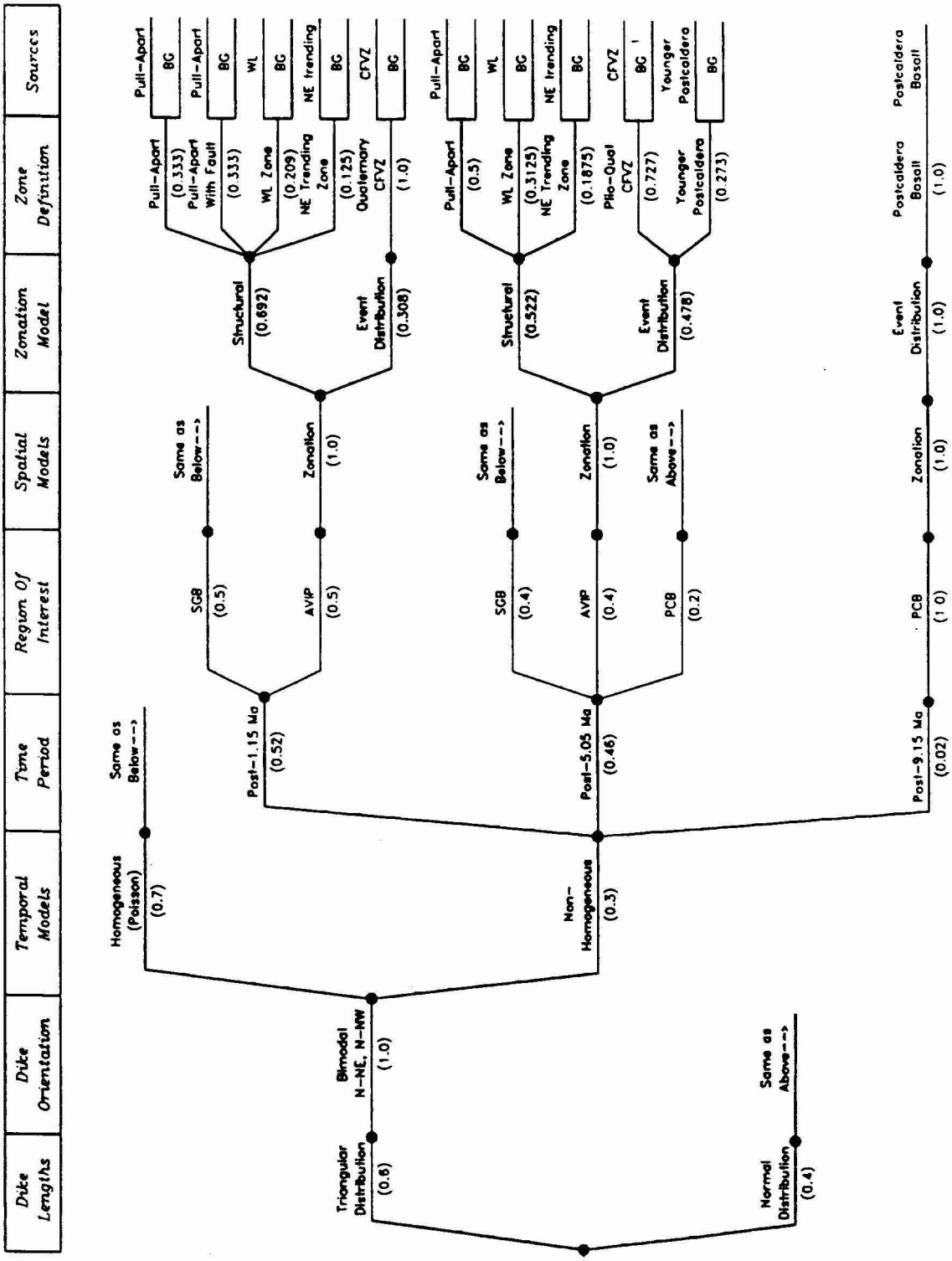

Figure 3-21 Logic tree for the PVHA model developed by Bruce Crowe.

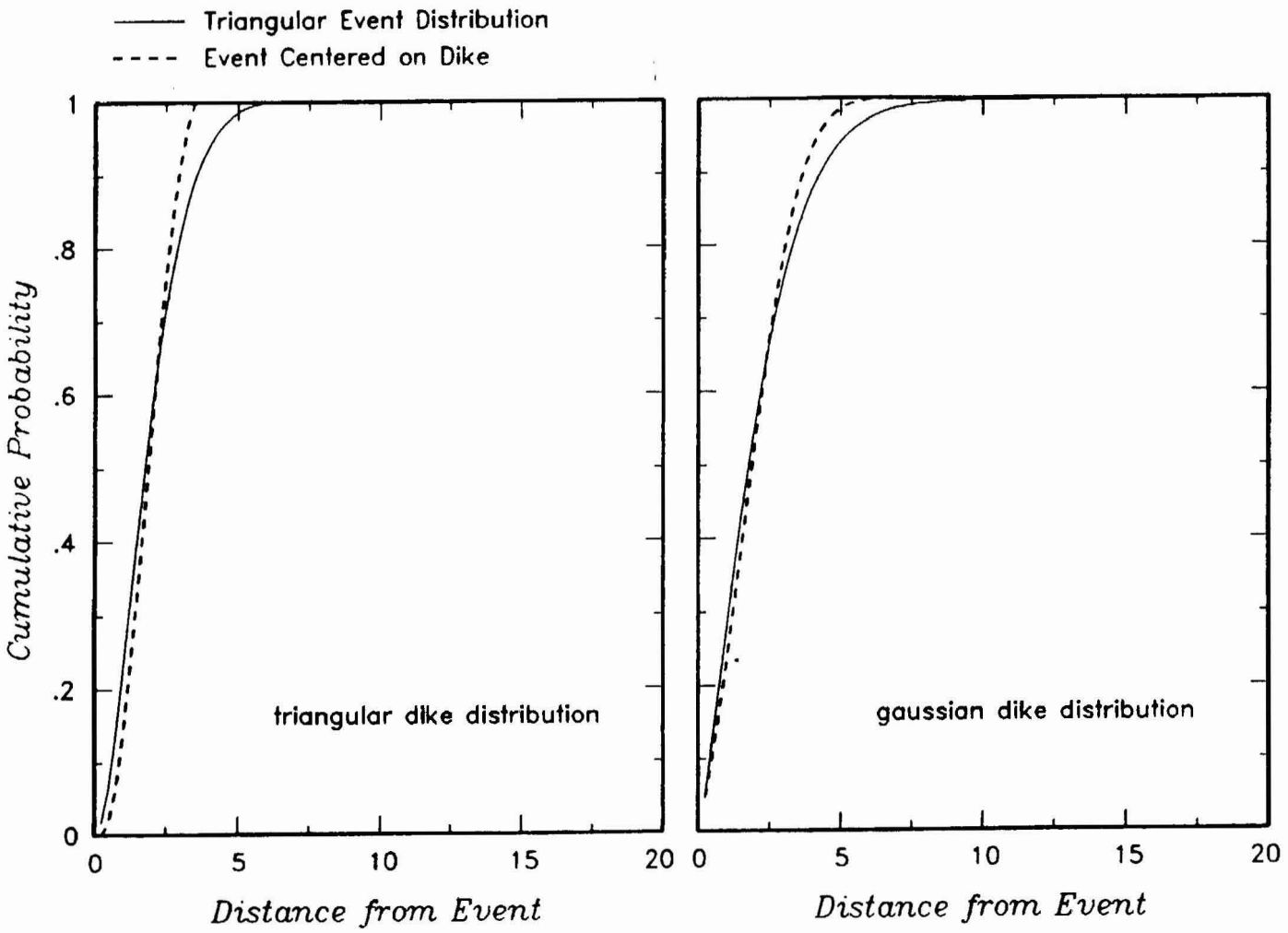

Figure 3-22 Alternative distributions for the length of an event *f(l)* developed from the assessments by Bruce Crowe.

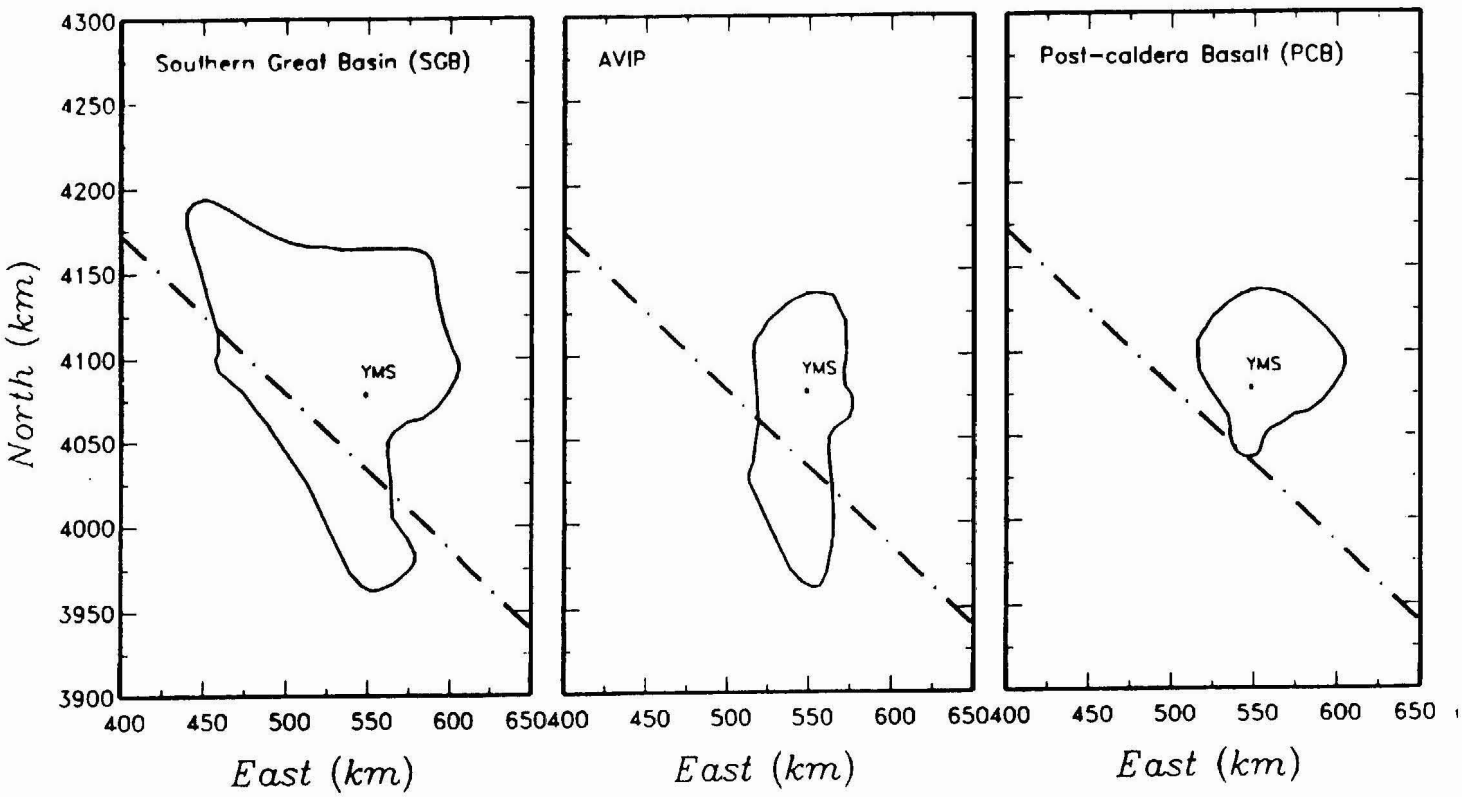

Figure 3-23 Alternative regions of interest used as background source zones in Bruce Crowe's PVHA model. YMS refers to the proposed Yucca Mountain repository site and the dash-dot line is the Nevada-California border.

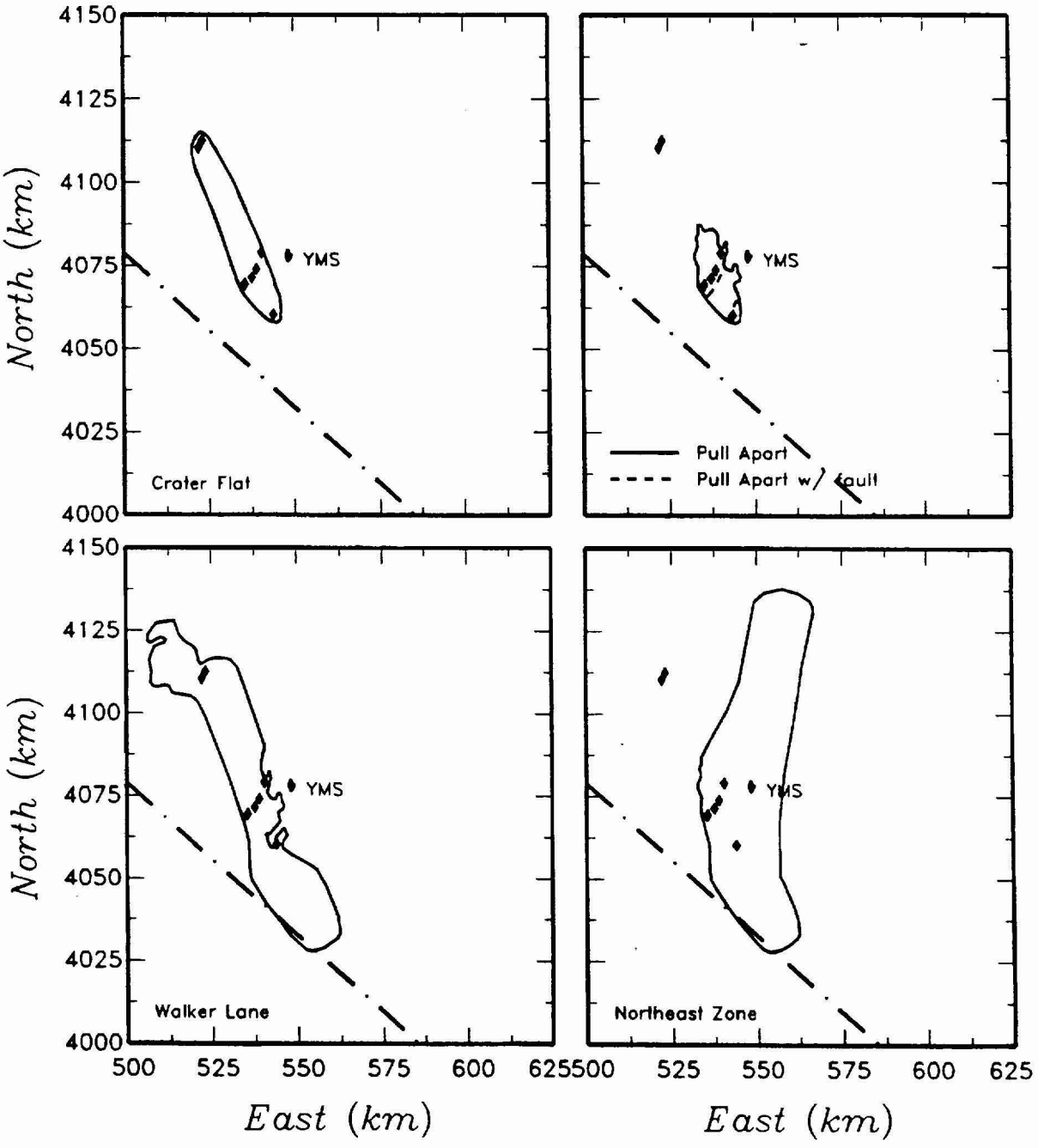

Figure 3-24 Alternative source zones defined by Bruce Crowe for the post-1.15 Ma time period. Diamonds represent volcanic events for the post-1.15 Ma time period. YMS refers to the proposed Yucca Mountain repository site and the dash-dot line is the Nevada-California border.

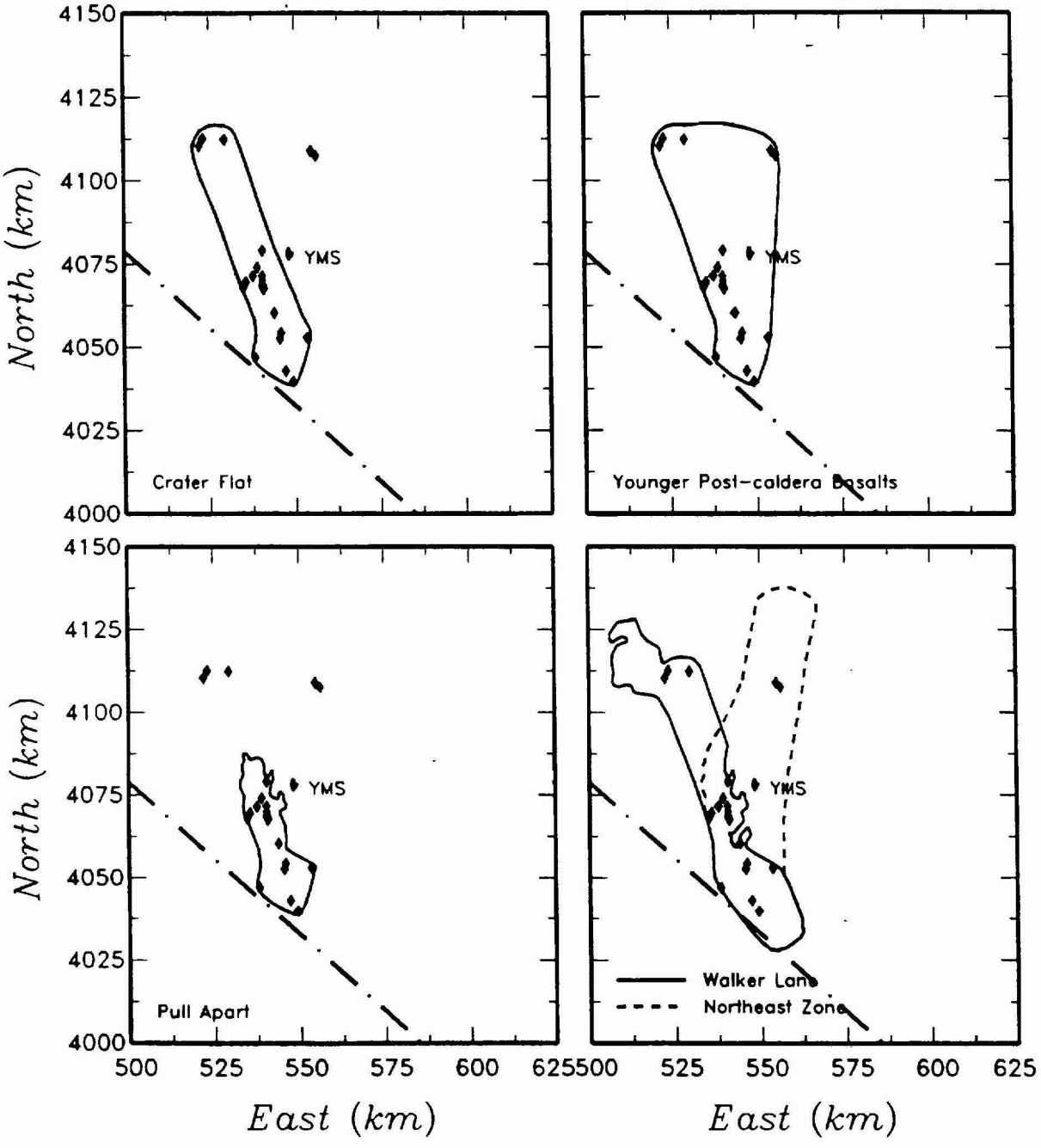

Figure 3-25 Alternative source zones defined by Bruce Crowe for the post-5.05 Ma time period. Diamonds represent volcanic events for the post-5.05 Ma time period. YMS refers to the proposed Yucca Mountain repository site and the dash-dot line is the Nevada-California border.

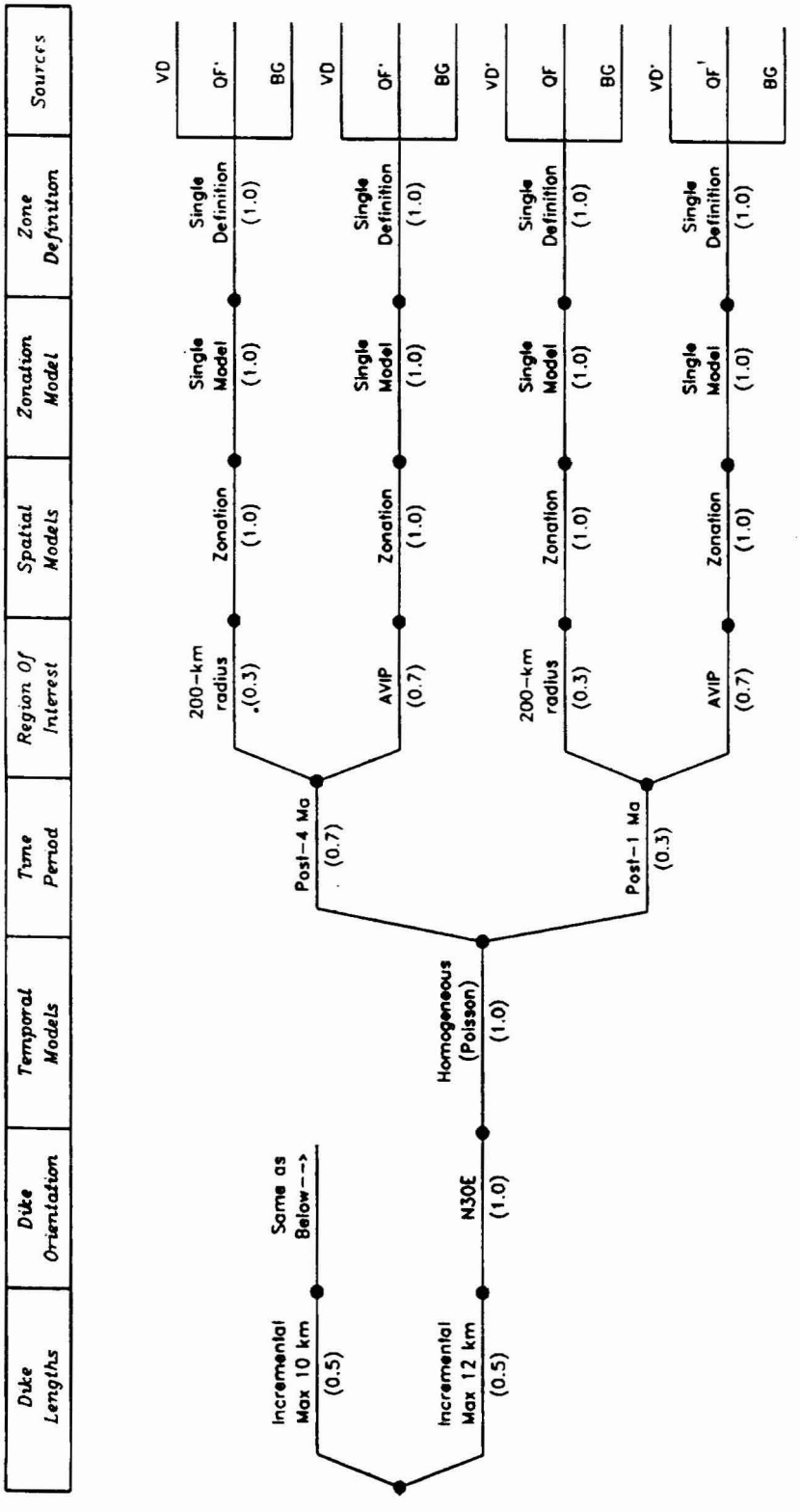

Figure 3-26 Logic tree for the PVHA model developed by George Thompson.

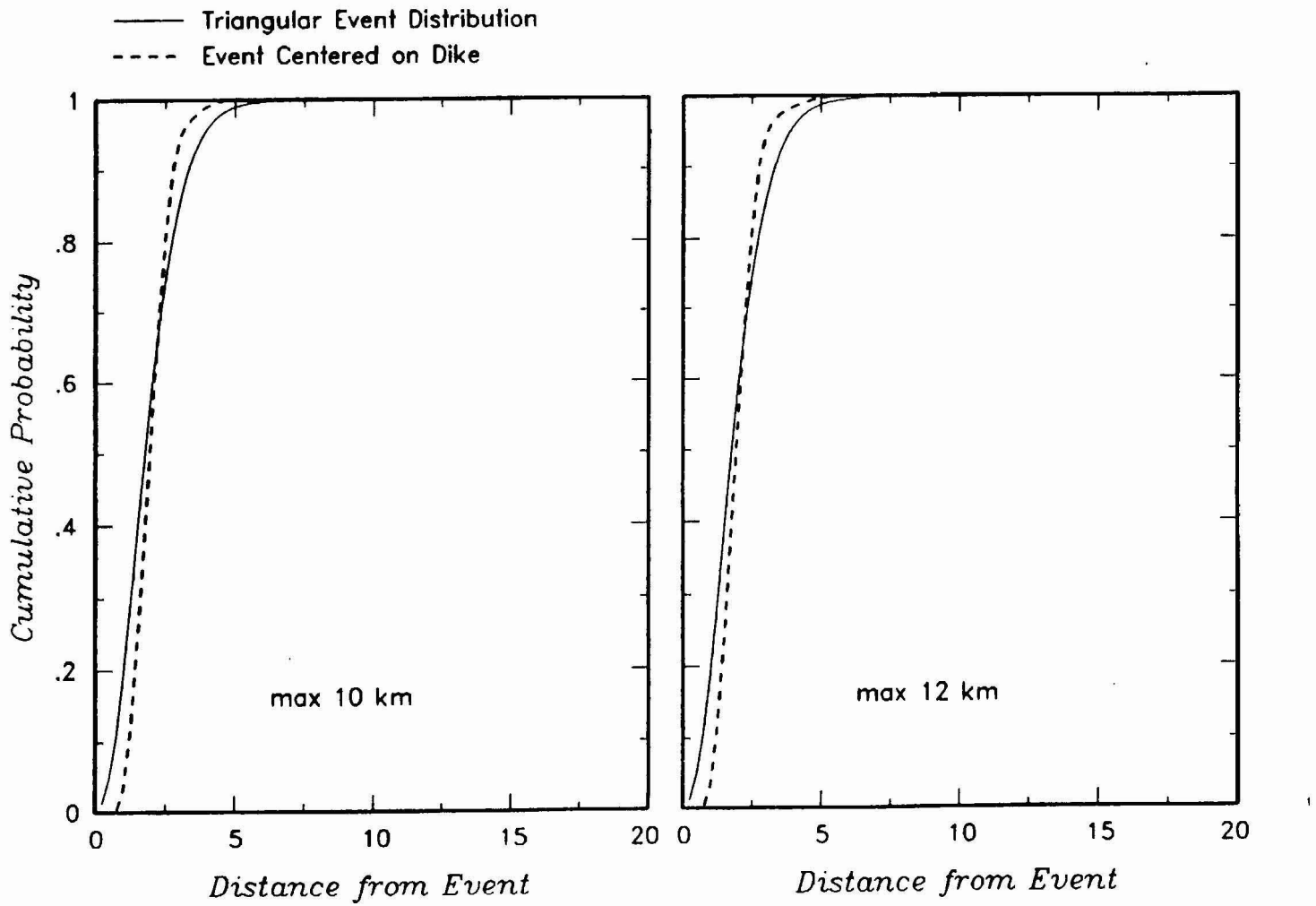

Figure 3-27 Alternative distributions for the length of an event *f(l)* developed from the assessments by George Thompson.

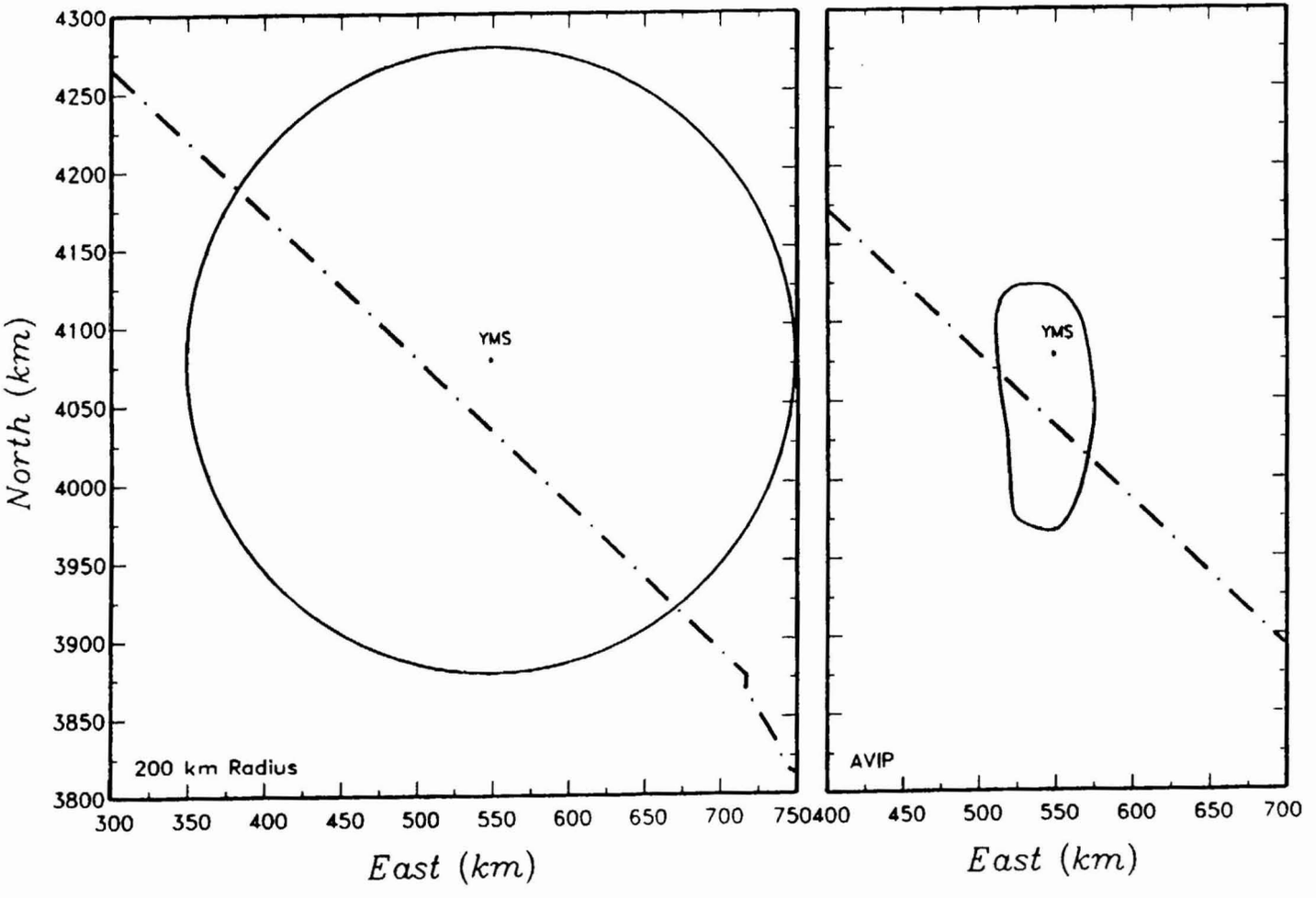

Figure 3-28 Alternative regions of interest used as background source zones in George Thompson's PVHA model. YMS refers to the proposed Yucca Mountain repository site and the dash-dot line is the Nevada-California border.

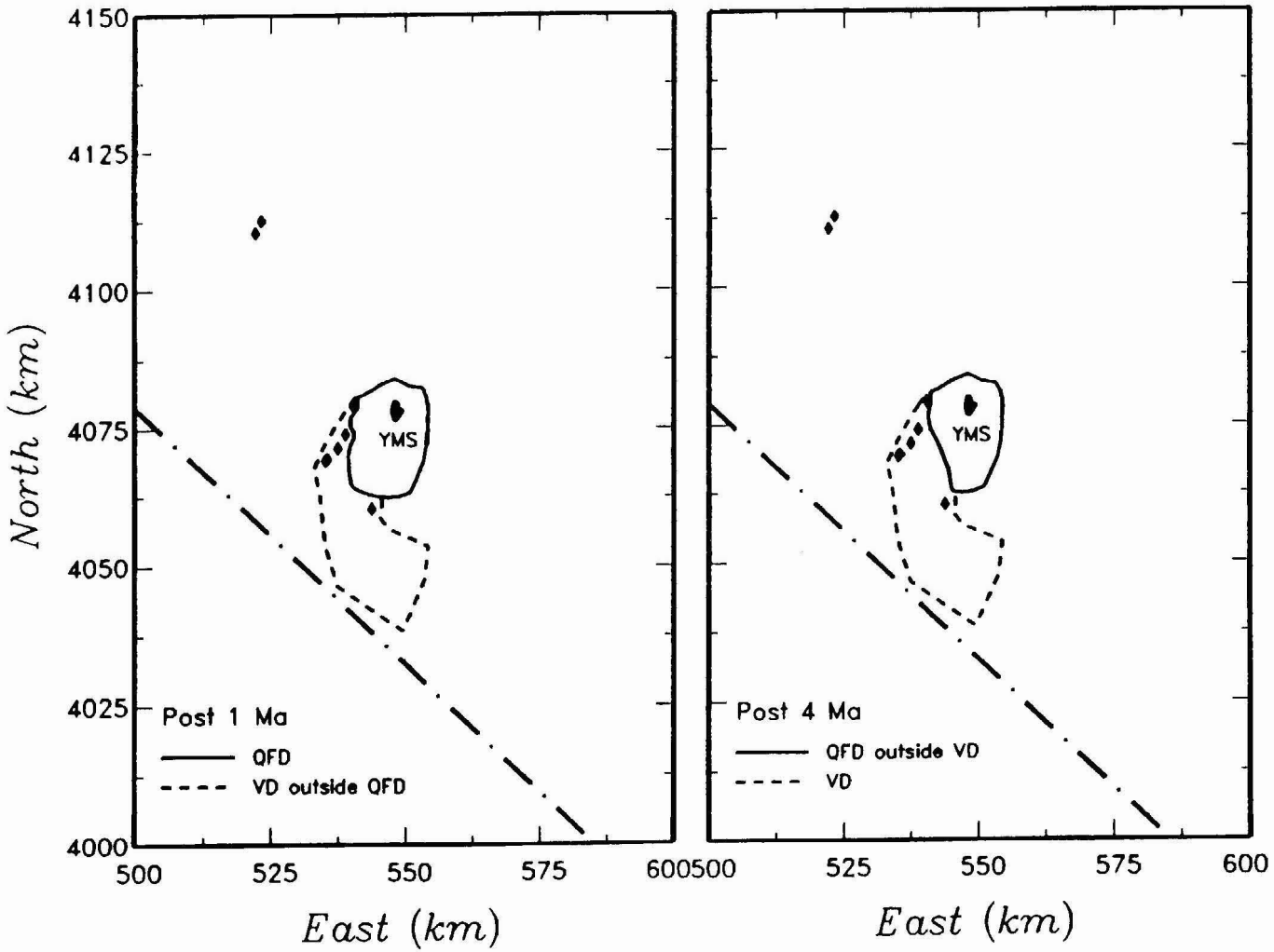

Figure 3-29 Alternative source zones defined by George Thompson. Diamonds represent volcanic events for the post-1 Ma and post-4 Ma time periods. YMS refers to the proposed Yucca Mountain repository site and the dash-dot line is the Nevada-California border.

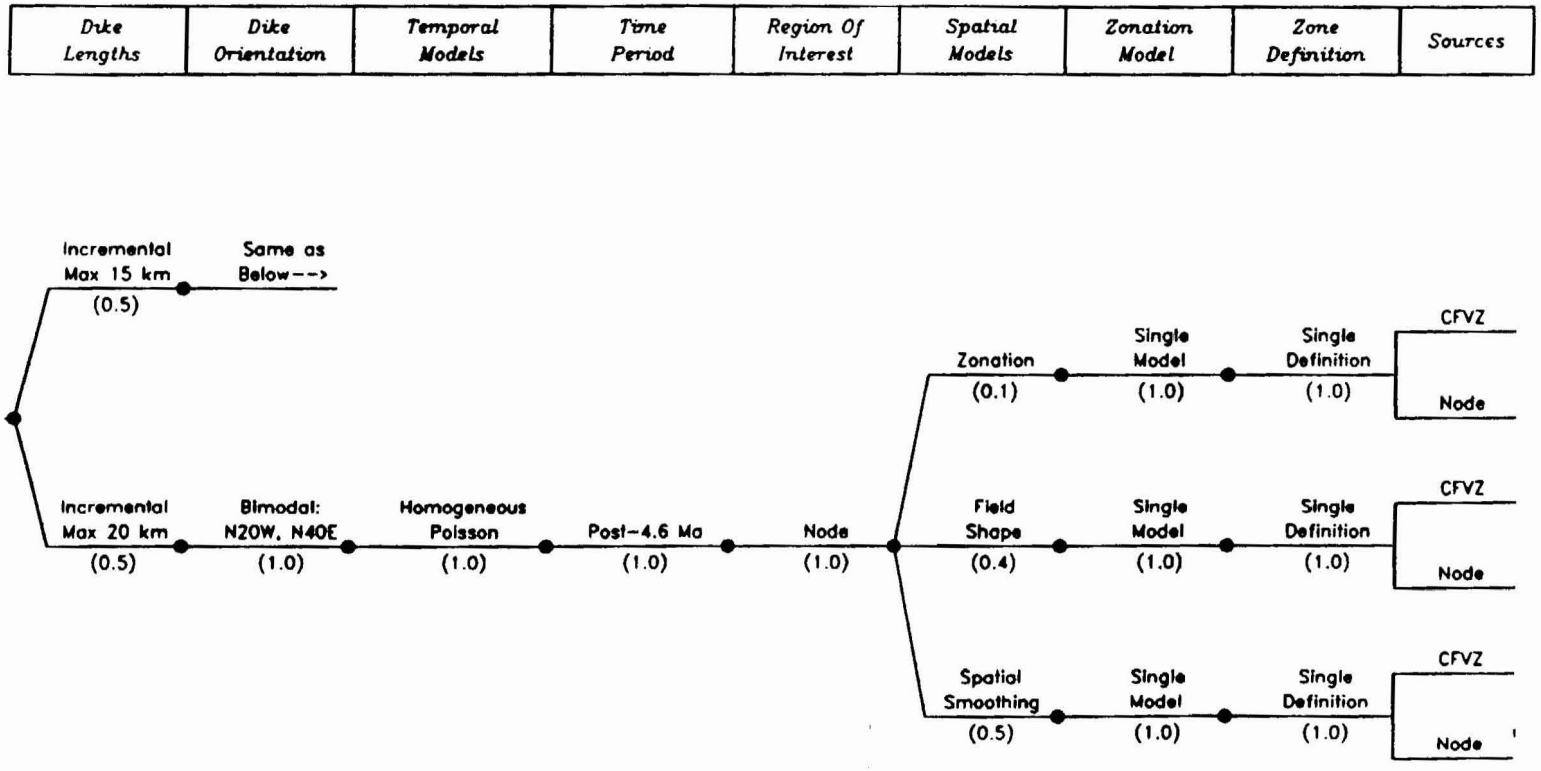

Figure 3-30 Logic tree for the PVHA model developed by George Walker.

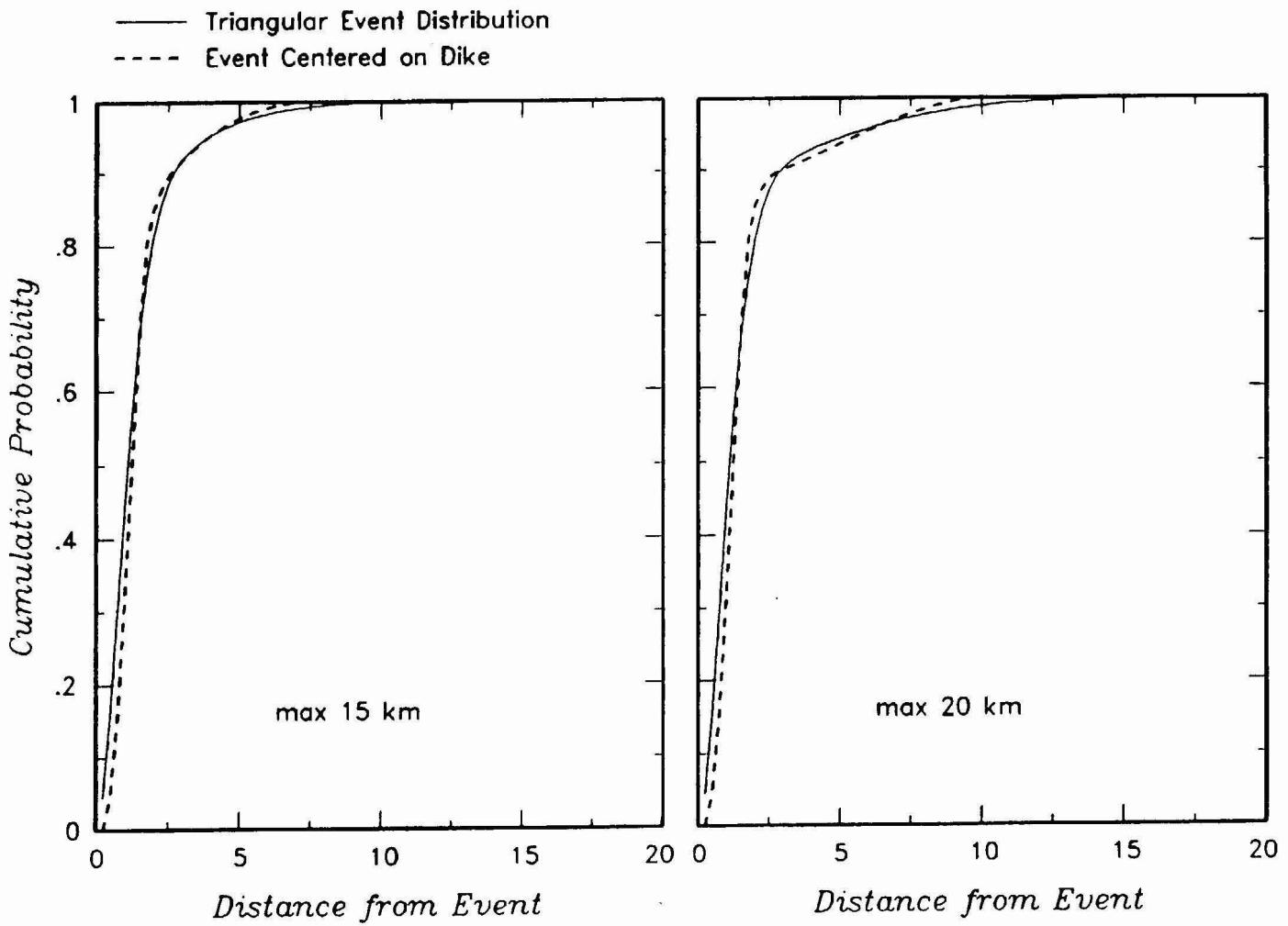

Figure 3-31 Alternative distributions for the length of an event *f(l)* developed from the assessments by George Walker.

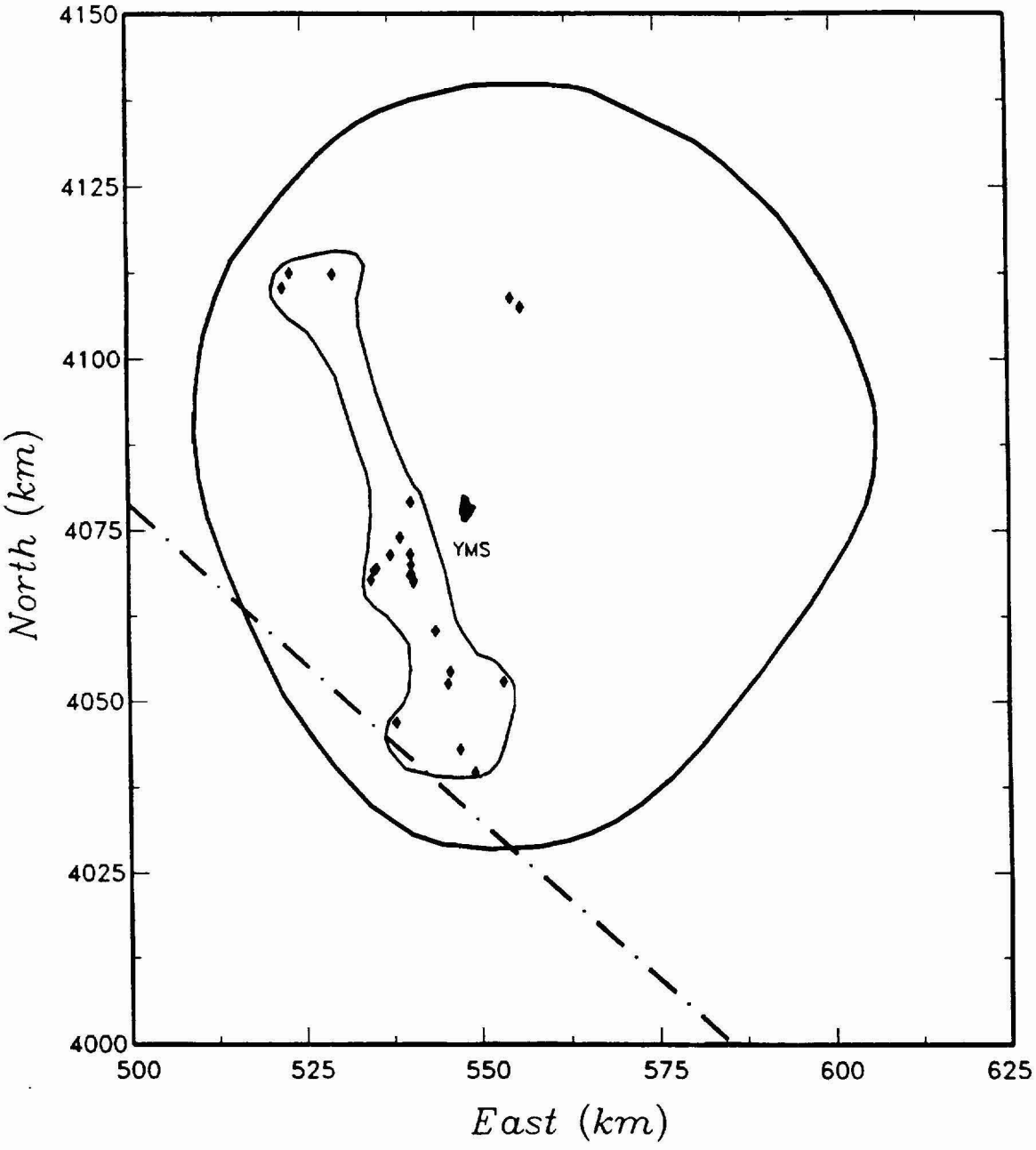

Figure 3-32 Volcanic source zone model developed by George Walker. Diamonds represent volcanic events for the post-5 Ma time period. YMS refers to the proposed Yucca Mountain repository site and the dash-dot line is the Nevada-California border.

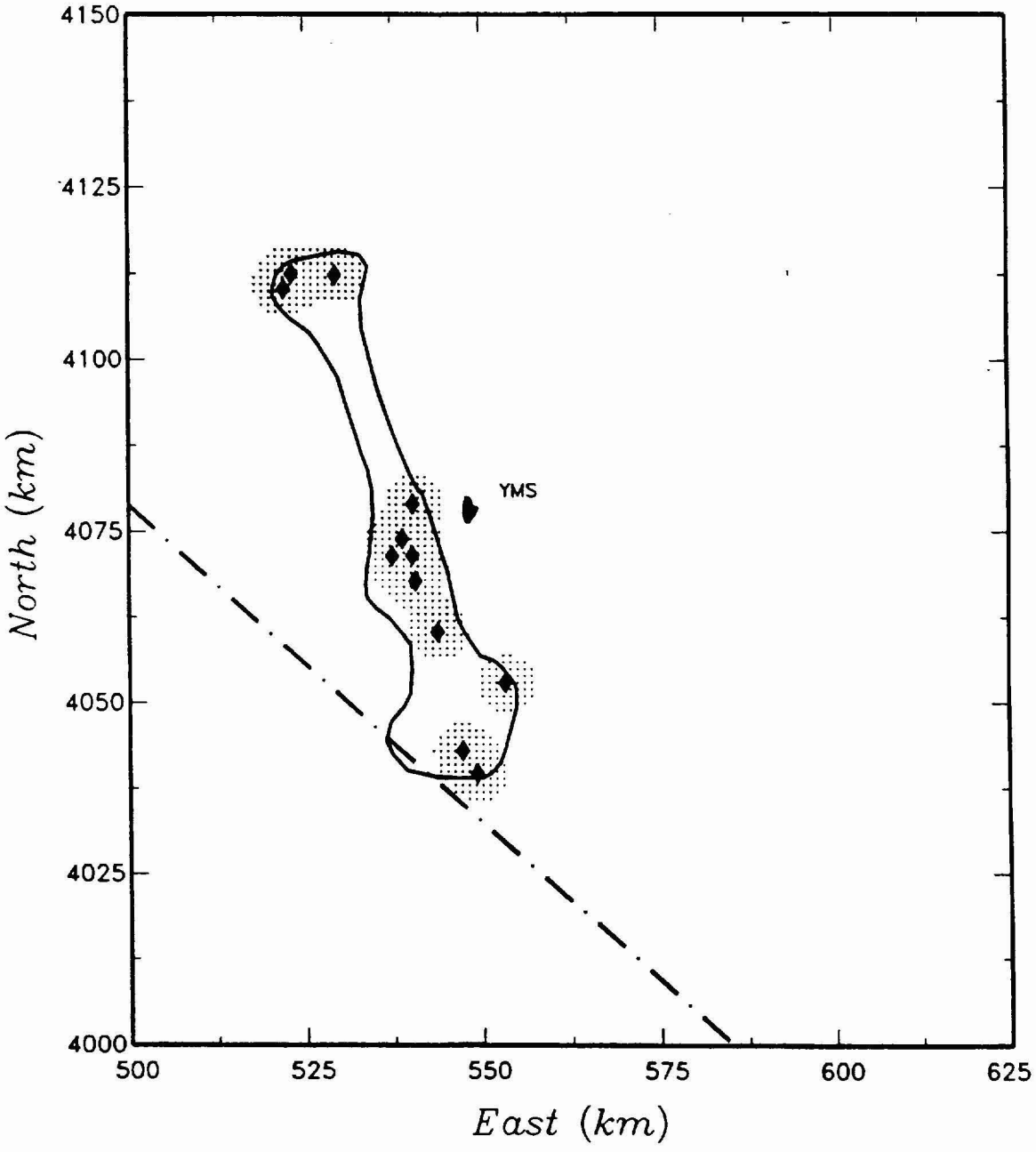

Figure 3-33 Example of a kernel density estimate based on George Walker's preferred event counts for the post-5 Ma time period (shown by diamonds) and the Crater Flat Volcanic Zone representing an approximation of the 90-percent density contour (the stippled area). The resulting Epanechnikov kernel smoothing parameter, *h*, is 5.8 km. YMS refers to the proposed Yucca Mountain repository site and the dash-dot line is the Nevada-California border.

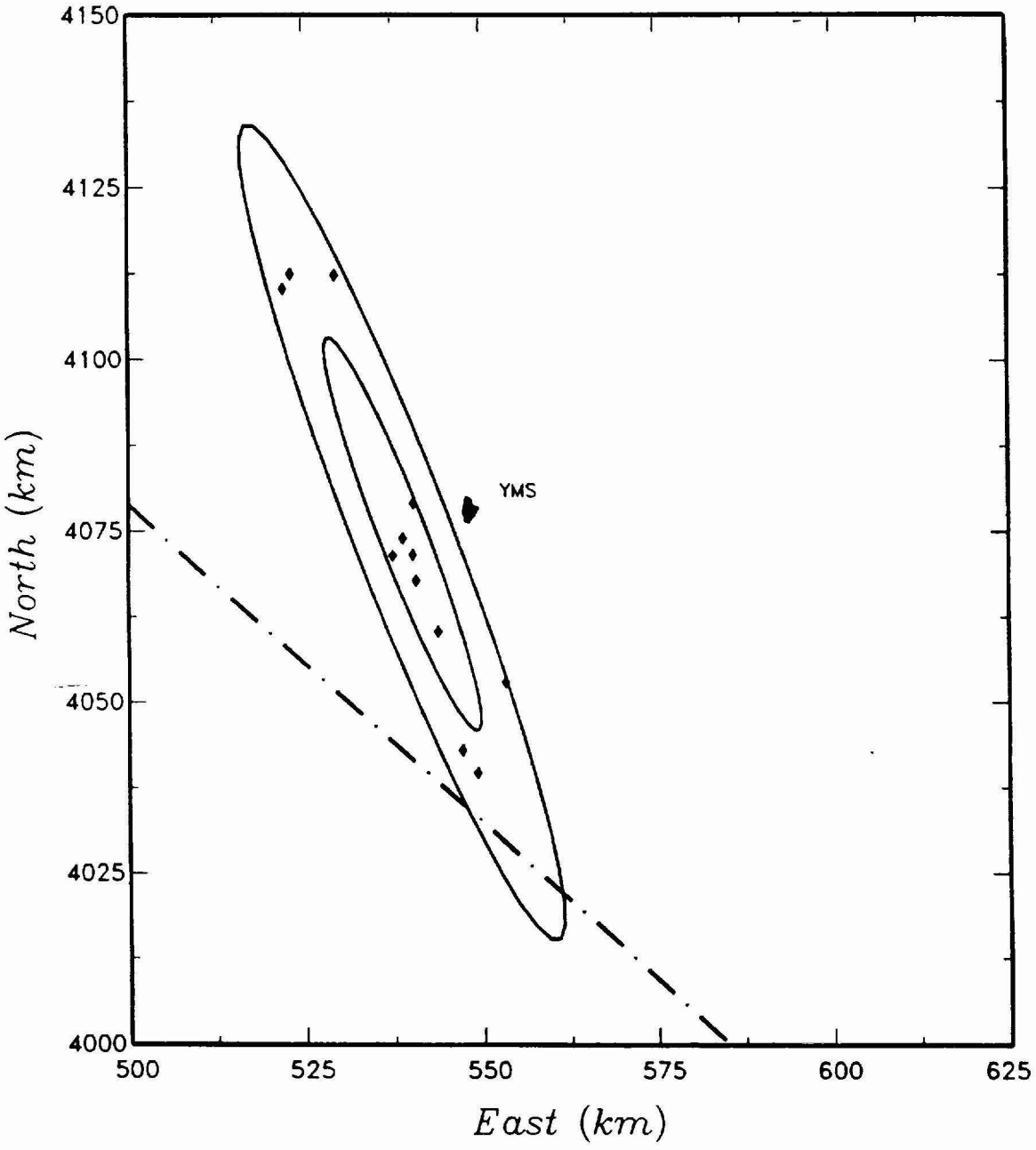

Figure 3-34 Example of the fit of a Gaussian field to George Walker's preferred event counts for the post-5 Ma time period (shown by diamonds) in the Crater Flat Volcanic Zone. The 50th and 95th percentile density contours are shown. YMS refers to the proposed Yucca Mountain repository site and the dash-dot line is the Nevada-California border.

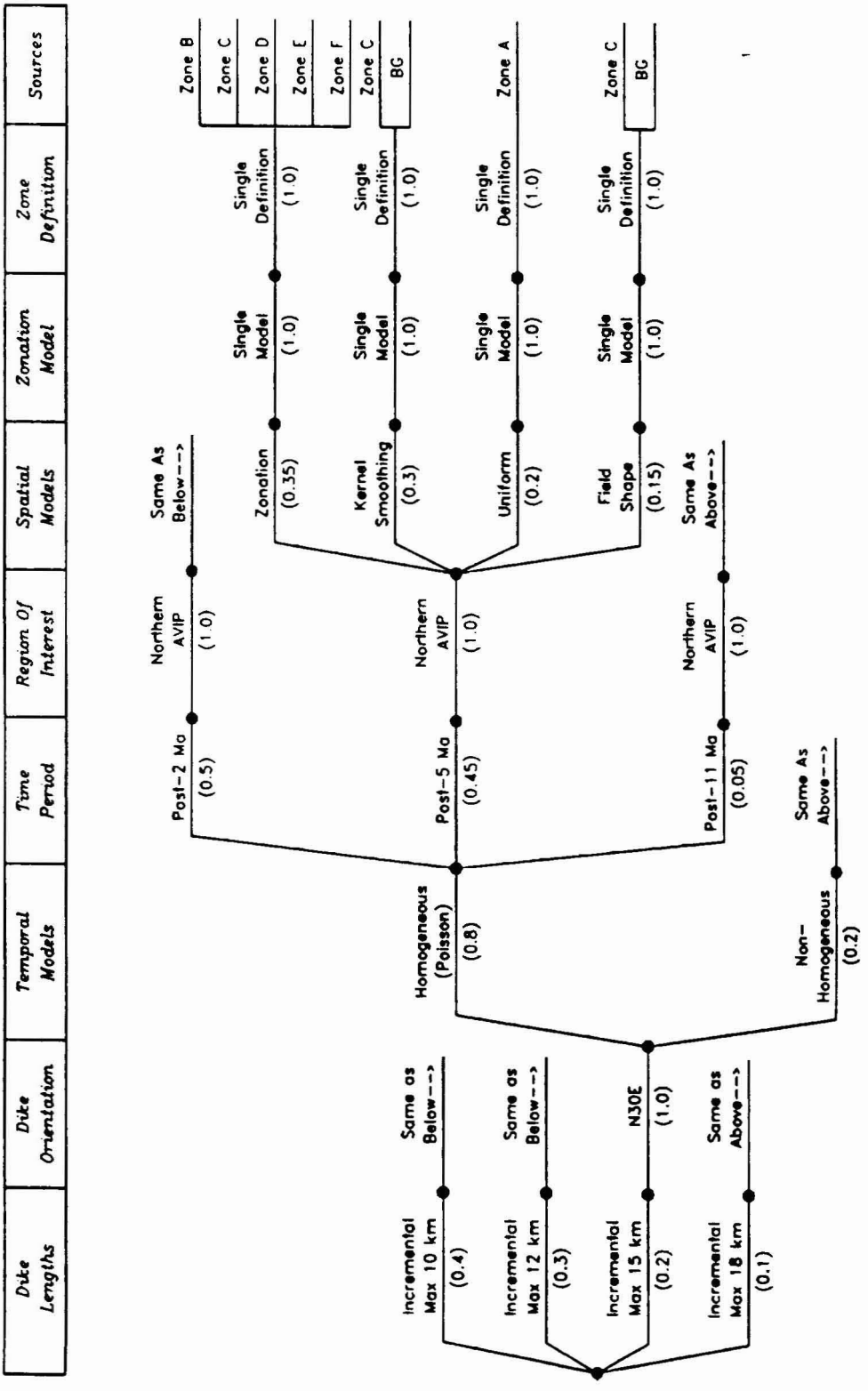

Figure 3-35 Logic tree for the PVHA model developed by Mel Kuntz.

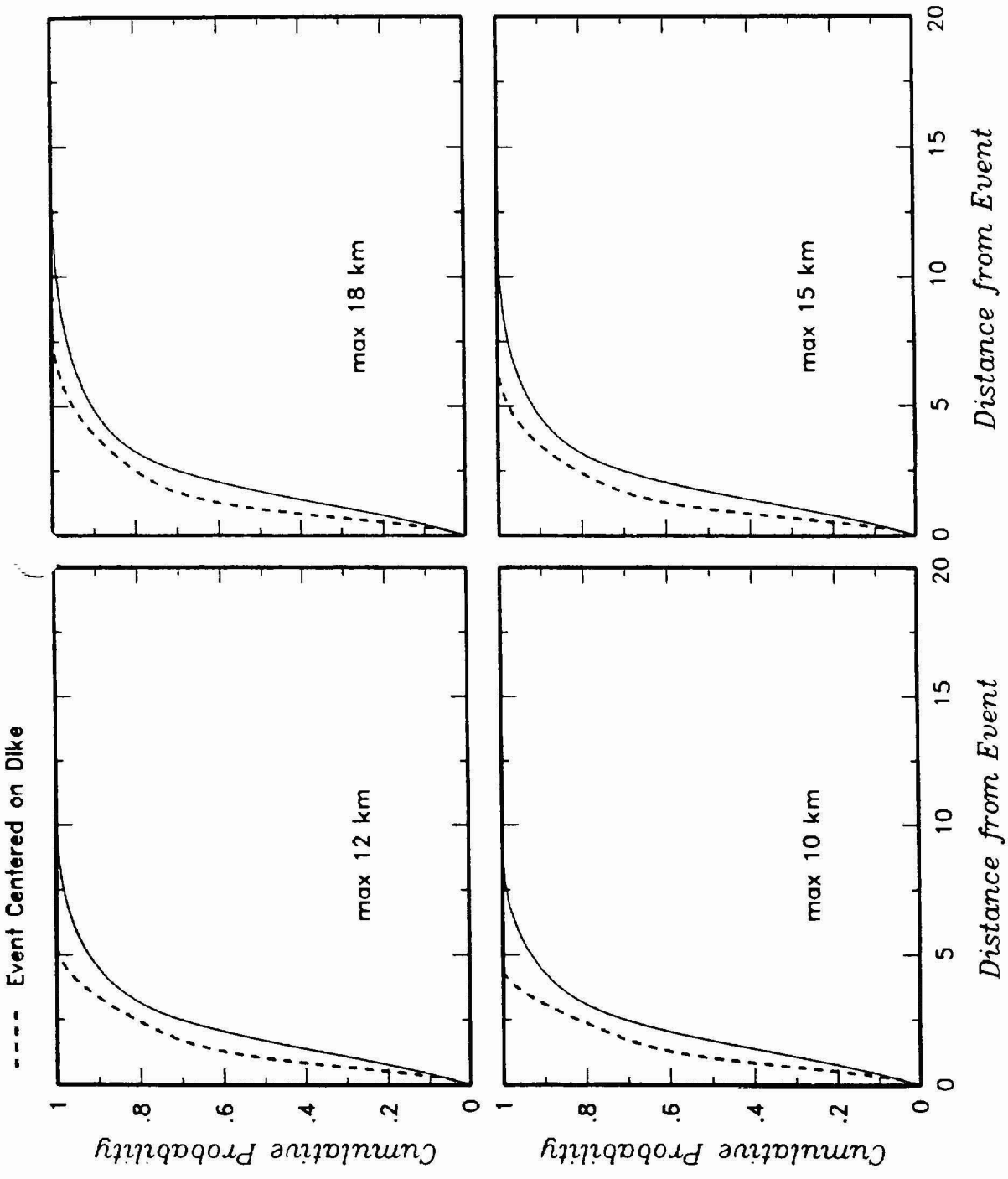

Figure 3-36 Alternative distributions for the length of an event *f(l)* developed from the assessments by Mel Kuntz.

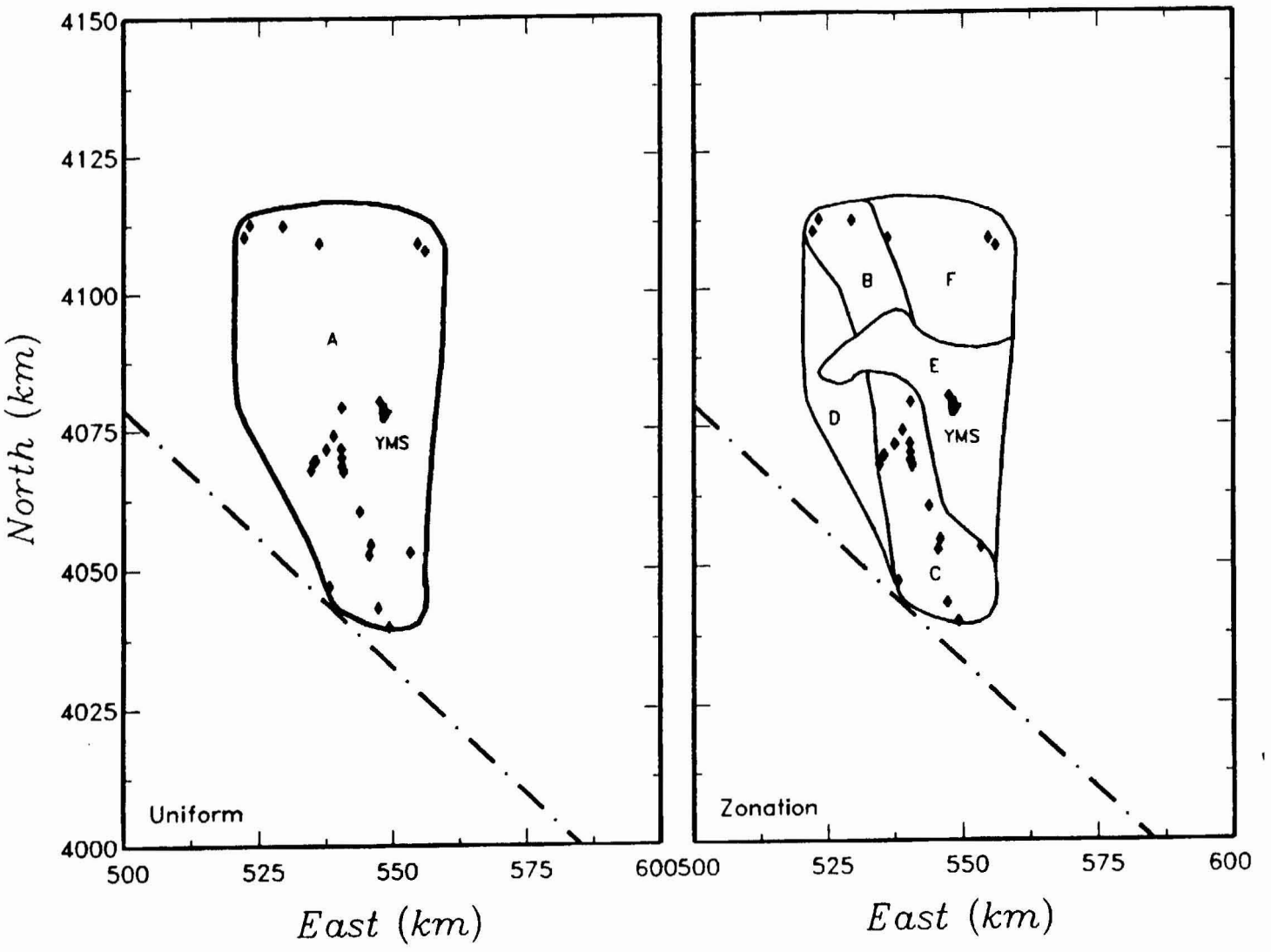

Figure 3-37 Region of interest and volcanic source zone model developed by Mel Kuntz. Diamonds represent volcanic events for the post-11 Ma time period. YMS refers to the proposed Yucca Mountain repository site and the dash-dot line is the Nevada-California border.

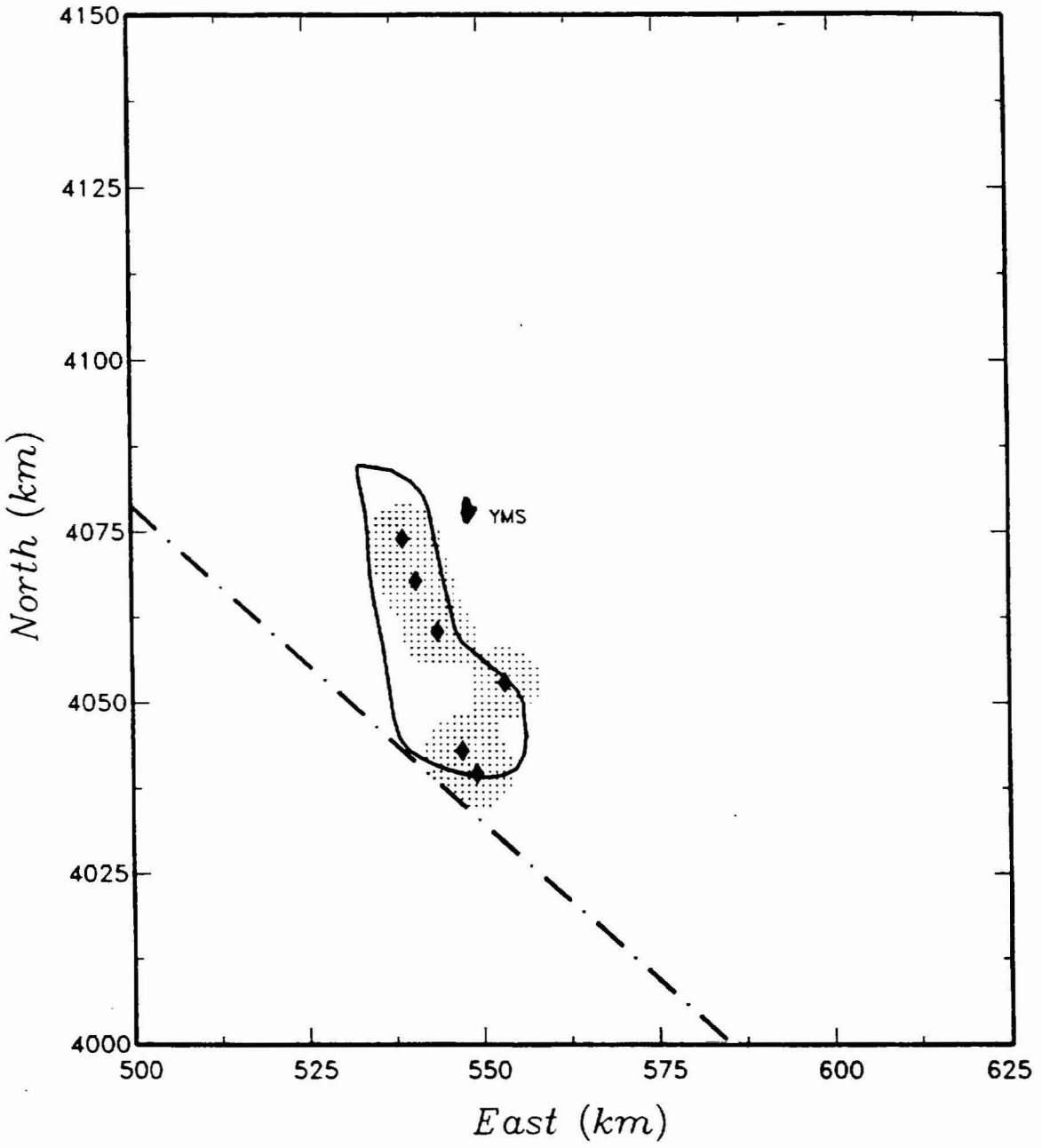

Figure 3-38 Example of a kernel density estimate based on Mel Kuntz's preferred event counts for the post-5 Ma time period (shown by diamonds) and Zone C (Crater Flat) representing an approximation of the 90-percent density contour (the stippled area). The resulting Gaussian kernel smoothing parameter, *h*, is 2.8 km. YMS refers to the proposed Yucca Mountain repository site and the dash-dot line is the Nevada-California border.

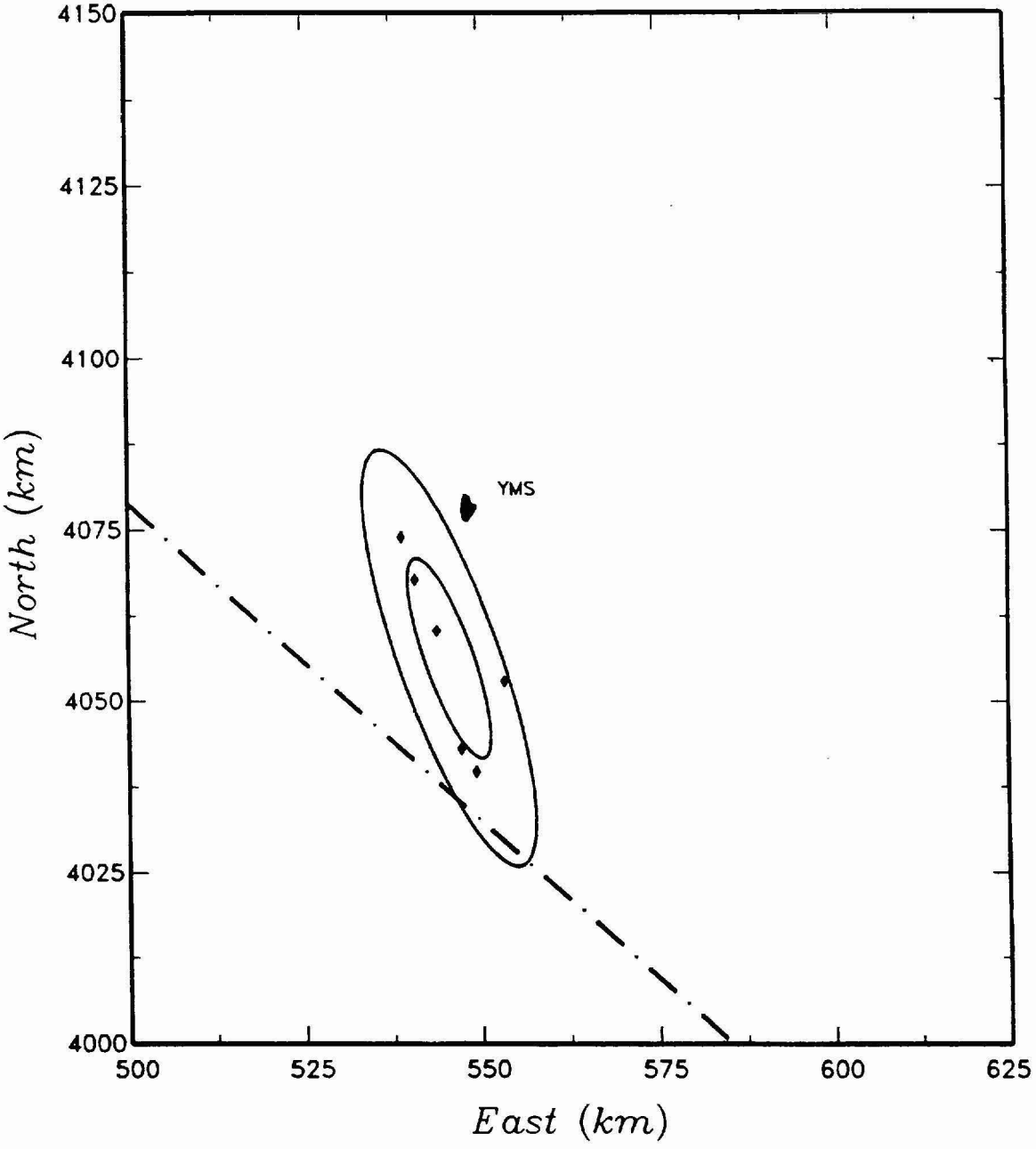

Figure 3-39 Example of the fit of a Gaussian field to Mel Kuntz's preferred event counts for the post-5 Ma time period (shown by diamonds) in Zone C (Crater Flat). The 50th and 95th percentile density contours are shown. YMS refers to the proposed Yucca Mountain repository site and the dash-dot line is the Nevada-California border.

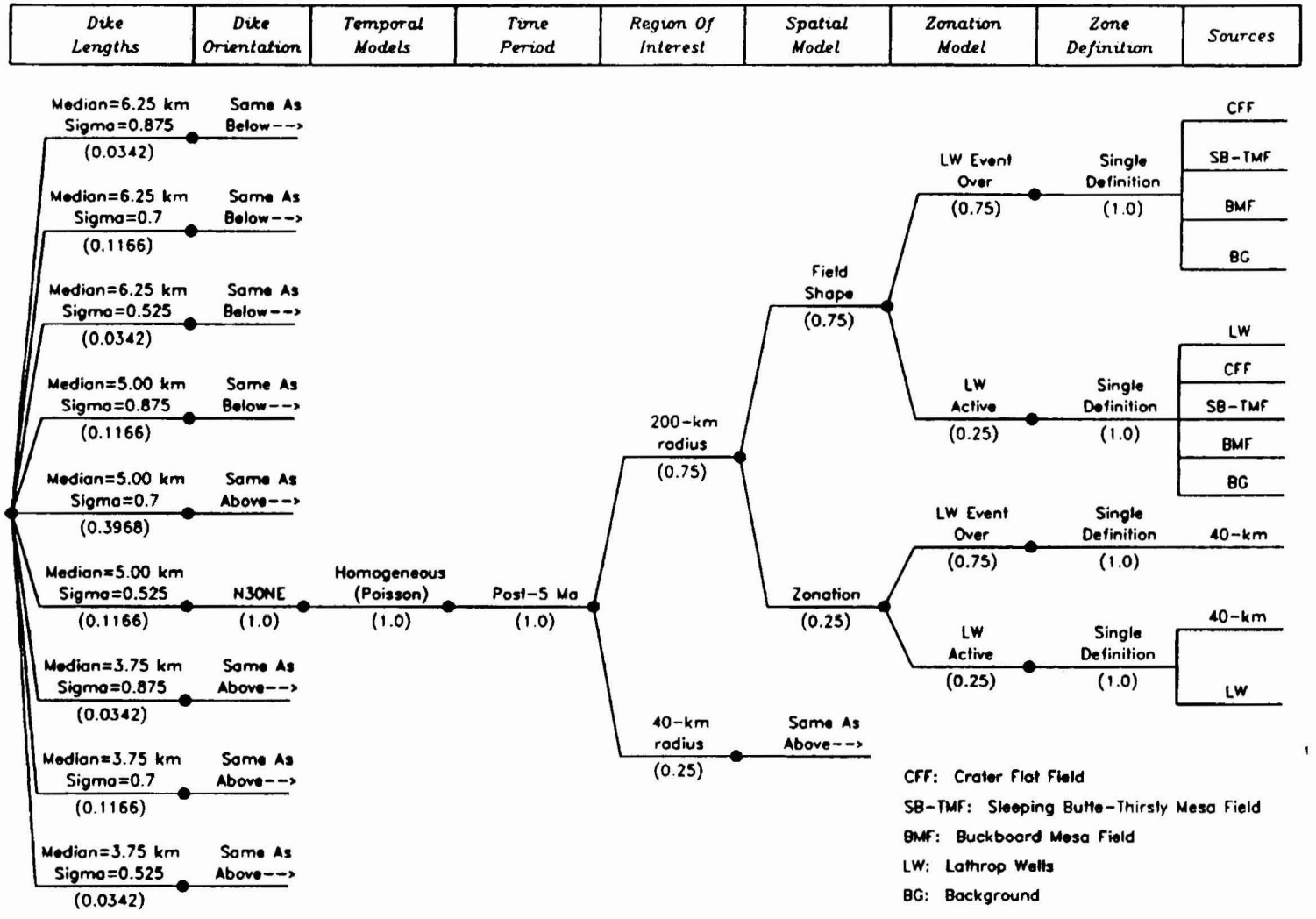

Figure 3-40 Logic tree for the PVHA model developed by Michael Sheridan.

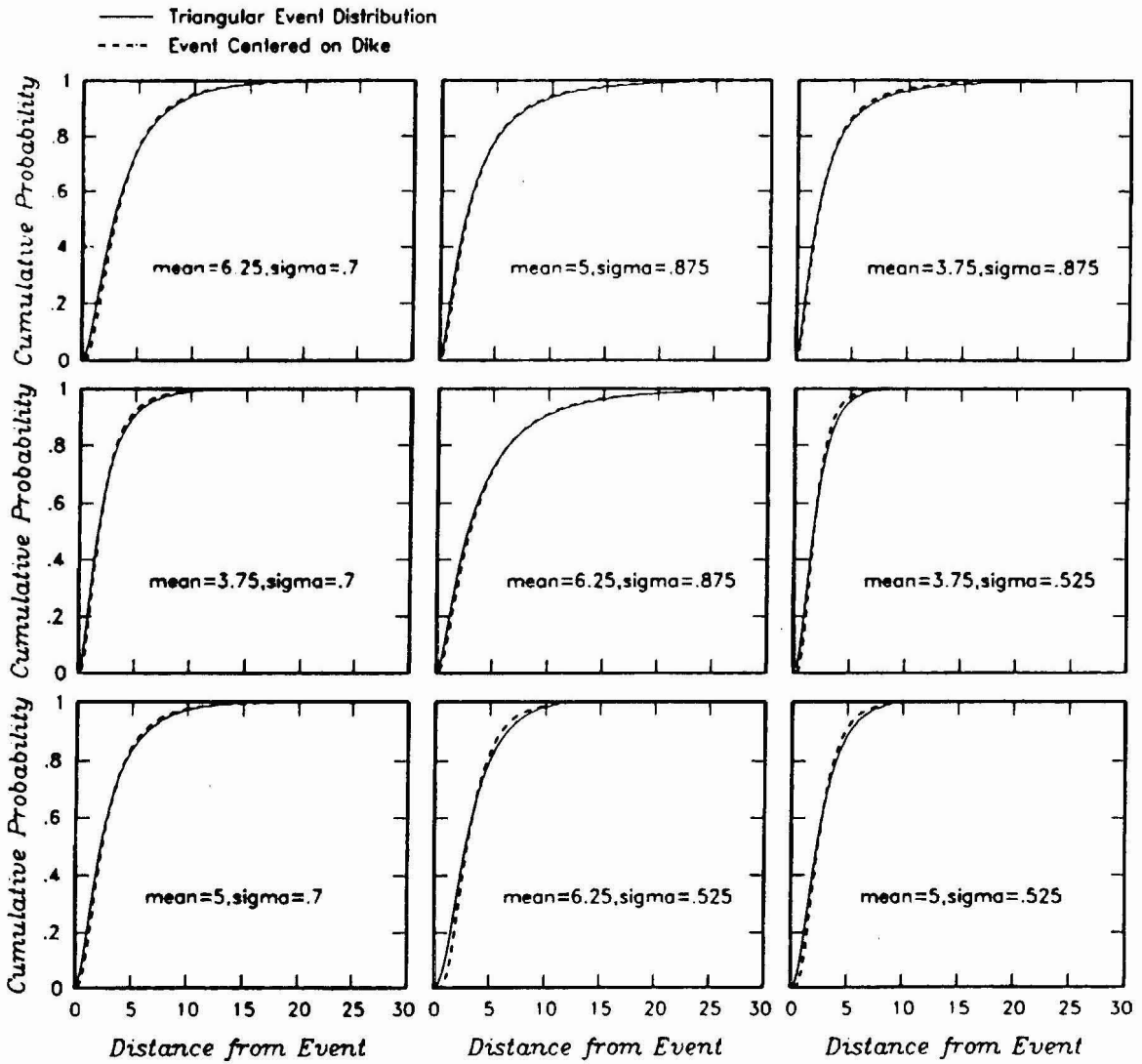

Figure 3-41 Alternative distributions for the length of an event *f(l)* developed from the assessments by Michael Sheridan.

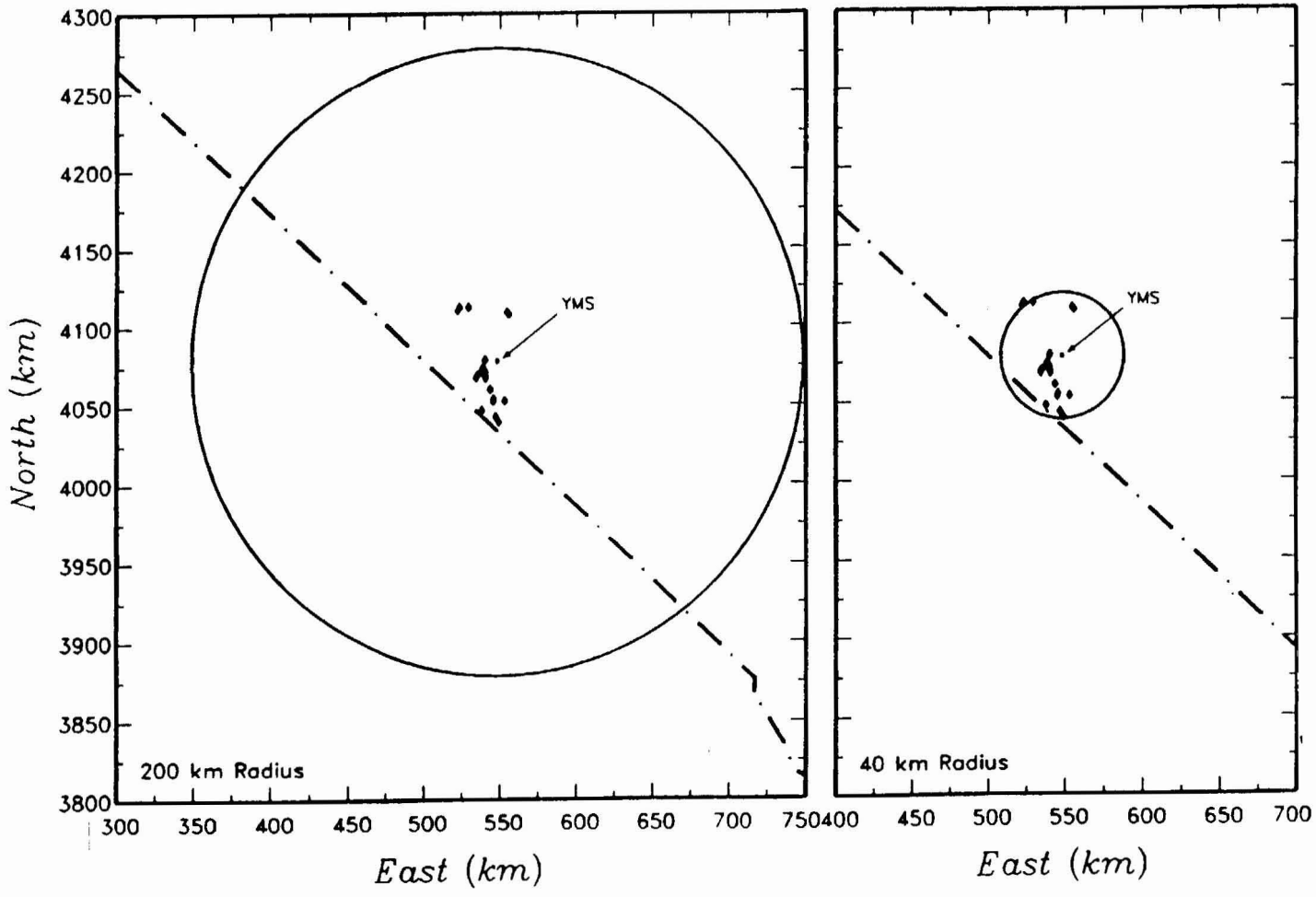

Figure 3-42 Regions of interest specified by Michael Sheridan. Diamonds represent volcanic events for the post-5 Ma time period. YMS refers to the proposed Yucca Mountain repository site and the dash-dot line is the Nevada-California border.

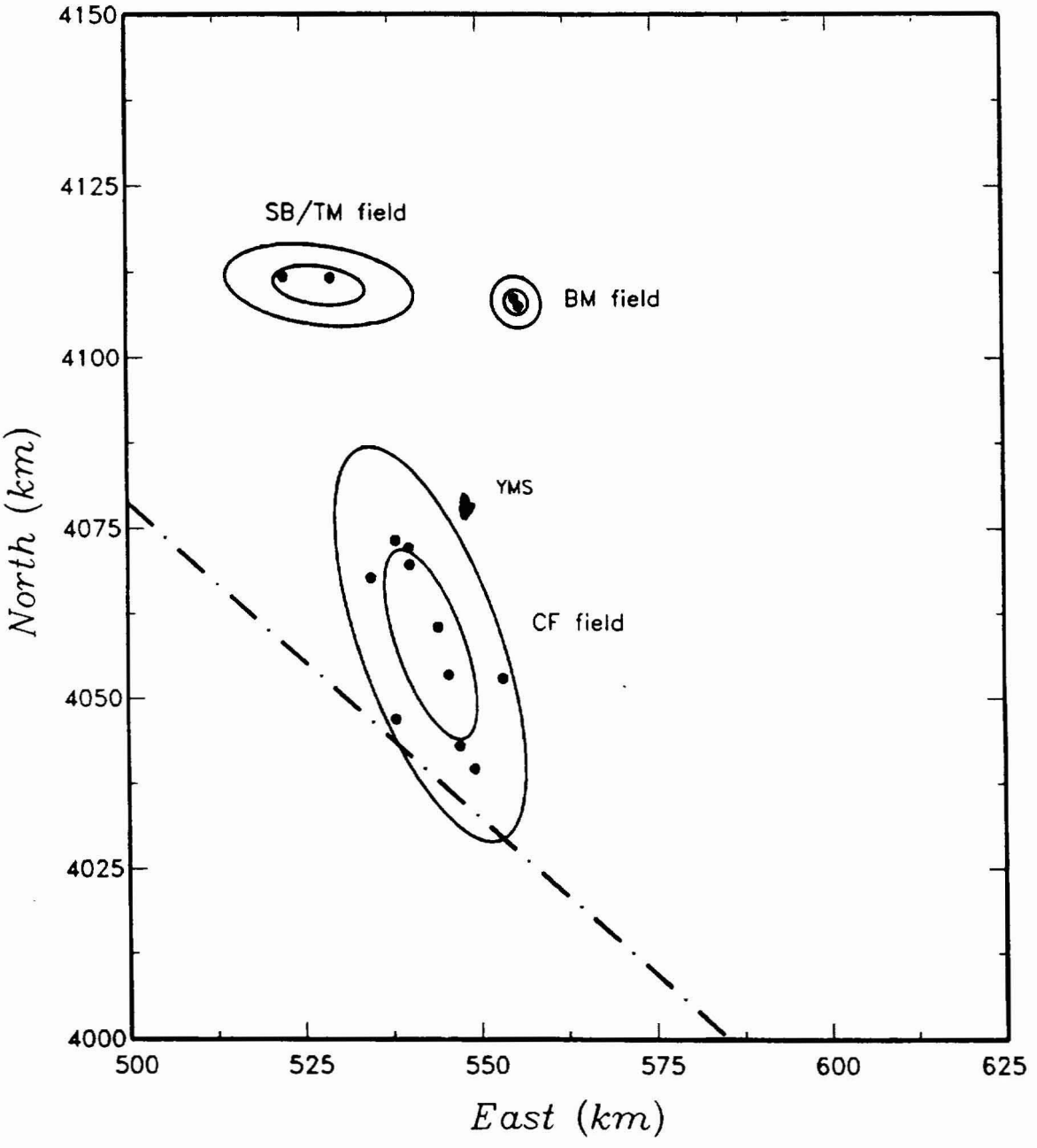

Figure 3-43 Example of the fit of Gaussian fields to Michael Sheridan's preferred event counts for the Crater Flat (CF), Sleeping Butte/Thirsty Mesa (SB/TM), and Buckboard Mesa (BM) fields. The 50th and 95th percentile contours are shown. YMS refers to the proposed Yucca Mountain repository site and the dash-dot line is the Nevada-California border.

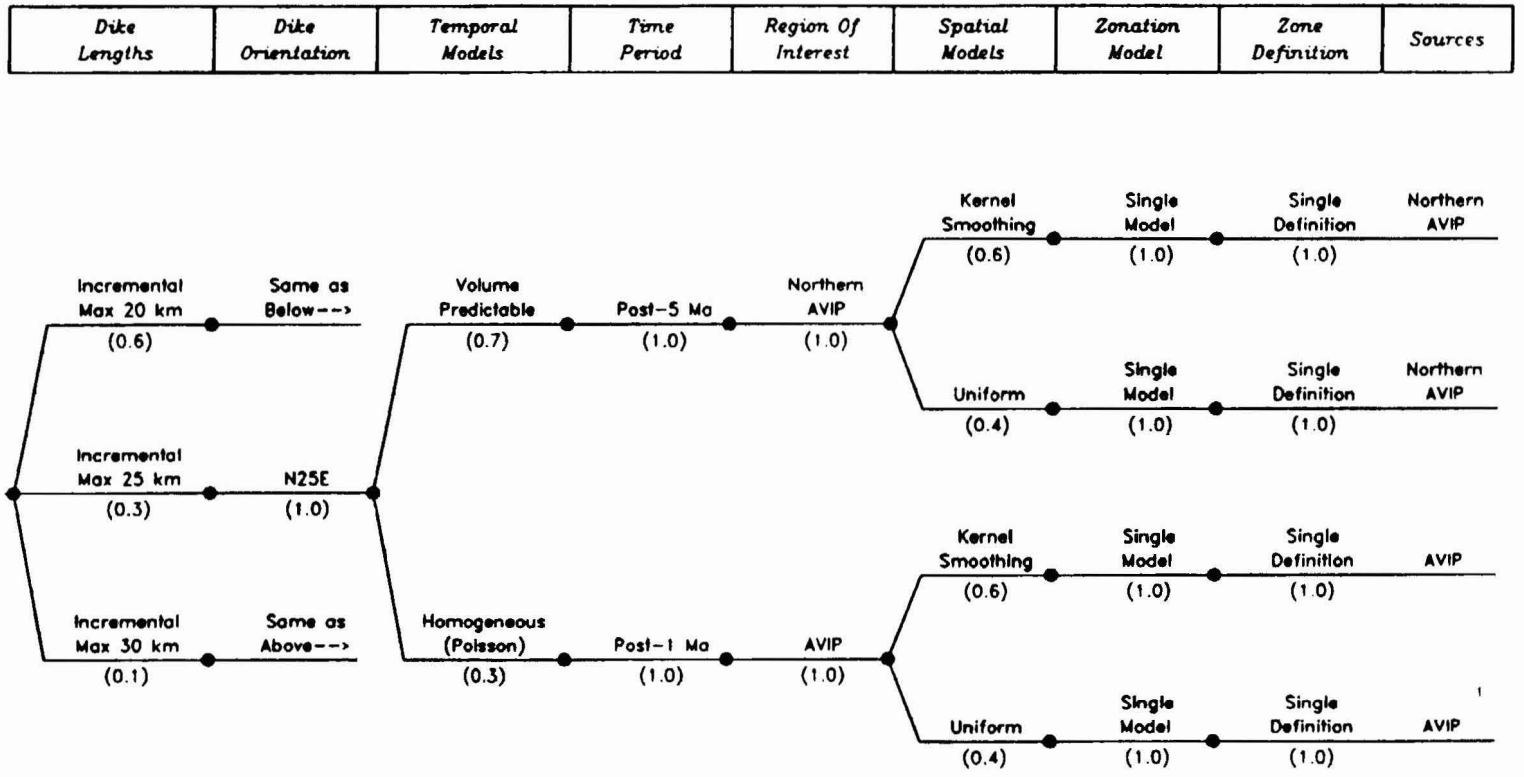

Figure 3-44 Logic tree for the PVHA model developed by Richard Carlson.

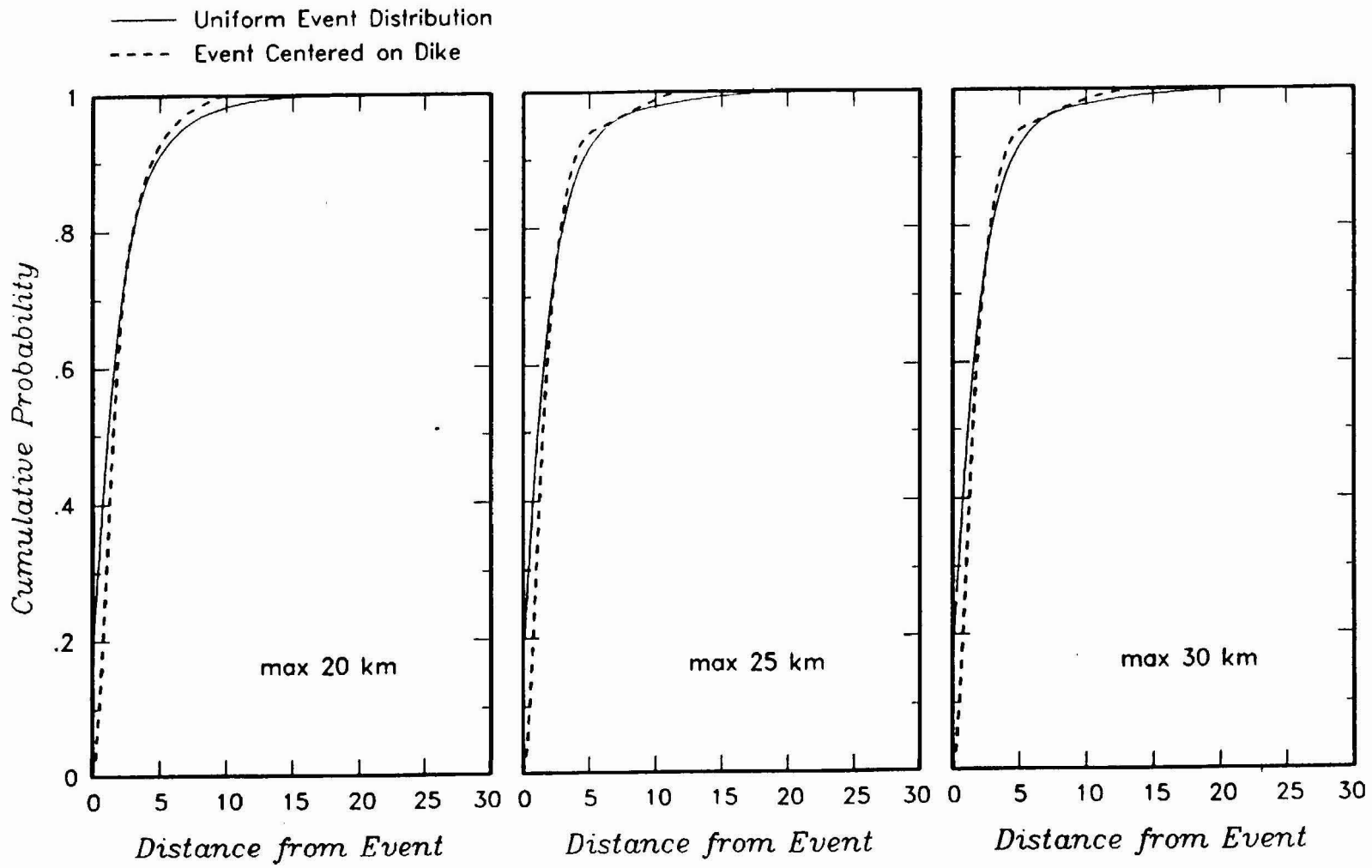

Figure 3-45 Alternative distributions for the length of an event *f(l)* developed from the assessments by Richard Carlson.

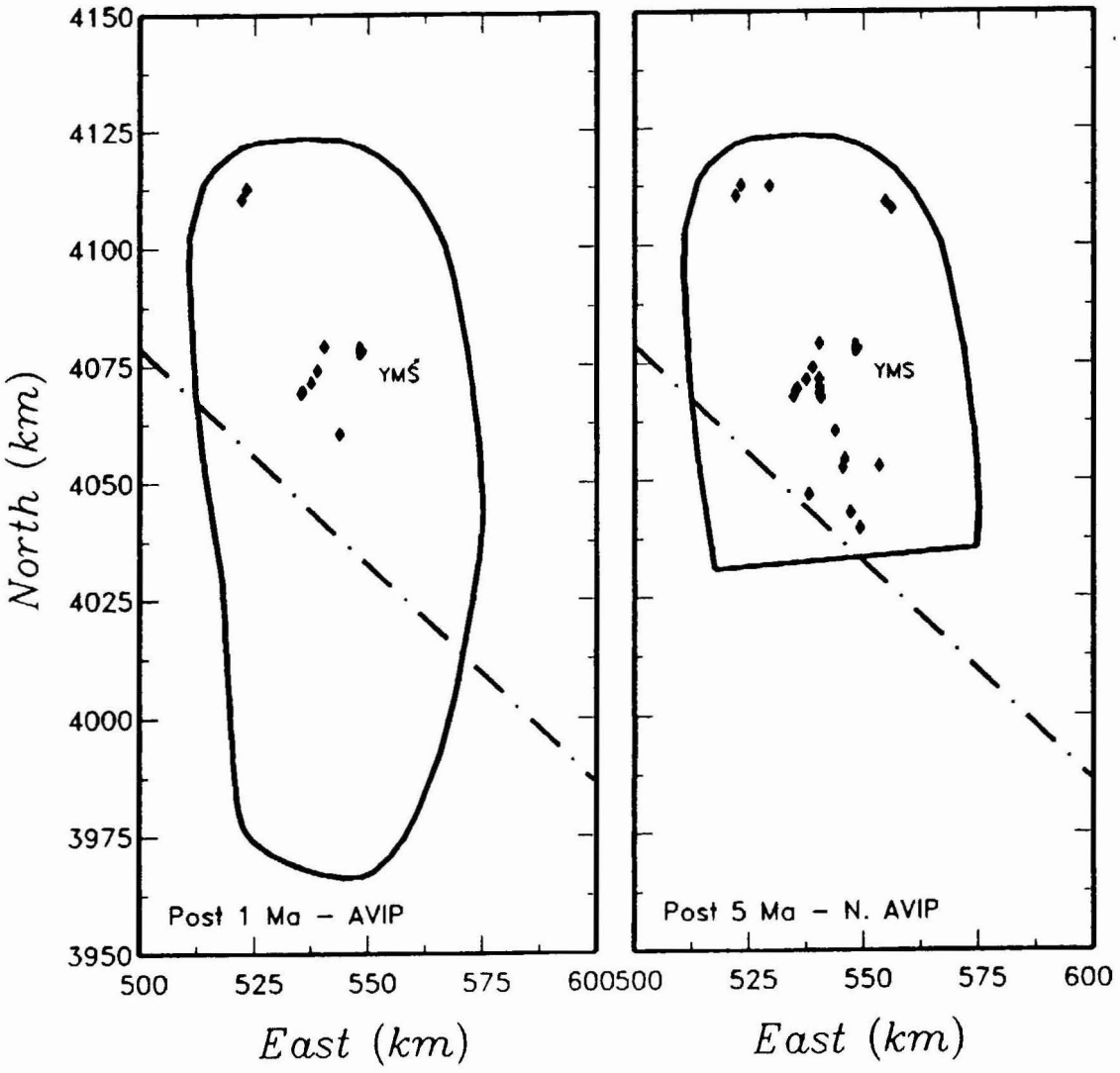

Figure 3-46 Regions of interest specified by Richard Carlson. Diamonds represent volcanic events for the post-1 Ma and the post-5 Ma time periods. YMS refers to the proposed Yucca Mountain repository site and the dash-dot line is the Nevada-California border.

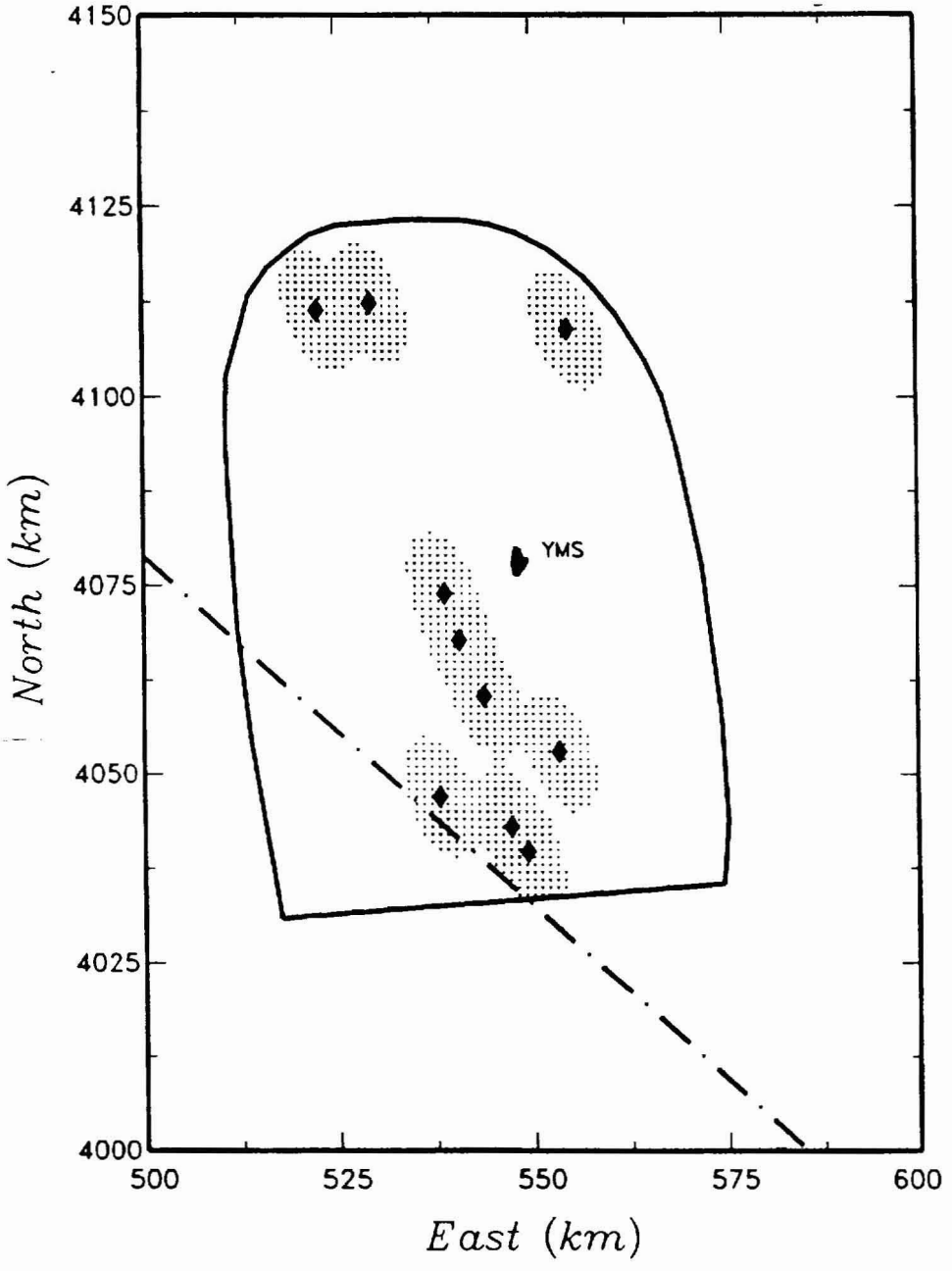

Figure 3-47 Example of the fit of an Epanechnikov kernel with a 2:1 aspect ratio and *h* for the major axis of 10 km to Richard Carlson's preferred event counts for the northern AVIP region and the post-5 Ma time period. The stippled area outlines the 95th percentile density contour. YMS refers to the proposed Yucca Mountain repository site and the dash-dot line is the Nevada-California border.

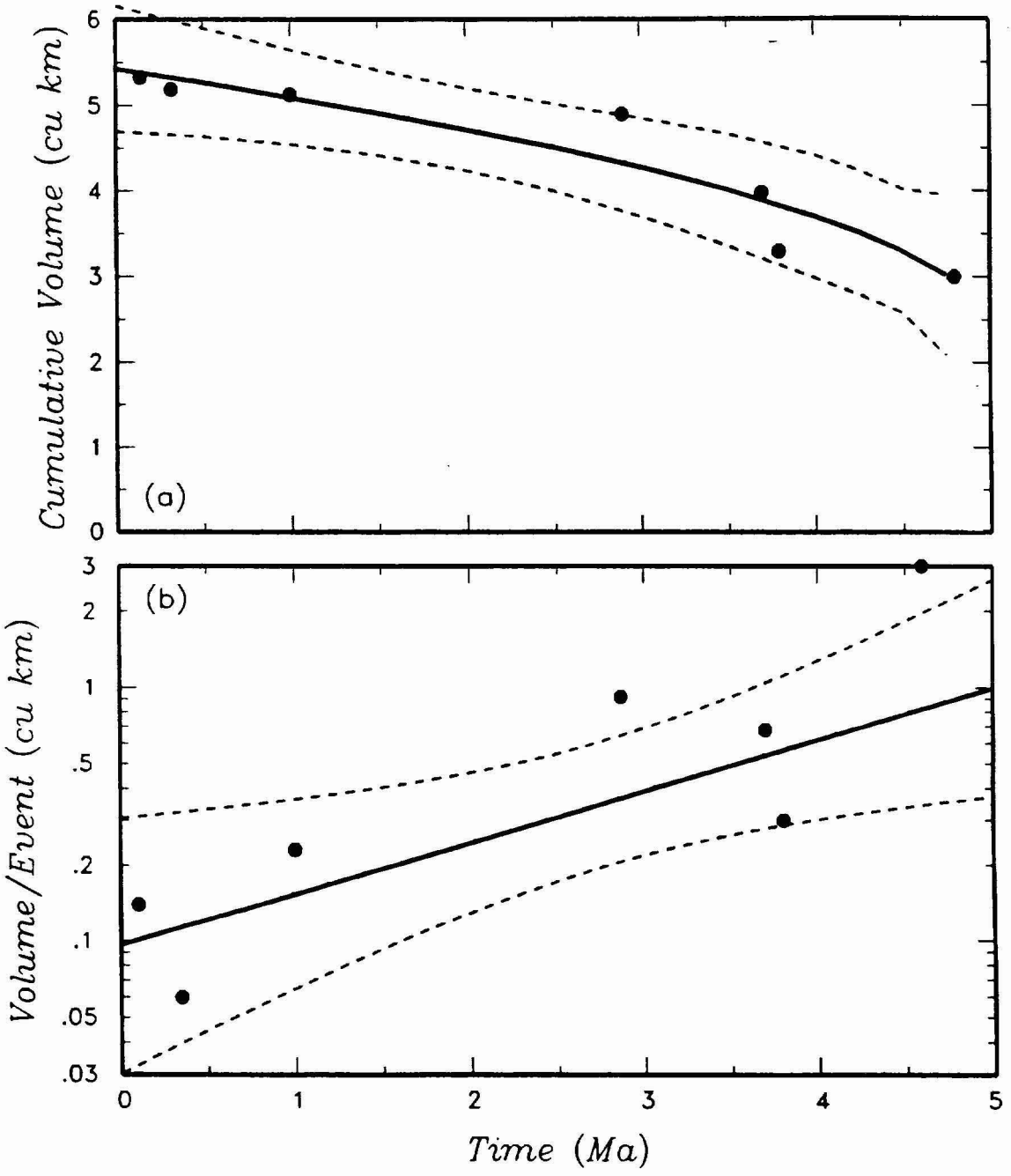

Figure 3-48 Parameters for the volume predictable rate model used by Richard Carlson. (a) Relationship for cumulative volume $V_M(t)$. (b) Example of relationship for volume per event, $V_E(t)$ computed for the most likely event counts in the northern AVIP zone.

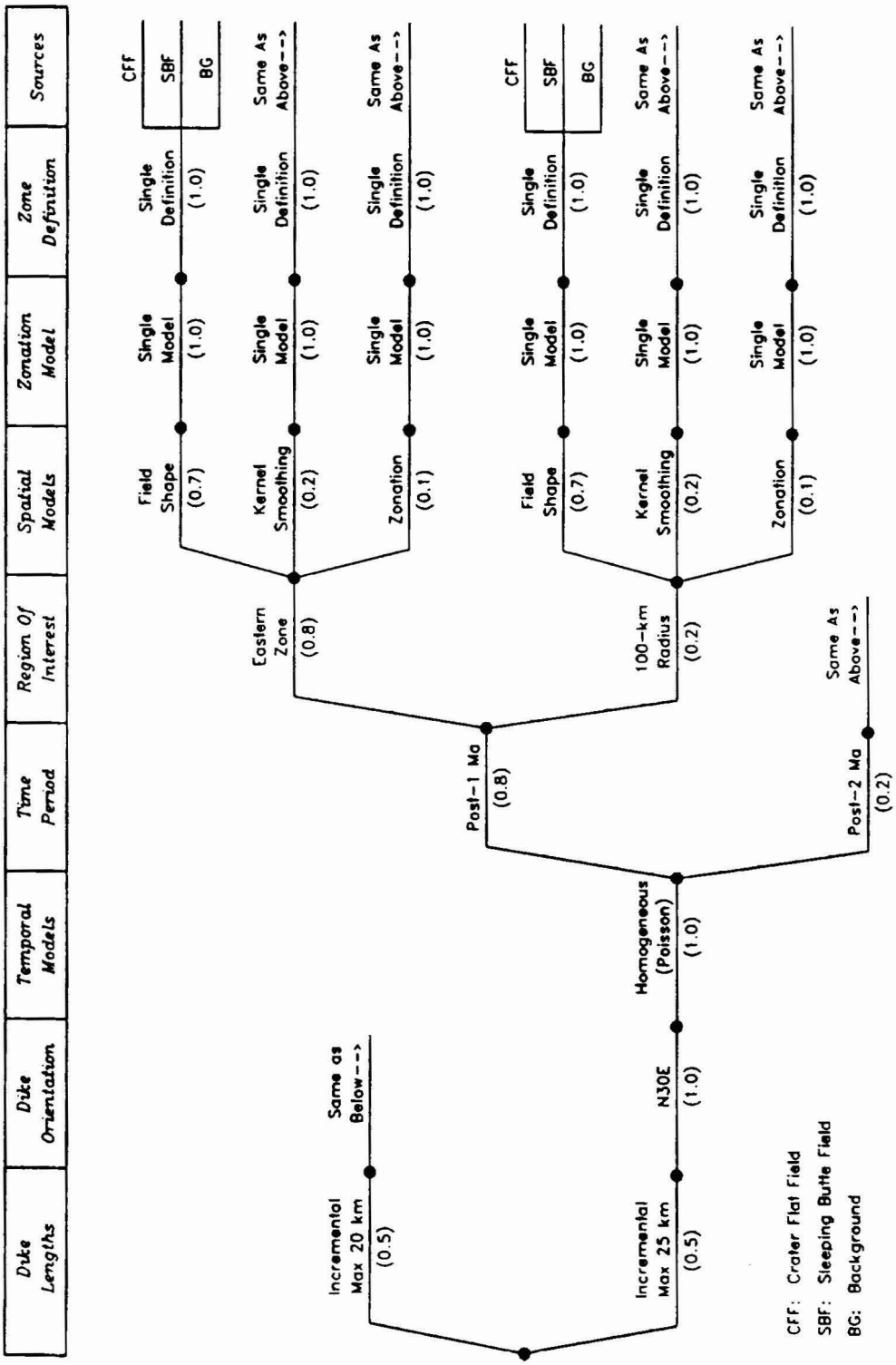

Figure 3-49 Logic tree for the PVHA model developed by Richard Fisher.

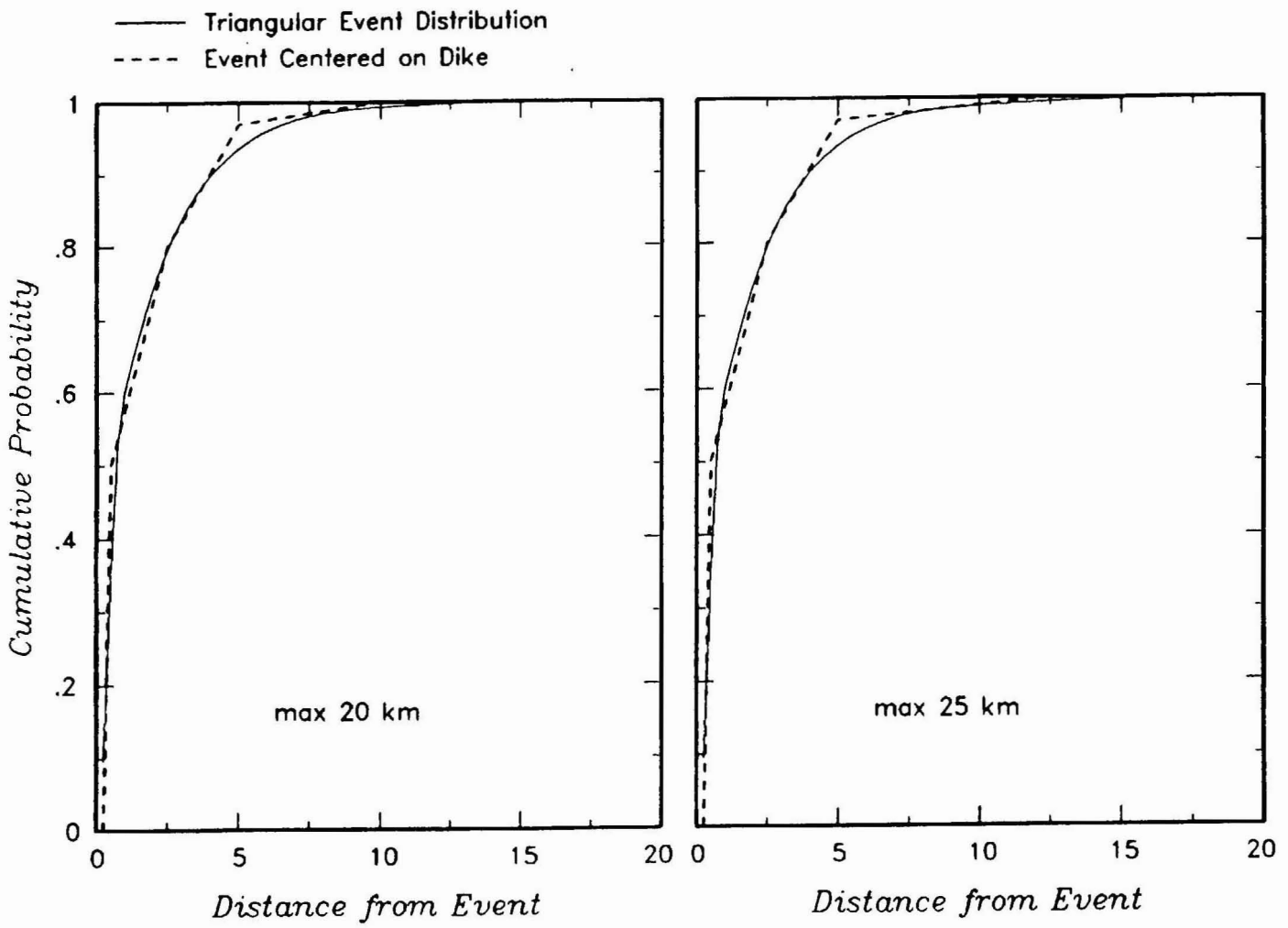

Figure 3-50 Alternative distributions for the length of an event *f(l)* developed from the assessments by Richard Fisher.

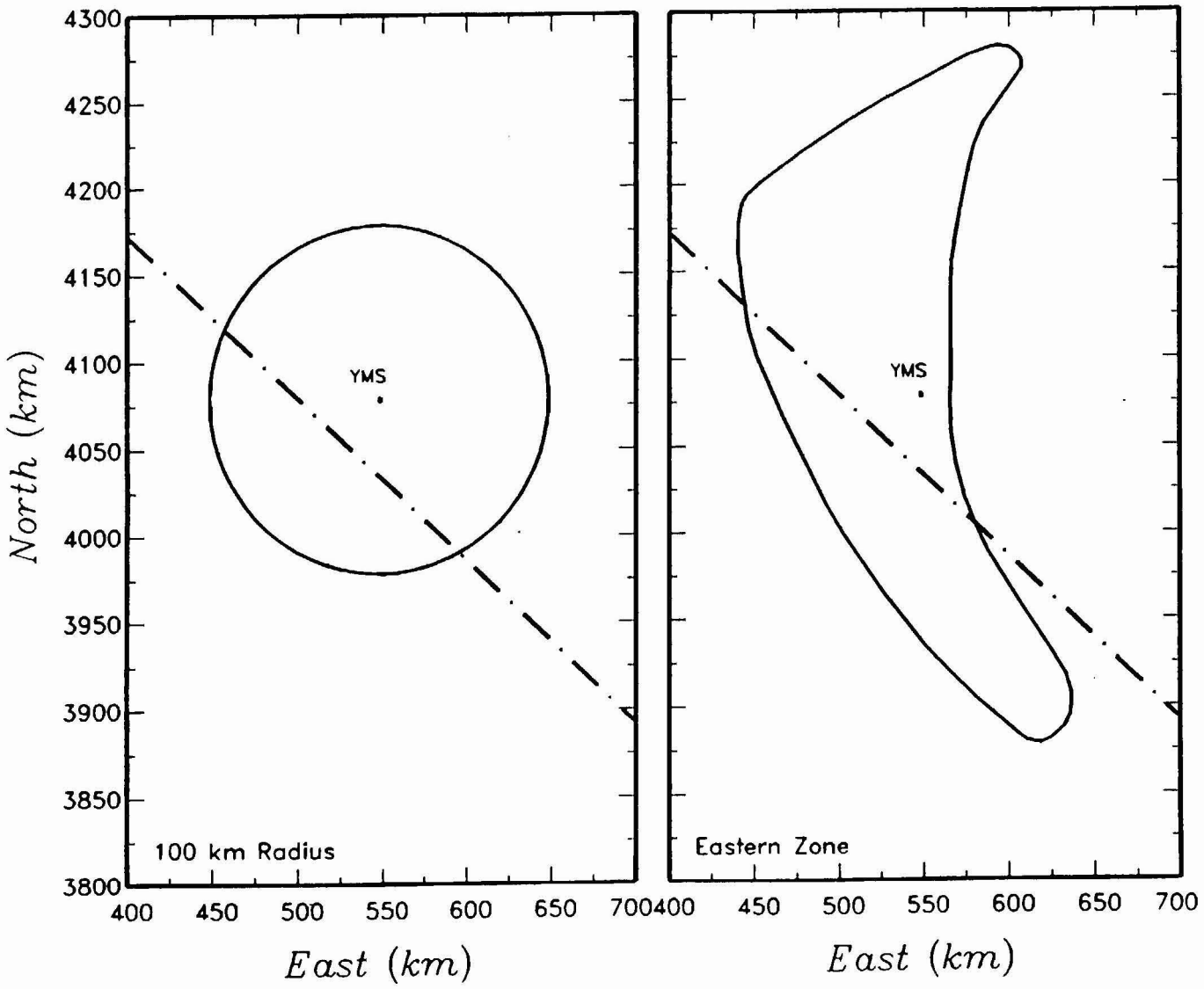

Figure 3-51 Alternative regions of interest considered by Richard Fisher. YMS refers to the proposed Yucca Mountain repository site and the dash-dot line is the Nevada-California border..

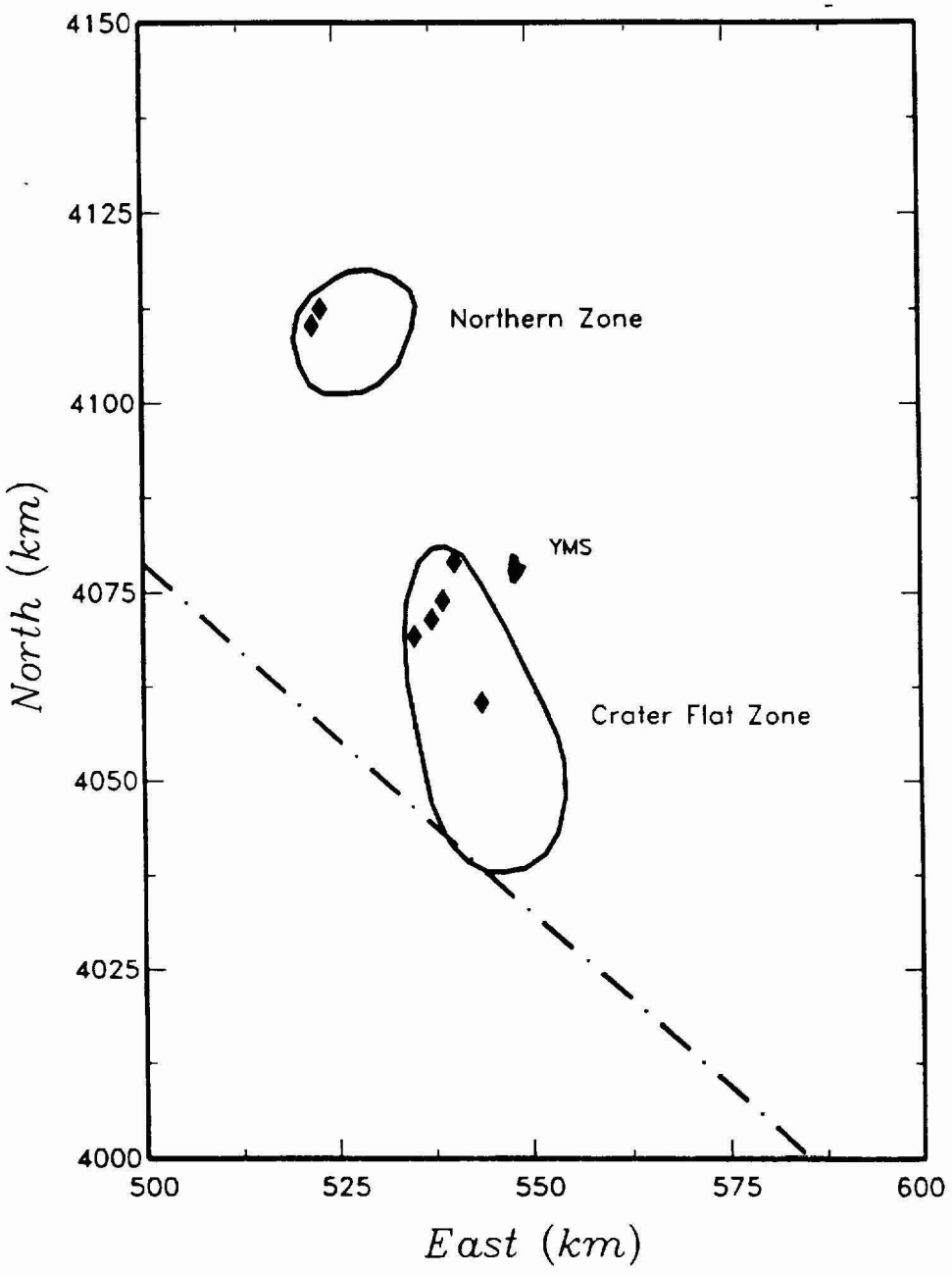

Figure 3-52 Volcanic source zone model developed by Richard Fisher. Diamonds represent volcanic events for the post-2 Ma time period. YMS refers to the proposed Yucca Mountain repository site and the dash-dot line is the Nevada-California border.

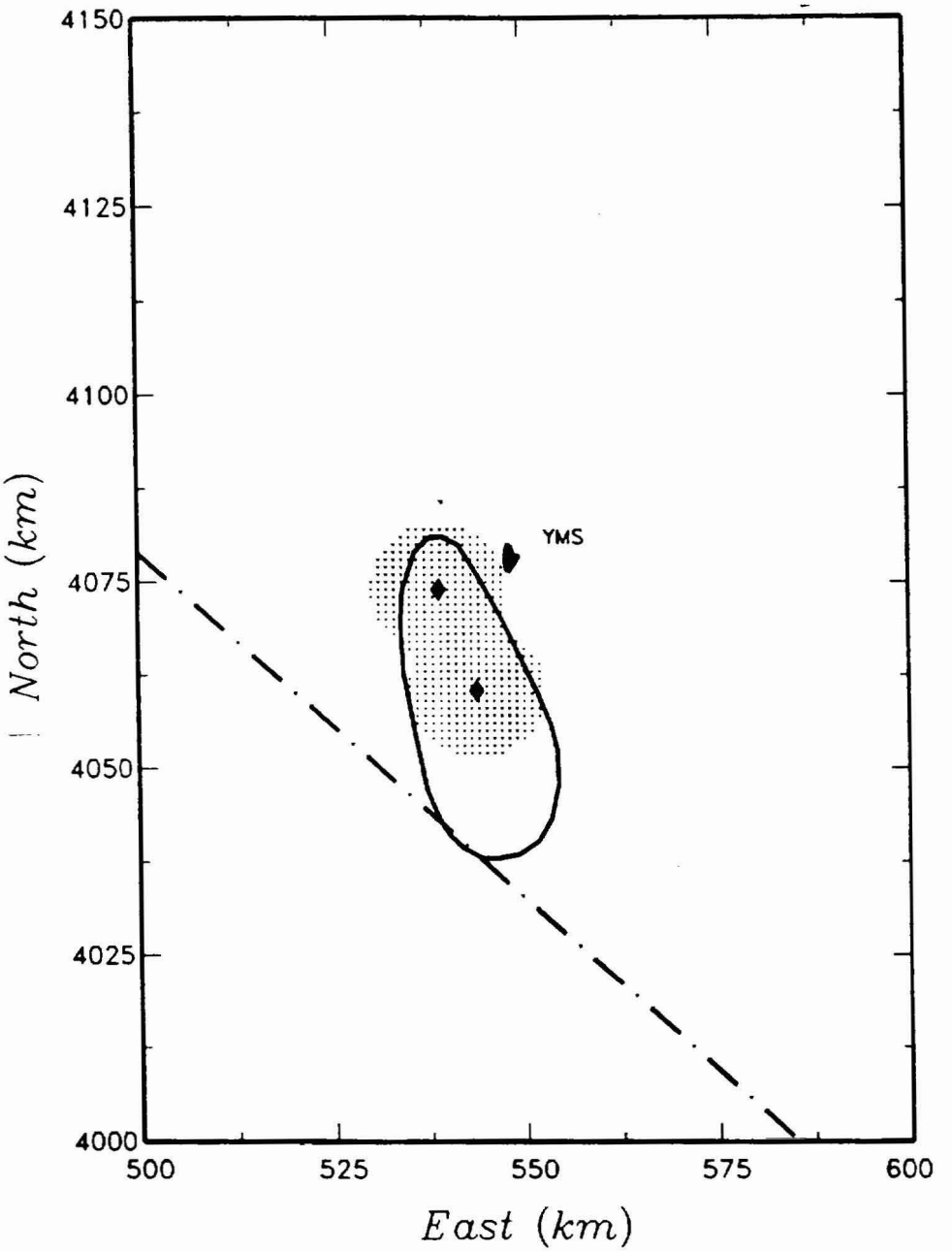

Figure 3-53 Example of a kernel density estimate based on Richard Fisher's preferred event counts for the post-2 Ma time period (shown by diamonds) and the Crater Flat zone representing an approximation of the 90-percent density contour (the stippled area). The resulting Epanechnikov kernel smoothing parameter, *h*, is 10.4 km. YMS refers to the proposed Yucca Mountain repository site and the dash-dot line is the Nevada-California border.

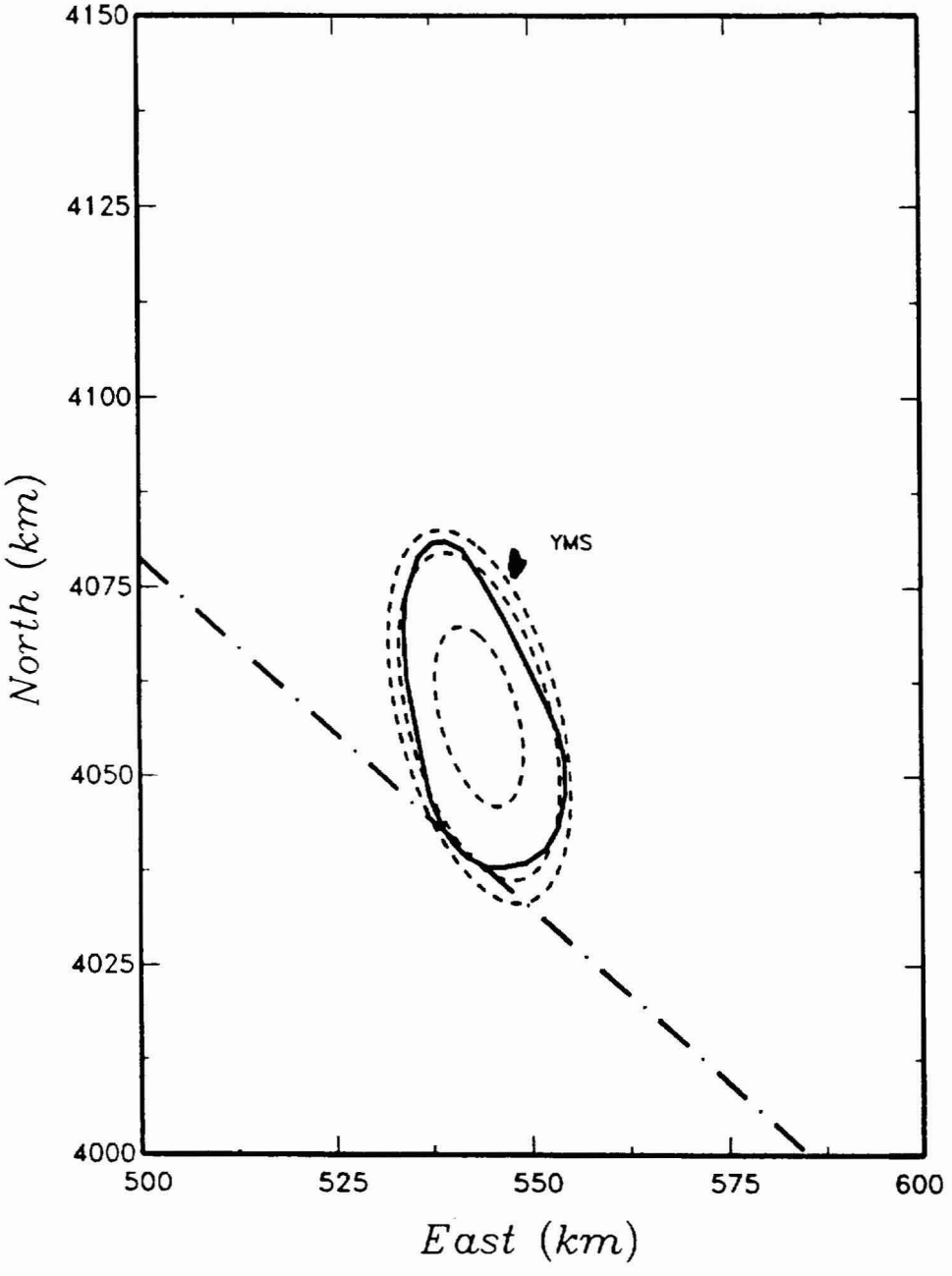

Figure 3-54 Example of the fit of a Gaussian field shape to Richard Fisher's Crater Flat zone boundary assuming it represents a 90-percent density contour. The 50th and 95th percentile density contours are also shown. YMS refers to the proposed Yucca Mountain repository site and the dash-dot line is the Nevada-California border.

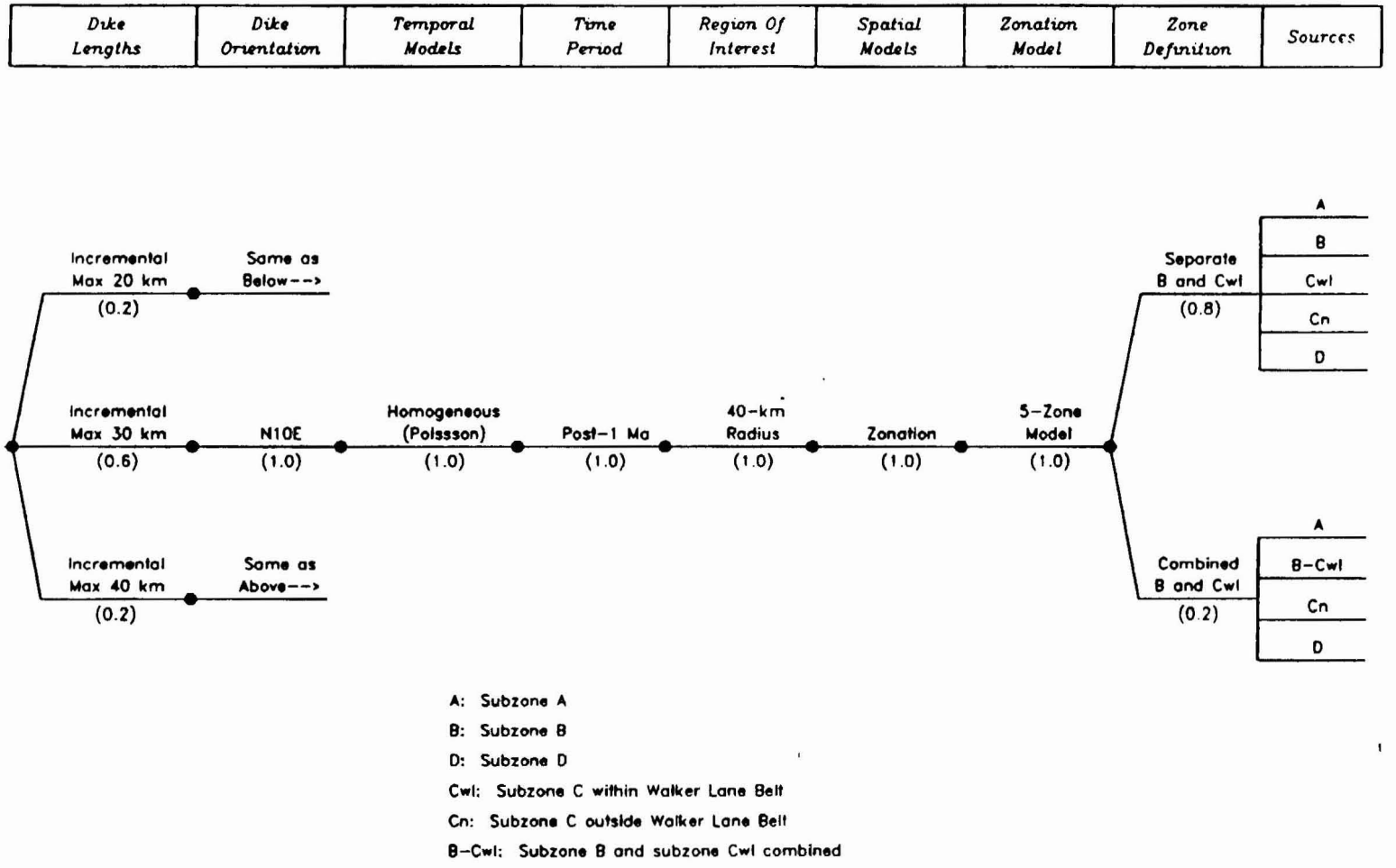

Figure 3-55 Logic tree for the PVHA model developed by Wendell Duffield.

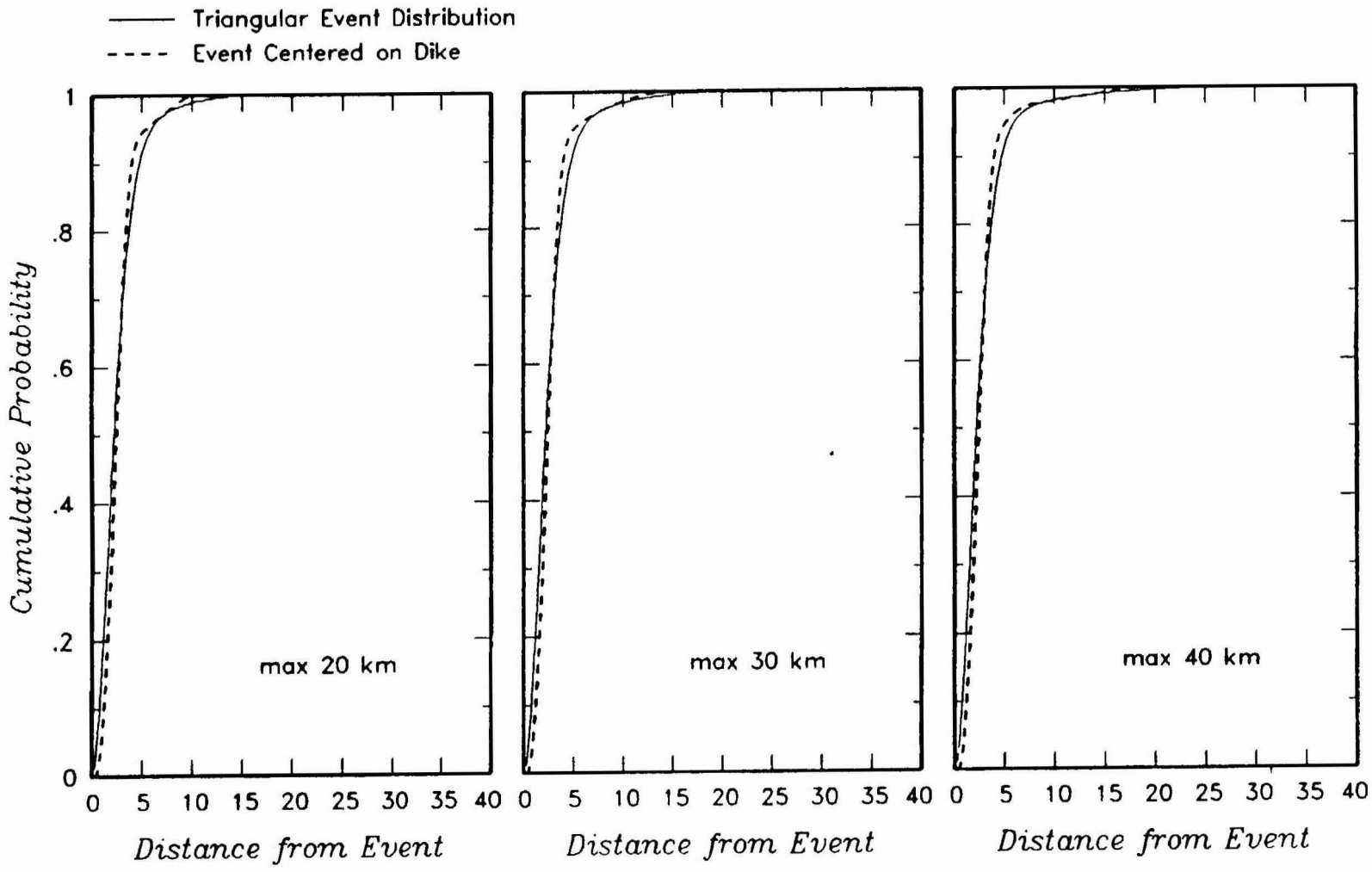

Figure 3-56 Alternative distributions for the length of an event *f(l)* developed from the assessments by Wendell Duffield.

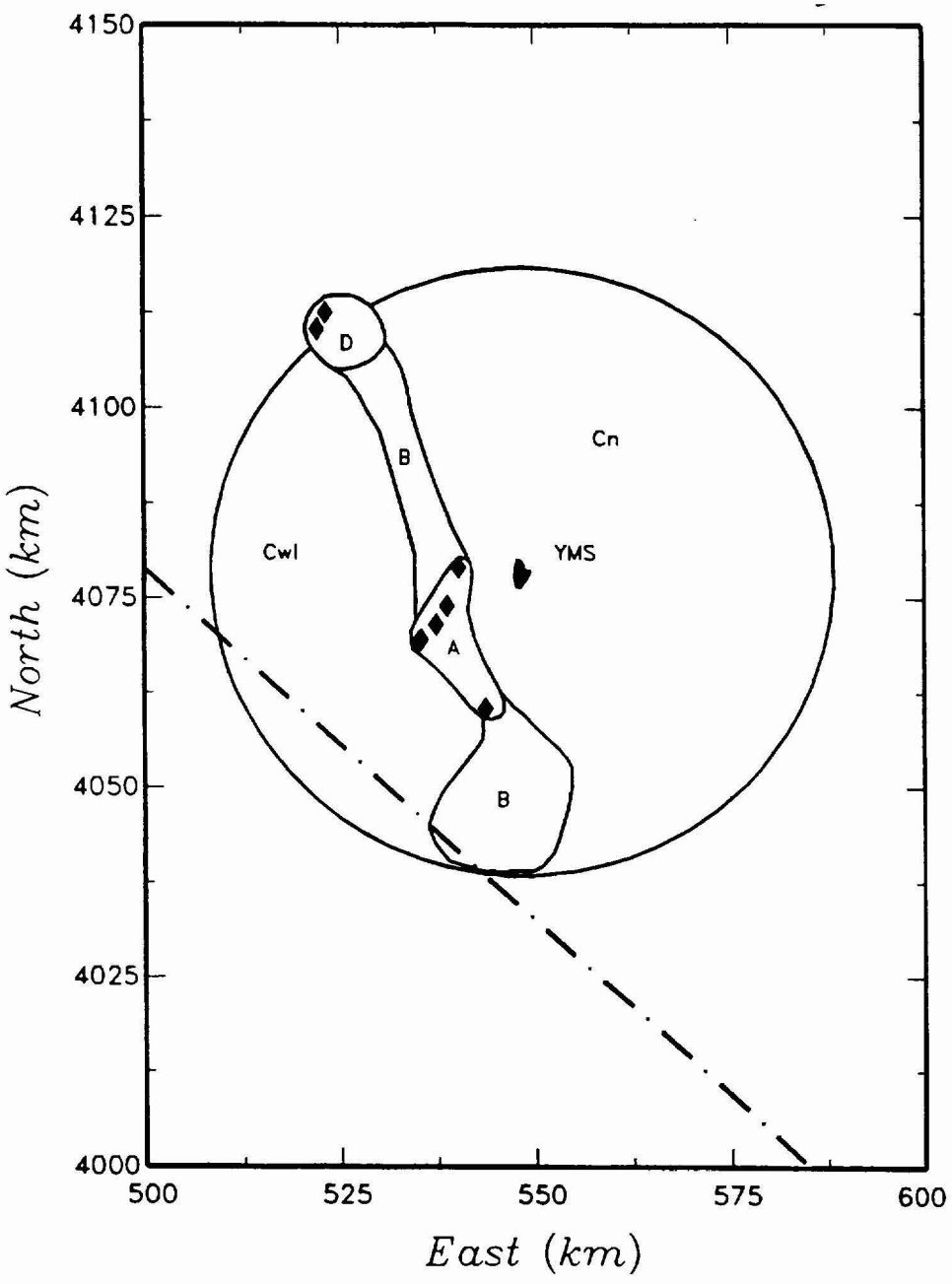

Figure 3-57 Regions of interest and source zones defined by Wendell Duffield. Diamonds represent volcanic events for the post-1 Ma time period. YMS refers to the proposed Yucca Mountain repository site and the dash-dot line is the Nevada-California border.

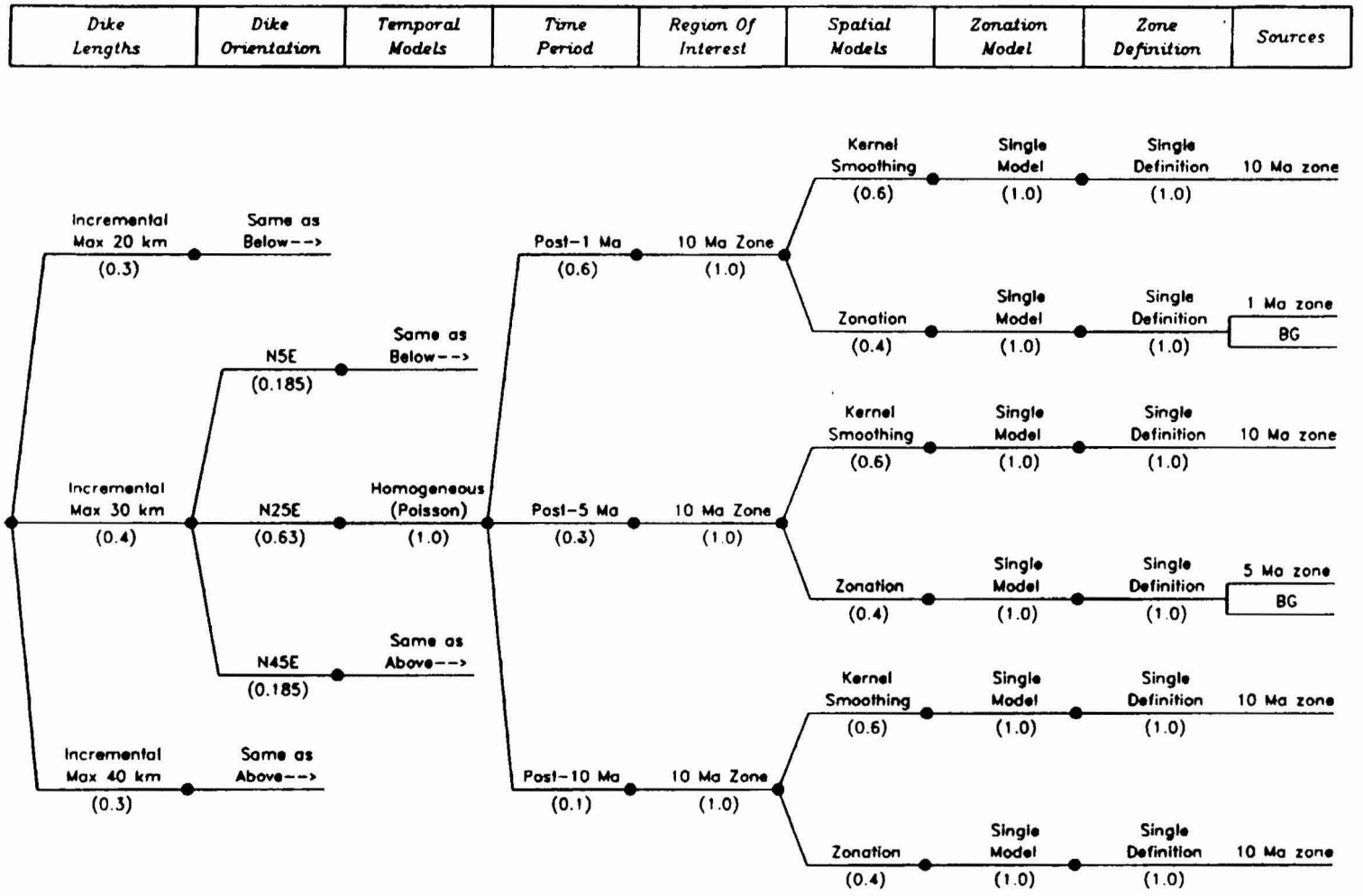

Figure 3-58 Logic tree for the PVHA model developed by William Hackett.

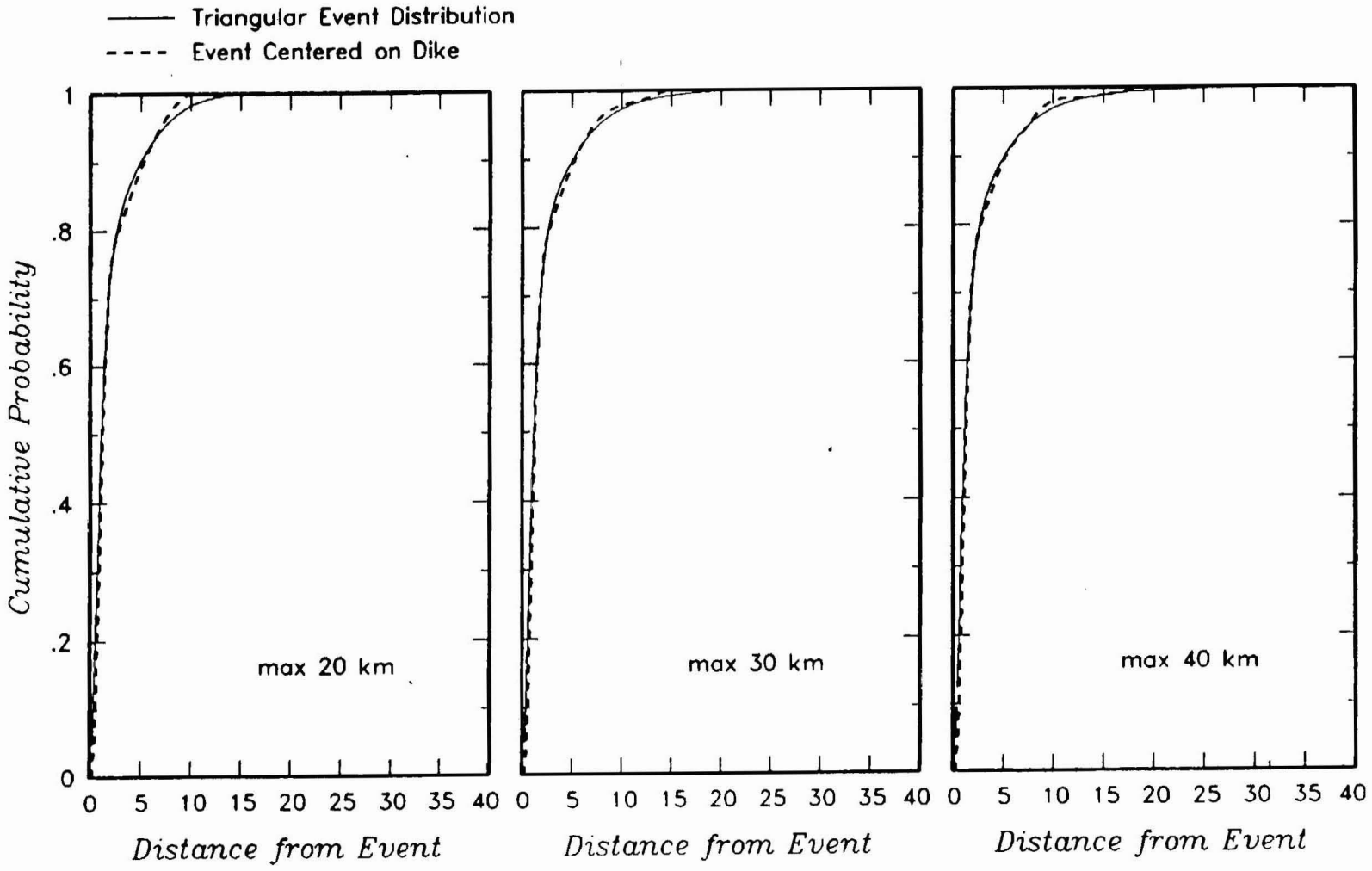

Figure 3-59 Alternative distributions for the length of an event *f(l)* developed from the assessments by William Hackett.

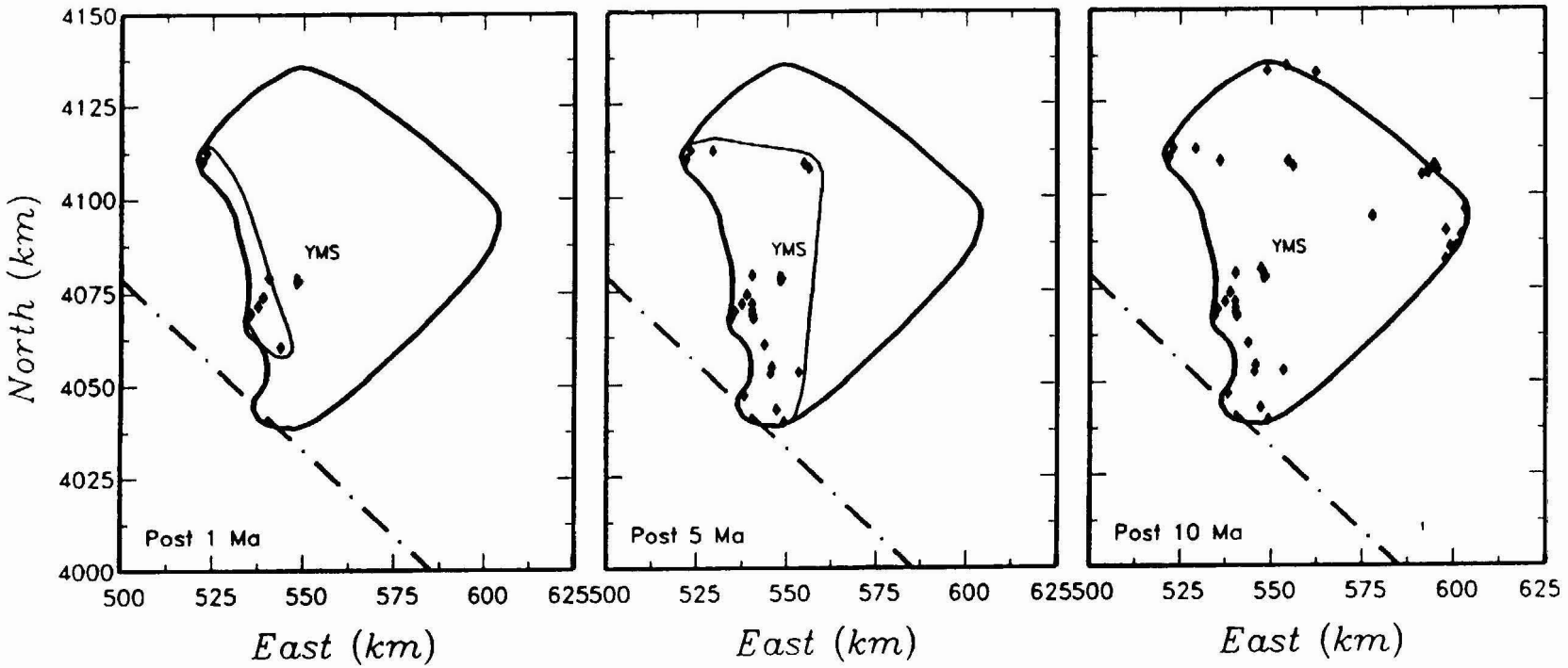

Figure 3-60 Region of interest and source zones defined by William Hackett.. Diamonds represent volcanic events for the indicated time periods. YMS refers to the proposed Yucca Mountain repository site and the dash-dot line is the Nevada-California border.

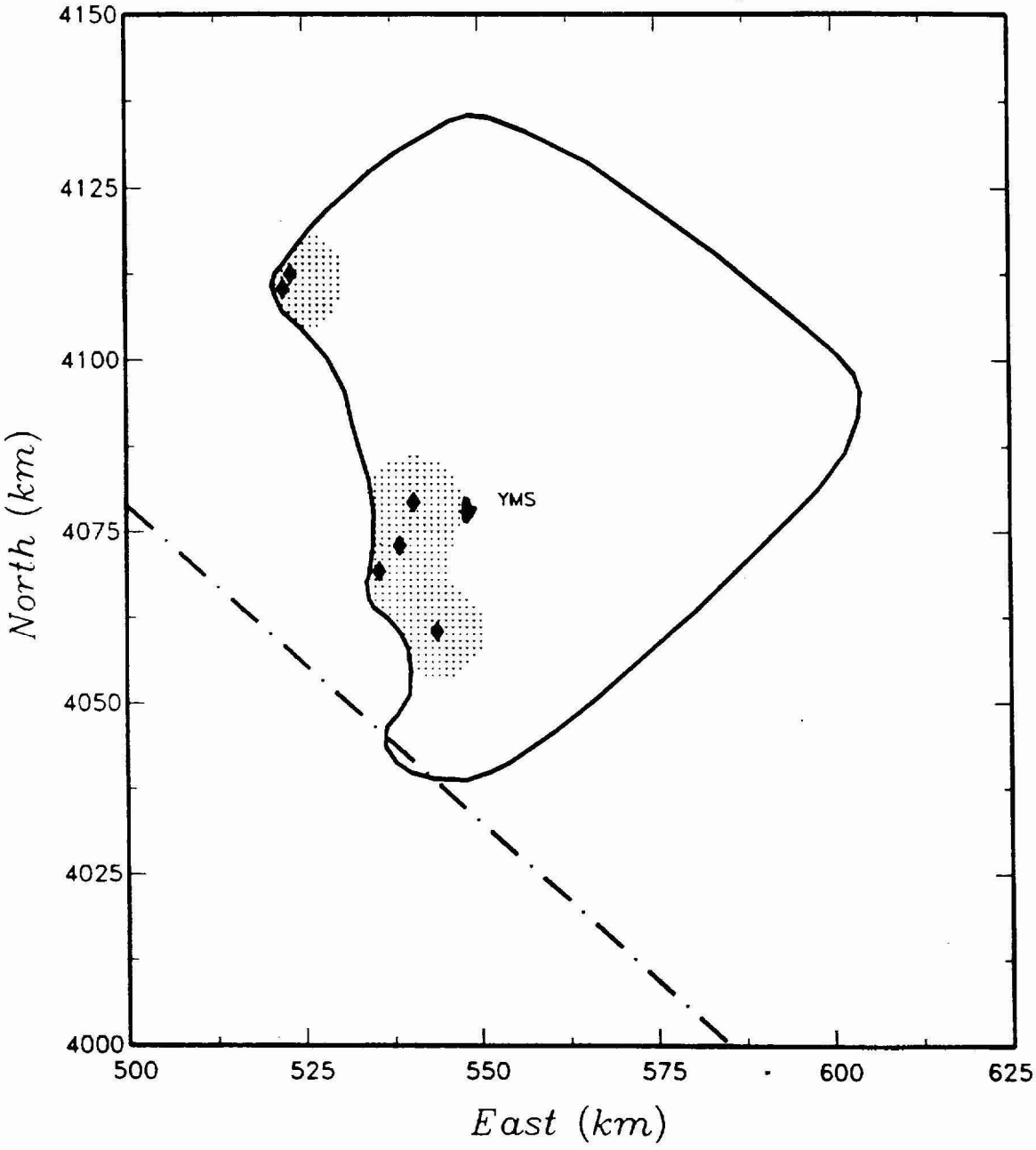

Figure 3-61 Example of the fit of a Gaussian kernel with h equal to 3.2 km to William Hackett's preferred event counts for the post-1 Ma time period. The stippled area outlines the 95th percentile density contour. YMS refers to the proposed Yucca Mountain repository site and the dash-dot line is the Nevada-California border.

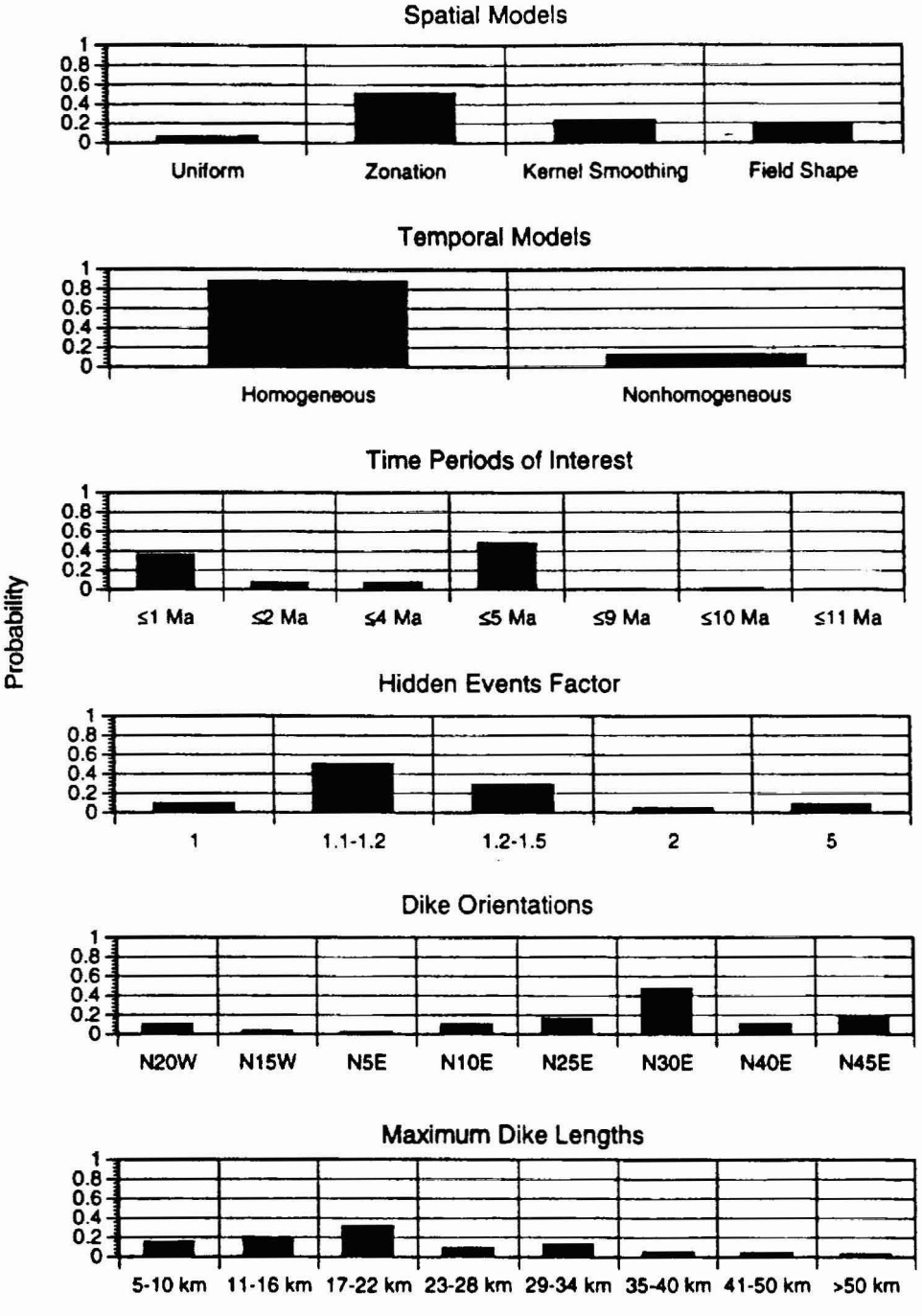

Figure 3-62 Summary of experts' assessments for components of the PVHA model.

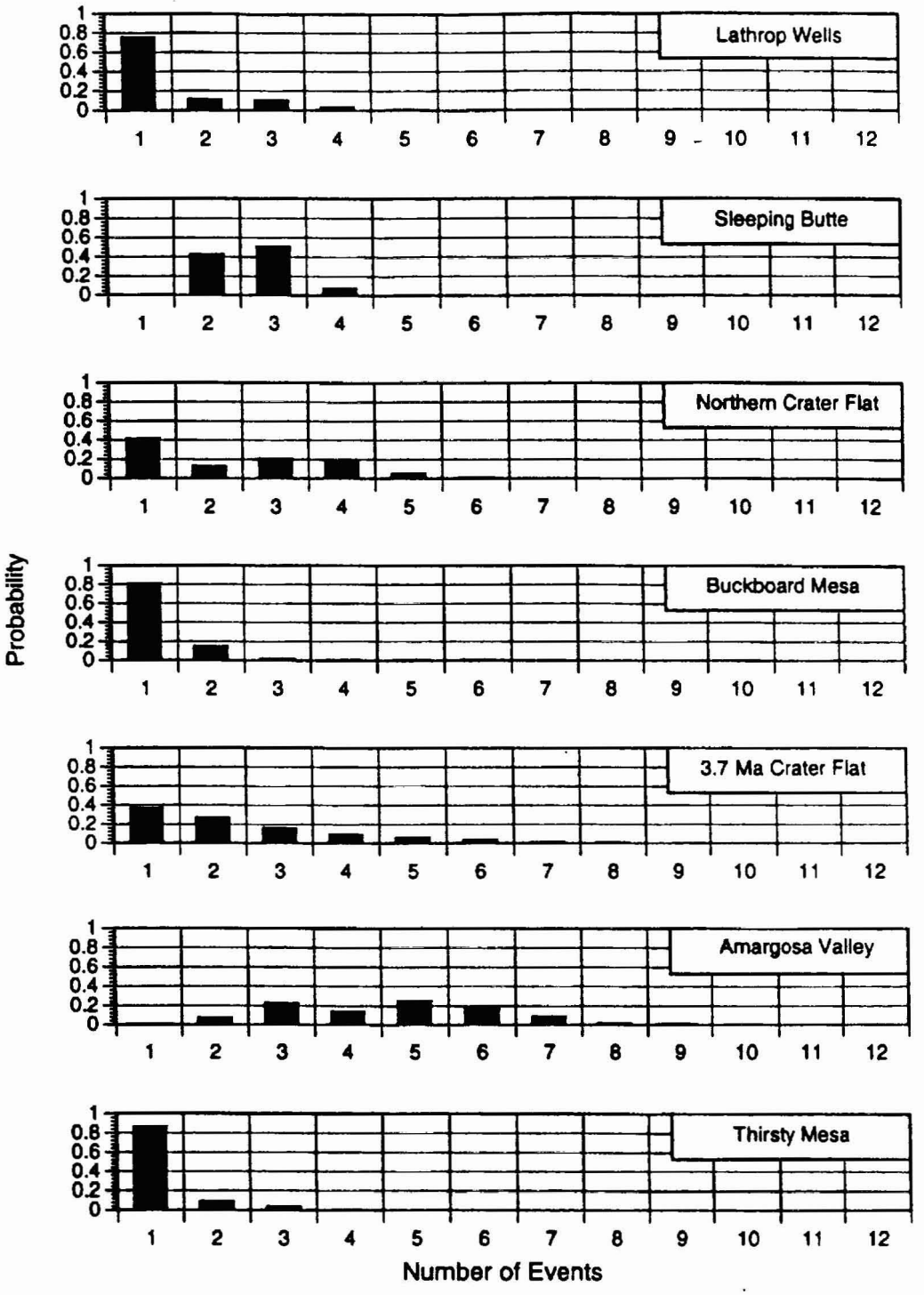

Figure 3-63 Summary of experts' assessments of the number of events at the various volcanic centers.